EXPERIMENTAL INVESTIGATION OF PARTICLE FILTRATION IN COMPRESSION RESIN TRANSFER MOLDING OF ADVANCED COMPOSITES

A THESIS SUBMITTED TO
THE GRADUATE SCHOOL OF NATURAL AND APPLIED SCIENCES
OF
MIDDLE EAST TECHNICAL UNIVERSITY

BY

TUĞÇE AYDİL DALKIRAN

IN PARTIAL FULFILLMENT OF THE REQUIREMENTS
FOR
THE DEGREE OF MASTER OF SCIENCE
IN
MECHANICAL ENGINEERING

SEPTEMBER 2014

Approval of the thesis:

EXPERIMENTAL INVESTIGATION OF PARTICLE FILTRATION IN COMPRESSION RESIN TRANSFER MOLDING OF ADVANCED COMPOSITES

submitted by **TUĞÇE AYDİL DALKIRAN** in partial fulfillment of the requirements for the degree of **Master of Science in Mechanical Engineering Department, Middle East Technical University** by,

Prof. Dr. Canan Özgen
Dean, Graduate School of **Natural and Applied Sciences** _____

Prof. Dr. Süha Oral
Head of Department, **Mechanical Engineering** _____

Assist. Prof. Dr. Merve Erdal Erdoğmuş
Supervisor, **Mechanical Engineering Dept., METU** _____

Examining Committee Members:

Prof. Dr. Mustafa İlhan Gökler
Mechanical Engineering Dept., METU _____

Assist. Prof. Dr. Merve Erdal Erdoğmuş
Mechanical Engineering Dept., METU _____

Prof. Dr. Levend Parnas
Mechanical Engineering Dept., METU _____

Prof. Dr. Altan Kayran
Aerospace Engineering Dept., METU _____

Assoc. Prof. Dr. Metin Yavuz
Mechanical Engineering Dept., METU _____

DATE: 05.09.2014

I hereby declare that all information in this document has been obtained and presented in accordance with academic rules and ethical conduct. I also declare that, as required by these rules and conduct, I have fully cited and referenced all material and results that are not original to this work.

Name, Last Name : Tuğçe Aydil Dalkıran

Signature :

ABSTRACT

EXPERIMENTAL INVESTIGATION OF PARTICLE FILTRATION IN COMPRESSION RESIN TRANSFER MOLDING OF ADVANCED COMPOSITES

Aydil Dalkıran, Tuğçe
M.S., Department of Mechanical Engineering
Supervisor: Asisst. Prof. Dr. Merve Erdal Erdoğmuş
September 2014, 139 pages

With the inclusion of particle fillers in advanced continuous fiber reinforced composites, issues such as impregnation with increased viscosity of the injected resin leading to high process pressures and possible nonhomogeneous/directional composite properties due to filtering of filler particles necessitate the study of the relations between processing parameters and the resulting particle distributions. In this study, the particle-resin interaction during compression resin transfer molding (CRTM) and resin transfer molding (RTM) of particle filled advanced composites is experimentally investigated to propose particle filtration models that can predict composite microstructure. For this purpose an experimental set-up is developed and composite specimens are produced using RTM and CRTM processes for different fiber volume fractions and particle concentrations. The produced specimens are characterized to obtain particle filler distributions along the composites. A nearly constant particle distribution profile along the flow direction was found, indicating little filtration in RTM however in CRTM, particle content in composite increased towards the end of the flow length in composite. To model particle filled resin impregnation, a Darcy law-based porous flow model, coupled with particle filtration kinetics is adapted to RTM and CRTM processes. An appropriate commercial software tool, Comsol Multiphysics® version 4.3 is used for numerical implementation and solution. The filtration kinetics of the model is adjusted with respect to the experimental results by

tuning the model parameters to match simulated particle filler distributions with experimental ones.

Key words: Particle filled advanced composites, Compression resin transfer molding, Experimental study, Filtration model.

ÖZ

BASKILI REÇINE TRANSFER KALIPLAMA İŞLEMİNDE PARÇACIK FİLTRASYONUNUN DENEYSEL OLARAK İNCELENMESİ

Aydil Dalkıran, Tuğçe
Yüksek Lisans, Makina Mühendisliği Bölümü
Tez Yöneticisi: Yard. Doç. Dr. Merve Erdal Erdoğmuş
Eylül 2014, 139 sayfa

Sürekli elyaf katkılı ileri kompozit malzemelere parçacacık eklenmesi enjekte edilen reçinenin viskozitesinin yükselmesiyle proses basıncının yükselmesi ve kompozit mikro yapısında homojen olmayan özelliklerin oluşumuna sebep olan eklenen parçacıkların filtrelenmesi, proses paremetreleri ve parçacık dağılımı sonuçları arasındaki ilişkinin araştırılmasını gerektirmektedir. Bu çalışmada parçacık katkılı ileri kompozit, baskılı reçine transfer kalıplama (CRTM) ve reçine transfer kalıplama yöntemleri (RTM) süresince parçacık reçine etkileşimi kompozit mikroyapısını (parçacık filtrasyonunu) öngörecek parçacık filtrasyon modellerini tasarlamak için deneysel olarak incelenmiştir. Bu amaçla deneysel bir düzenek geliştirilmiş ve kompozit malzemeler RTM ve CRTM prosesleri kullanılarak farklı elyaf oranları ve farklı parçacık konsantrasyonları için üretilmiştir. Üretilen kompozit malzemeler kompozit boyunca oluşan parçacık dağılımını elde etmek için karakterize edilmiştir. RTM prosesinde akış doğrultusunda çok az parçacık filtrasyonunu gösteren yaklaşık sabit parçacık dağılımı bulunmuş fakat CRTM prosesinde kompozitteki parçacık miktarı akış uzunluğunun sonuna doğru artmıştır. Parçacık katkılı reçine emilimini modellemek için parçacık filtrasyon kinetiği ile birleştirilmiş poröz akış modeline bağlı Darcy kanunu, RTM ve CRTM yöntemlerine uyarlanmıştır. Sayısal analiz ve çözüm için uygun bir paket yazılımı olan Comsol çoklu-fizik 4.3 sürümü kullanılmıştır. Modelin filtrasyon kinetiği deneysel sonuçlara bağlı olarak model

parametrelerinde değişiklikler yapılıp parçacık dağılımı simülasyonunun deneysel olanlarla eşleşmesi için ayarlanmıştır.

Anahtar Kelimeler: Parçacık katkılı ileri kompozitler, Baskılı reçine transfer kalıplama, Deneysel çalışma, Filtrasyon modeli.

to my dear family

ACKNOWLEDGEMENTS

I would like to thank to my supervisor Asisst. Prof. Dr. Merve Erdal Erdoğmuş for her valuable advice, guidance and patience at each grade of this thesis.

My special thanks go to Hamed Tanabi, Hatice Sinem Şaş, Betül Macit, Dilek Adalı Kızılören, Yelda Meyva, Sinem Gözde Defterli, Gülsüm Çaylan for helping me get through the hard time, and for all support, entertainment.

I would like to express my deepest thankfulness to my mother, Feray Aydil, my father, Fazıl Aydil and my lovely husband, Mehmet Ceyhun Dalkıran. They have been a constant love and encouragement in each step of my life. This dissertation would certainly be not possible without their support.

TABLE OF CONTENTS

LIST OF TABLES

TABLES

LIST OF FIGURES

FIGURES

NOMENCLATURE

C: concentration of particles in the polymer (volume of particles/volume of suspension)

K: domain permeability [m^2]

p: flow pressure [Pa]

t: time [s]

u, v, w: superficial velocity components in x-, y- and z- directions [m/s]

u′, v′, w′: actual (interstitial) velocity components in x-, y- and z- directions [m/s]

U_z: top mold plate closing speed [m/s]

V: superficial velocity [m/s]

V′: actual (interstitial) velocity [m/s], $V' = \frac{V}{\varepsilon}$

h: mold cavity height

w: mold cavity width

Q: volume flow rate

$\dot{m}$: mass flow rate

C_o: particle concentration (by volume) in injected suspension

v_{fo}: fiber volume fraction in mold (volume of fibers/volume of mold cavity)

$\nu_{fo,initial}$: initial fiber volume fraction of CRTM

ν_f: solids volume fraction in mold (volume of fibers and filtered particles/volume of mold cavity), $\nu_f = \nu_{fo} + \sigma$

$\nu_{f,particle}$: Particle volume fraction in the composite

x,y,z: cartesian coordinates

ε_0: porosity of the fiber preform, $\varepsilon_0 = 1 - \nu_{fo}$

ε: porosity (volume of pores/volume of mold cavity), $\varepsilon = \varepsilon_0 - \sigma$

μ: viscosity [Pa·s]

ρ: density [kg/m^3]

σ: specific particle deposit (volume of filtered particles/volume of mold cavity)

ACRONYMS

LCM: liquid composite molding

RTM: resin transfer molding

CRTM: compression resin transfer molding

VARTM: vacuum assisted resin transfer molding

2-D: two dimensional

3-D: three dimensional

CV: control volume

FEM: finite element method

SSE: sum of squares of errors

CHAPTER 1

INTRODUCTION

1.1 Continuous Fiber Reinforced Composites

Composite materials are made of two or more constituents, which have different physical or chemical properties to give a unique combination of properties. Having the flexibility of constituting these combinations helps produce superior and unique material properties compared to other materials. Therefore, they are preferred in many industrial applications such as aerospace, automotive, defense, construction, biomedical.

Composites have two main phases: the matrix and the reinforcement. The matrix materials can be polymeric, metallic and ceramic. The main function of matrix, the primary phase of composites, is transferring the load to the reinforcement. Polymeric matrix composites can have thermoset or thermoplastic matrix phase. These composites can yield outstanding mechanical properties with low density. Thermoset resins that are utilized in the particular composite production methods of this study are used in about 75% of all composite products. The wide use of thermoset resins is due to their processability at liquid state, with less heat and pressure requirements, low cost tooling and the ability to wet fibers relatively easily [1].

The secondary phase of composite, the reinforcement, carries the load and provide the mechanical properties such as strength, stiffness in the composite. Reinforcements are classified as particulate and fibrous reinforcements according to their geometry.

Particle fillers are used as particulate reinforcement in composite materials. Fibrous form of reinforcements which have much greater length than their cross sections can be discontinuous fibers (short fibers) and continuous fibers according to their shape and size as shown in Figure1.1 [2].

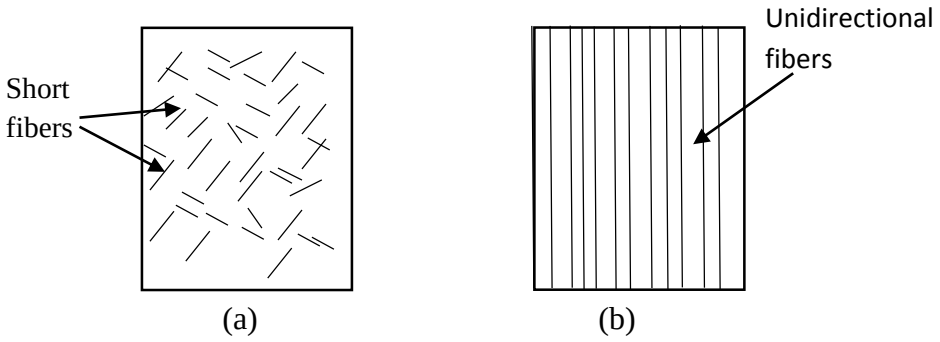

Figure 1.1 a) Discontinuous (short) and, b) Continuous fiber reinforced composites

Fibrous composite containing continuous fibers have high strength-to-weight ratio. Therefore, they are crucial in applications where light weight along with structural integrity is needed, such as in aerospace, defense, marine and automotive industries. The orientation of load bearing component (continuous fiber) of these composites can be unidirectional as shown in Figure 1.1 (b), bidirectional (e.g. woven fabric layers) or three-dimensional (e.g. 3-D woven fiber architecture). So one can acquired the desired strength or modulus of composite by using different orientation of continuous fibers. The continuous fibers in polymeric composite fibers can be glass, carbon, aramid or their combinations. These reinforcements are in the form of woven or nonwoven fabric layers (for 2-D orientation) or 3-D woven architecture. Examples of continuous fiber reinforcement are presented in Figure 1.2

Chopped fiberglass mat (unwoven)

Twill weave glass fiber fabric

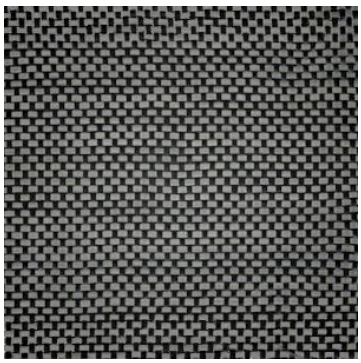

Plain weave carbon fiber fabric

Figure 1.2 Examples of continuous fiber reinforcements that are used in polymeric composites

1.2 Liquid Molding of Advanced Composites

Composite products are made by various composites processing techniques depending on requirements in engineering such as geometry of products, the mechanical properties and cost. For thermoset composites, a number of processing methods exist. The most prominent ones are hand-lay-up, autoclave molding, liquid molding and filament winding. This study focuses on liquid molding.

In liquid composite molding (LCM) processes, the dry fibrous reinforcement, usually being glass, carbon or aramid, is impregnated with the liquid thermosetting resin. Producing large and complex shaped composite parts, versatility and good surface finish are the leading advantages of LCM processes [2]. LCM encompasses a number of processes. These are resin transfer molding (RTM), compression resin transfer molding (CRTM), vacuum assisted resin transfer molding (VARTM) and their variations. The focus of the current study is the two processes: RTM and CRTM.

1.2.1 Resin Transfer Molding

RTM process enables producing somewhat large and complex shaped composites relatively fast with low labour requirement and smooth part surface finish [3–5]. In RTM, the fiber reinforcements can be continuous strand mats, chopped fiber strand mats, woven/ uni-directional fabric layers.

In the first step of RTM; the dry fiber reinforcements is placed in a mold cavity that has the shape of the part to be produced. The reinforcement in the shape of the composite part is usually referred to as preform. Then the mold is closed for the injection phase of the process. After closing the mold, the thermosetting resin is injected through one or more injection gates until all of dry fibrous reinforcement is impregnated (and the mold is completely filled). During the filling stages, the air in the mold is discharged through the air vents in the mold. In order to form a rigid composite the liquid resin ‘‘cures’’, that is, the resin molecules cross-link through an exothermic chemical reaction. The injection times are usually much faster than the resin curing times therefore, there is no significant heat transfer or chemical reaction taking place during injection (except in structural reaction injection molding process where fast-reacting resins such as polyurethanes are used). Filling times can vary from a few minutes to several hours [6]. When the injection is completed, the mold can be heated to accelerate the cure. In various cases, the produced part is also post-cured (after being removed from the mold). These processing steps of RTM process are presented in Figure 1.3.

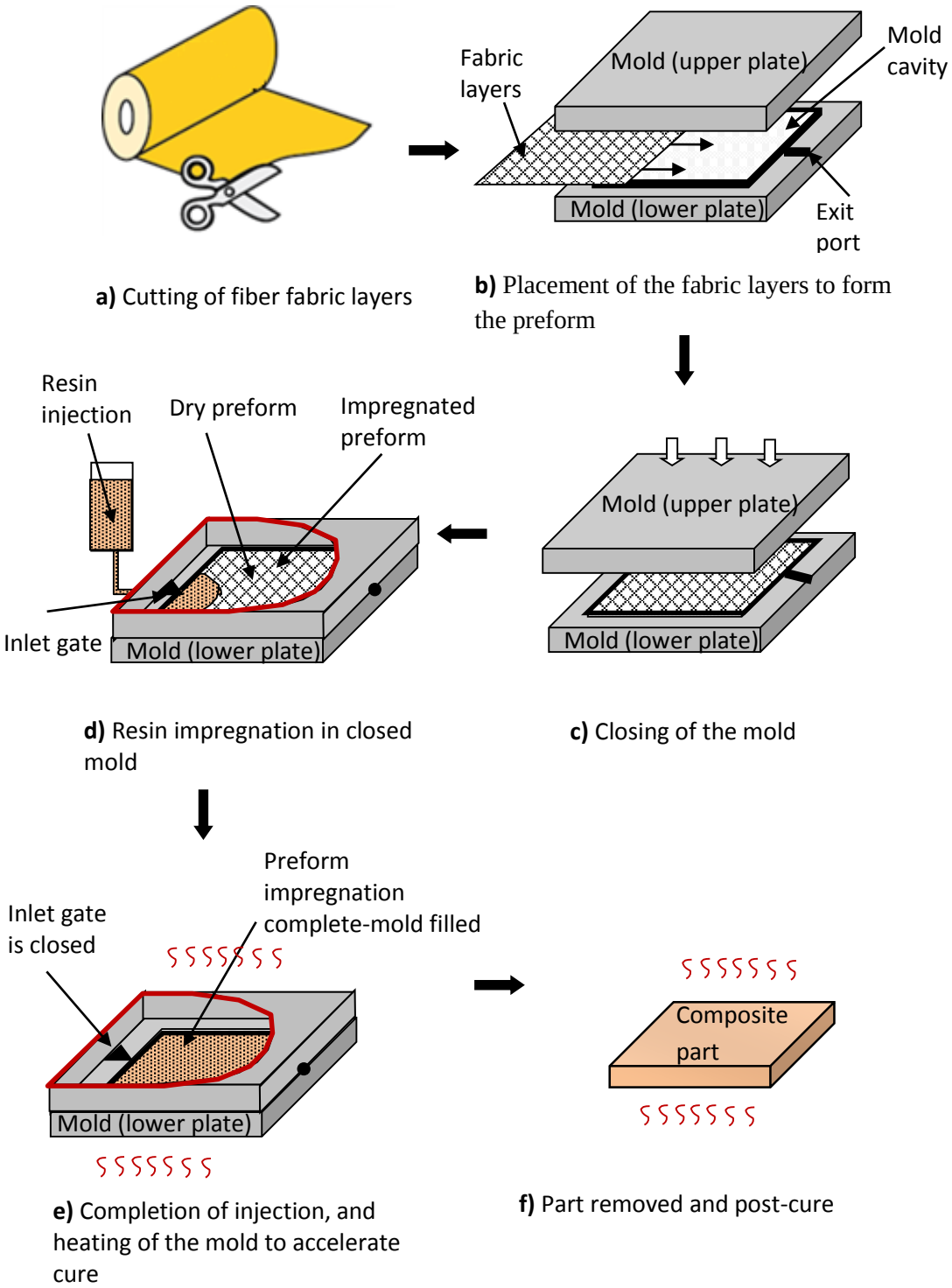

a) Cutting of fiber fabric layers

b) Placement of the fabric layers to form the preform

c) Closing of the mold

d) Resin impregnation in closed mold

e) Completion of injection, and heating of the mold to accelerate cure

f) Part removed and post-cure

Figure 1.3 Stages of resin transfer molding process

1.2.2 Compression Resin Transfer Molding

Compression resin transfer molding (CRTM) is a modification of RTM which is best suitable producing relatively large advanced composites. The fibrous reinforcement is placed into the mold cavity and then the mold is partially closed. In this process, the resin is injected when the fibrous preform is not at its final (design) fiber volume fraction (the fiber volume fraction is significantly less than the design fiber volume fraction). After a sufficient amount of resin is injected, injection is stopped and the inlet gate is closed. The injection phase is then followed by the compression phase in which the mold closes (by bringing down the upper mold plate) and forces the injected resin to impregnate the rest of the fiber preform as the preform thickness is brought down to its final thickness (the design fiber volume fraction is achieved). After the desired thickness of the preform is achieved by the compression phase, the curing occurs. Figure 1.4 presents the schematic of the CRTM process.

In CRTM, better consolidation of the composite part, better wettability of the fibrous reinforcement, larger composite production and lower injection pressure are aimed comparison to RTM. If the fiber loading or the fiber volume fraction is increased in RTM, the flow pressure or the filling time increases due to the reduction in permeability of the preform [7]. With CRTM, it is possible to consolidate composites of fairly high fiber volume fractions.

In literature, the description of the CRTM process shows some differences depending on whether the upper mold is in contact with the preform or if there is a gap between the upper mold and the fiber preform. When the upper mold plate is not in contact with the preform, the desired volume of resin is injected directly to the gap. Since the gap permeability is higher than that of the preform, at first, most of the resin spreads across the gap instead of penetrating the preform. The penetration of resin through preform happens during the compression phase [8]. In the case where the preform is not in contact with the upper mold plate, the resin directly preform. The injection phase is followed by the compression phase [9]. These are also other variations of the process

such as simultaneous in injection and compression [10]. In this case, the process is called injection/compression molding(I/CM).

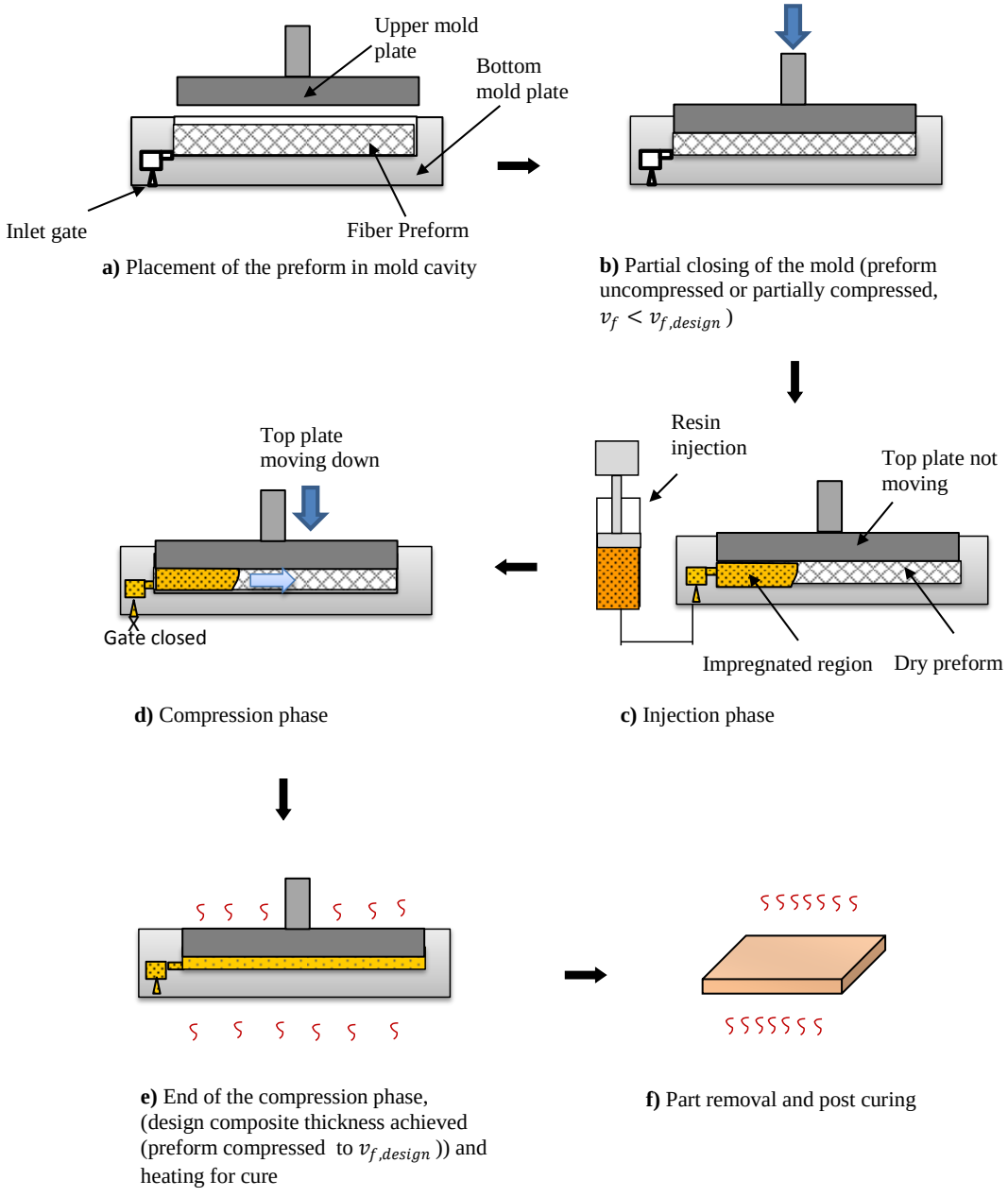

a) Placement of the preform in mold cavity

b) Partial closing of the mold (preform uncompressed or partially compressed, $v_f < v_{f,design}$)

c) Injection phase

d) Compression phase

e) End of the compression phase, (design composite thickness achieved (preform compressed to $v_{f,design}$)) and heating for cure

f) Part removal and post curing

Figure 1.4 Stages of the CRTM process

1.3 Particle-Filled Continuous Fiber Reinforced Composites

In advanced composites particle fillers may be included in the composite to enhance certain properties ranging from mechanical properties [11], flame-retardance [12] to wear resistance [13,14], thermal and electrical conductivities [15]. For example, the outstanding electrical and thermal conductivities and mechanical properties of carbon nanotubes combined with the structural and properties of lightweight fiber composites render such composites an attractive class of materials [16]. Another possible advantages of using particle fillers in the matrix is that they may help prevent the development of cracks throughout the composite by toughening the composite. [17]

1.4 Issues in Production of Particle-Filled Continuous Reinforced Composites

Particle filled composites can be produced via liquid molding processes, most commonly using RTM and vacuum assisted resin transfer molding (VARTM), by transferring the particles into the fiber preform through impregnation with a particle-resin suspension. Before the impregnation of fiber preform, nano or micro particle fillers are mixed with the resin in desired amounts to form the particle resin suspension.

The use of particle fillers in advanced composites introduces several issues to the production of such composites via liquid molding processes. Processing pressure can rise significantly, especially in high fiber volume fraction composites with high particle concentrations. The high particle concentrations in injected particle-resin suspension lead to high suspension viscosity, which requires higher pressure to impregnate the preform. High pressure can lead to higher manufacturing cost and at the same time, inadequate resin-fiber bonding and weak composite properties due to the difficulty the viscous resin experiences in penetrating the dense fiber preforms. In addition to these issues, the dense preform may also act as a filter and the process may yield a nonhomogeneous particle distribution in the composite, leading to nonhomogeneous/directional properties. [9, 10]. Such process outcome possibilities

necessitate the understanding of the relations between the process/processing parameters and the resulting particle distribution in the composite.

1.5 Objective of the Thesis

The aim of this thesis is to experimentally investigate the effect of various process parameters in resin transfer molding (RTM) and compression resin transfer molding (CRTM) of particle-filled, continuous fiber reinforced composites, on the resulting particle distribution within the composite. For this purpose, an experimental set-up for RTM and CRTM has developed and particle-filled continuous fiber reinforced composites samples are produced and characterized for particle distribution. The impregnation processes in both RTM and CRTM processes are also simulated using a previously developed particle-filled impregnation model [17,19] in order to assess the applicability of a filtration model , as well as to fine-tune the filtration model constants.

1.6 Literature Survey

In this section, a brief literature survey on key subjects of the thesis work is presented.

1.6.1 Particle-Filled Advanced Composite Production

In literature, several experimental studies on particle filled advanced composites exist. These range from investigating the change in the composite properties with the inclusion of particle fillers to the limitations in the amount of particle fillers that can be introduced and understanding particle deposition and how it affects the quality of the particle dispersion in the produced composites. Costa and Skordos [20] investigated carbon nano-tube (CNT) filled continuous fiber reinforced composites manufactured via RTM and found that for acceptable CNT resin suspension viscosity

for impregnation, CNT content would have to be below 0.3 % by weight. Fan et al. [21] injected a multi-walled carbon nanotube vinylester resin suspension to a random glass fiber preform to understand the dependence of initial particle dispersion in the suspension to the particle dispersion after the production of the composite. They showed that the initial state of suspension and the fibrous medium affect the particle distribution in the composite sample. Nordlund et al. [22] manufactured particle filled advanced composites using VARTM to investigate two particle deposition mechanisms: ˝filtration during the fiber bundle impregnation" and ˝filtration induced by stationary flow through fiber bundles ". The filtration during the fiber bundle impregnation can be explained with the particle transport into fiber bundle, only occurs in a region close behind the flow front. In the second mechanism, a distance behind the flow front, the transient flow behavior present at the flow front is replaced by a stationary flow condition. They showed that particle deposition occurred around and in front of the fiber bundles for both mechanisms and proposed suggestions to achieve homogeneous particle distribution (such as particle size be smaller than fiber bundle spacing, and adjustable flow rate). Mohan et al. [13] investigated the effect of different fillers on wear resistance of glass epoxy composites produced via VARTM. They have obtained lower wear damage in particle filled composites than in composites sample with no particle fillers.

There are no published experimental studies involving particle filled composites manufactured by CRTM, which is the subject of this thesis.

1.6.2 Modeling of Resin Impregnation in Liquid Molding of Advanced Composites

1.6.2.1 Resin Transfer Molding

The need for modeling RTM process arised from the need to reduce production design costs due to expensive and time-consuming experiments. The flow models can be used for designing the mold features such as location of the inlet and the air vent gates, and

determining the appropriate process parameters for producing a composite part with the desired properties [19]. Shojaei et al. [23] distinguished the studies of simulation of RTM process into two fields: The simulation of the mold filling stage, and the simulation of the process cycle. The simulation of mold filling stage predicts the resin flow front location and flow pressure during injection in order to optimize the molding conditions and minimize the filling time. The simulation of the process cycle optimizes the production efficiency and performance of the produced part. Simacek and Advani [24] simulated mold filling for different air vent and injection gate positions and investigated fiber tow saturation.

Several issues may occur during RTM process and it is necessary to understand relationship between process parameters and these issues for finding and controlling the optimum process parameters. Variation in the thickness of the fiber preform was shown to be an important issue that affected the flow behavior as it lead to fiber anisotropic permeability of the flow domain [25]. Issues such as formation and amount of voids (unimpregnated regions in preform) and race tracking were investigated via numerical simulations to find optimum process parameters to avoid these [26,27].

Several studies exist that compare experimental results with numerical simulations. Trochu et al. [28] presented a numerical model of resin impregnation of RTM based on nonconforming finite element approximation (unlike conforming finite element approximation the computed flow rates remain continuous across the boundary of the elements). They also compared the numerical results with their experimental results to satisfy the optimum process variables for different mold geometries and multiple injection ports. Laurenzi et al. [29] simulated the RTM process for a large and complex aeronautic beam (which has an anisotropic permeability) based on finite element-modified control volume (FEM-CV) to obtain successful impregnation of the preform and a filling time compatible with the resin gel time. The results of the simulation were compared with a series of RTM experiment result, and were used to manufacture the beam. Poodts et al. [30] performed a series of RTM experiments and simulated the resin flow and curing cycle of the process to find the optimum process parameters for manufacturing. They performed some mechanical tests on the finished product, comparing RTM with other composite production method.

1.6.2.2 Compression Resin Transfer Molding

In literature, numerical studies of the CRTM have been conducted for mold design as well as to determine the influential process parameters and their effects. Pham et al. [31] simulated the impregnation phase of 2-D resin flow using finite element method. Numerical simulation of 3-D impregnation phase in CRTM on control volume/finite element method (CV/FEM) was presented by Shojaei [3]. Chang [10] presented a simultaneous resin injection/compression molding process(I/CM) using FEM. He used Hele-Shaw flow model for modeling the resin flow in the gap (between the fiber reinforcement and the upper mold) while Darcy's Law was used for modeling the resin flow through the fibrous reinforcement. In their work, a small gap existed between the mold top plate and the preform, and the resin was directly injected to the gap. Their results showed that the minimum total filling time was achieved by using a high compression speed and small initial gap. They also showed that mold filling time and injection pressure decreased significantly compared to RTM. Bhat et al. [8] simulated CRTM at three stages: Resin injection to the gap between the mold and the preform, compression by upper mold and penetration of the resin in the gap to the preform, continuation and completion of compression in which the resin moves solely through the preform. They investigated the effect of process parameters on filling time through a non-dimensional analysis. They assumed that during the compression stage, the preform deformation was uniform through the thickness. Merotte et al. [32] showed that the preform deformation could not be neglected and implemented the preform compression in their model.

Experimental studies and comparison of these studies with the numerical studies of CRTM also exist in literature. Merotte et al. [33] simplified and modeled the resin flow during compression stage as a one dimensional flow to obtain estimates for process time if the applied force is known. They verified numerical solution of the flow front progression and the change in the permeability thickness experimentally. Buntain and Bickerton [9] studied the forces applied on the mold in RTM and CRTM experimentally using two reinforcing materials with different compaction response.

They showed that mold clamping force strongly depended on non-elastic compaction effects (such as stress relaxation and an apparent lubrication by the injected fluid). They also simulated their experimental results to predict tooling forces on a mold [34].

Chang et al. [35] investigated the effect of various process parameters (injection pressure, mold opening distance (initial gap during the injection), resin temperature, compression pressure, pre-heated mold temperature, cure temperature) on the mechanical properties of composites produced via CRTM, experimentally. They found that low compression pressure and resin viscosity were most effective on the mechanical properties of the part.

1.6.3 Modeling of Particle Deposition in Flow through Porous Media

The inclusion of particle fillers in resin may leads a particle deposition in composite, which affects permeability of the preform, the injection pressure and also the resin flow in the media. Thus, the resin flow and the filtration phenomenon during the composite production processes affect each other. By developing modeling tools that can simulate the particle deposition in composite, a predict-and-verify type process design can be achieved [17].

The first mathematical model of particle-filled macroscopic resin impregnation of RTM, which is based on Darcy-flow and coupled with filtration kinetics, was presented by Erdal et al. [18]. They simulated the flow model to obtain particle filler content in composite, suspension viscosity, permeability, flow pressure with respect to time and position. Lefevre et al. [2,36] followed this model and modified the filtration kinetics by considering liquid retention. They produced particle filled composites via RTM and used the experimental results to modify the filtration kinetic model to match the simulation results.

Sas and Erdal [19] extended the model in [18] to injection and compression phase of compression resin transfer molding of particle-filled composites. They modeled the compression phase by modifying the mass conservation to account for the changing

the control volume. Chohra et al. [37] proposed another particle deposition model in multilayers preforms for VARTM process by using Darcy flow and extending it to include anisotropic preform. They validated their model by an experimental investigation.

Hwang et al. [38] simulated particle deposition in dual-scale porous media by considering interactions between particle-fluid and particle-porous wall. Moreover, Costa and Skordos [39] used an analytical solution to simulate the flow and filtration of liquid molding and compared it with a finite difference model.

1.7 Scope of the Thesis

The current study is presented in Chapters 2 to 5 of this thesis.

Chapter 2 presents the experimental work undertaken in this thesis. The experimental set-up and experimental procedure for producing composite samples using RTM and CRTM are presented in detail. The characterization of the produced composite samples for determining the particle distribution in them is explained.

Chapter 3 presents the particle –filled resin impregnation model for both RTM and CRTM processes. The governing equations and boundary conditions are given. The numerical implementation of mathematical model is also presented in this chapter.

Chapter 4 presents the results of the experimental work and process simulation based on the model given in Chapter 3, for RTM and CRTM processes. The comparison of experimental and numerical results is presented in this chapter. Effects of various process parameters on resulting particle distribution in the composites are presented and discussed. The production scenarios are simulated in order to obtain an appropriate filtration model that is valid for the production condition of the thesis work.

Finally, Chapter 5 presents the conclusion and contributions of the current study and outlines possible future work that can further extend the research topic.

CHAPTER 2

EXPERIMENTAL INVESTIGATION OF PARTICLE FILTRATION IN RESIN TRANSFER MOLDING AND COMPRESSION RESIN TRANSFER MOLDING

2.1 The Objective and Scope of Experimental Work

In this thesis, an experimental work has been perfomed to investigate the particle distribution in particle-filled, continuous fiber–reinforced composites produced via two liquid molding methods: RTM and CRTM. Composite specimens which are produced with these processes are characterized to compare and understand the effect of various process parameters on the composite microstructure (particle distribution) in each experiment.

An experimental set-up has been designed and constructed suitable for both RTM and CRTM processes. In order to monitor and record data during the processing experiments, suitable monitoring and data acquisition equipment was obtained. Appropriate composite material components were selected. After the production of particle filled continuous fiber reinforced composite samples, the particle distribution in the samples were characterized with an appropriate method.

2.2 The Experiment Design

In all production experiments, the dimensions of produced samples were targeted to be the same. The type of composite material constituents (fiber, resin and particles) did not vary in the composite.

In production experiments, process parameters, whose effects on particle distribution in the produced composites are to be investigated, are:

- The suspension injection speed
- The particle concentration in injected resin
- The fiber volume fraction
- The processing method (RTM or CRTM)

In order to capture the effect of each parameter, the remaining parameter values will be kept constant while production of varying values at the parameter of interest is carried out.

During the experiments the following data are recorded

- Injection pressure
- Piston speed
- Suspension flow front progression

After the production of composite samples, analysis and characterization are performed for the following

- Determination of suspension velocity impregnating the fiber preform, using the flow front progression data
- Obtaining the distribution of particle volume fraction in the composite samples.

2.3 Composite Material Constituents

The materials constitutents of particle filled continuous fiber reinforced samples are the resin matrix, the fiber reinforcements and the particle fillers. The type of the composite constitutents do not vary in production experiments.

For the matrix phase, epoxy resin (Hexion MGS L160, Momentive) is used. This resin is reported to have low shrinkage, good wettability, easy fabrication and chemical and moisture absorption [13]. Its nominal viscosity is reported to be 900 mPa-s and its density 1,13-1,17 g/cm^3. The resin is cured with the hardener (Hexion MGS H160, Momentive). The resin-hardener ratio is 100:30 by volume and the hardener viscosity is reported to be 0.77 Pa-s [40]. Table 2.1 presents the curing gel time of the epoxy-hardener at different temperatures. Figure 2.1 shows the epoxy resin, the hardener and their mixture. Though the resin is transparent, the resin and hardener mixture becomes ‘‘opaque”.

Table 2.1 Gel time of resin –hardener mixture (100:30 by vol) at different temperatures [40]

Temperature(℃)	Gel Time of Resin Hardener Mixture (100:30 by vol)
20 -25 ℃	Approximately 3-4 hours
40 -45 ℃	Approximately 60 minutes.

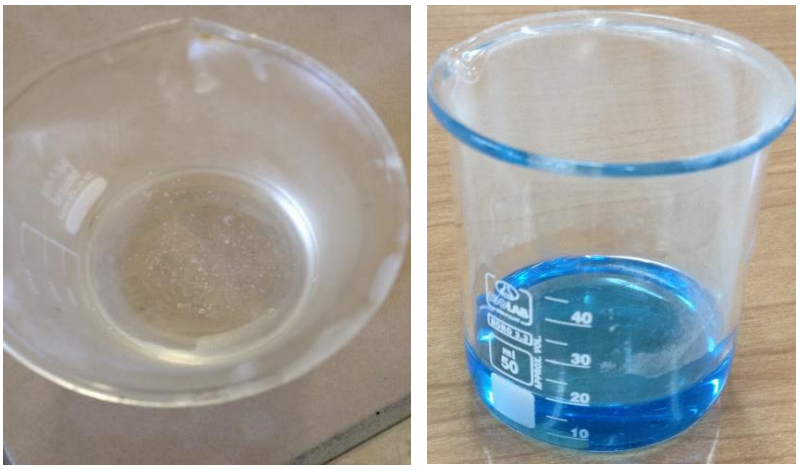

a.)Resin b.)Hardener

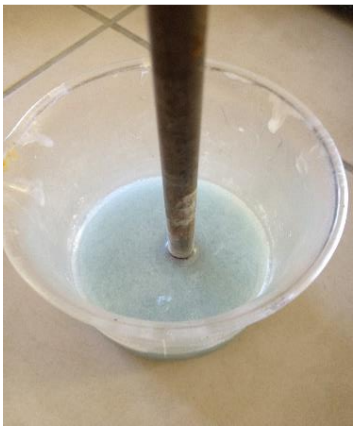

c.)Resin-hardener mixture

Figure 2.1 a.) Epoxy resin (Hexion MGS H160) **b**.) Hardener (Hexion MGS H160) **c.)** Mixture of the Epoxy resin and Hardener(100:30 by vol)

In the production experiments spherical glass particles (Microperl 050-20-215, Sovitec) with an average particle diameter of 20 μm and true density of 2.5 g/cm^3 were used as the particle fillers. These fillers can be seen in Figure 2.2.

Figure 2.2 Images of the spherical glass particles (Microperl 050-20-215) used as particle fillers in the production experiments

As the fiber reinforcement, layers of general purpose chopped strand glass fiber mat (CSM) with a nominal areal weight of 450 g/m^2 was used. The glass fiber density is 2.6 g/cm^3. Figure 2.3 shows the image of the glass fiber.

Figure 2.3 Chopped strand glass fiber mat used as the reinforcement in the production experiments

2.4 The Mold

Figure 2.4 presents the mold assembly. The mold consists of a top mold plate, a spacer plate and a bottom mold plate. The mold used is designed to produce thin, rectangular composite samples with the planar dimensions 150 mm length × 70 mm width. The thickness of the cavity is adjustable as the top mold plate can be lowered or raised to yield a thickness between 1.5 – 4 mm.

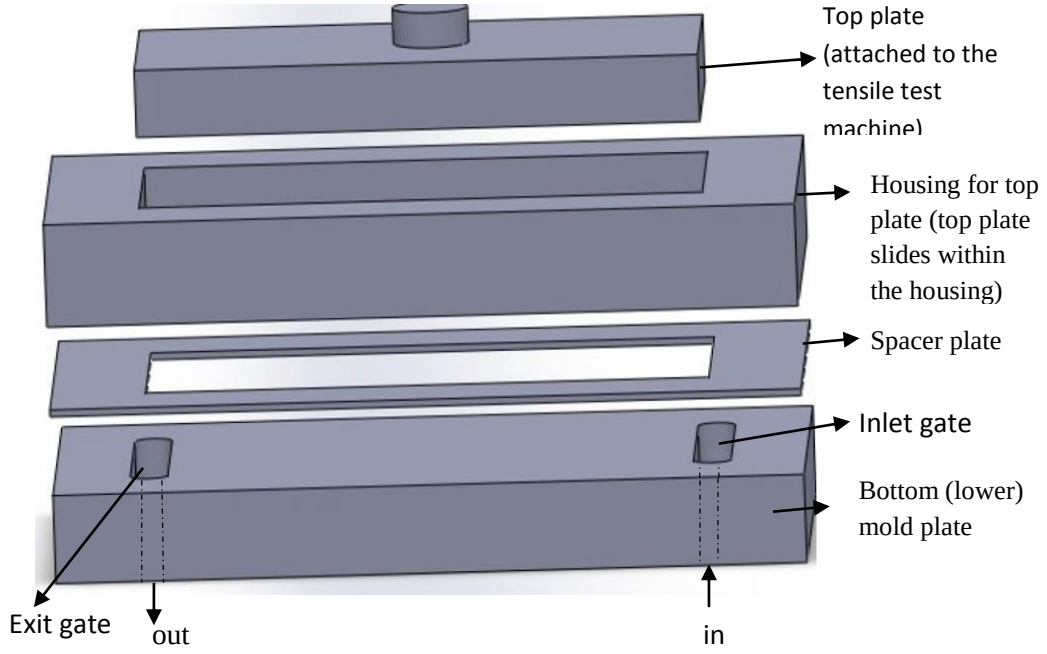

Figure 2.4 The mold assembly

In order to inject the suspension into the mold cavity, an inlet gate is constructed on the bottom mold plate. For 1-D, uniform resin flow front progression, the gate is constructed as a line gate in the form of a shallow pool at one end of the mold cavity, above the injection port. At the other end of the mold cavity, an exit gate (similar to the line gate) is constructed. The close-up image of the mold gates are shown in Figure 2.5.

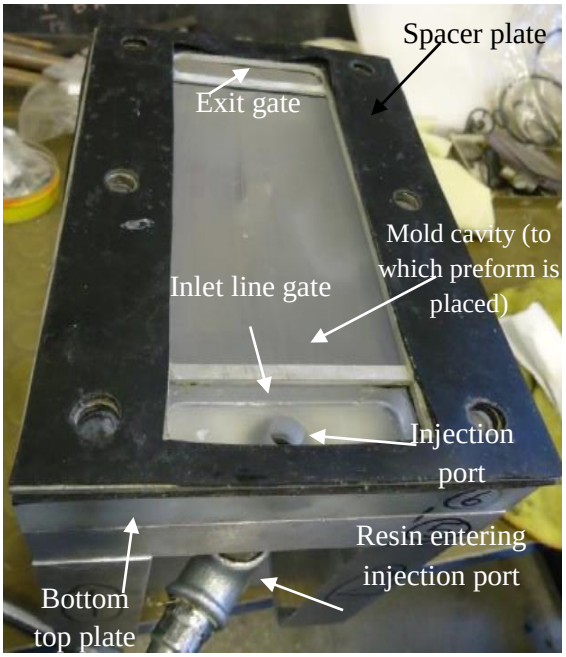

Figure 2.5 The close-up image of the mold gates

The lower plate of the mold is made of transparent PMMA in order to observe the flow during injection. The plate surface of this plate is marked with distance increments to quantify the flow front position at any time instant. Figure 2.6 presents the view from the bottom of the mold, facing the transparent lower mold plate.

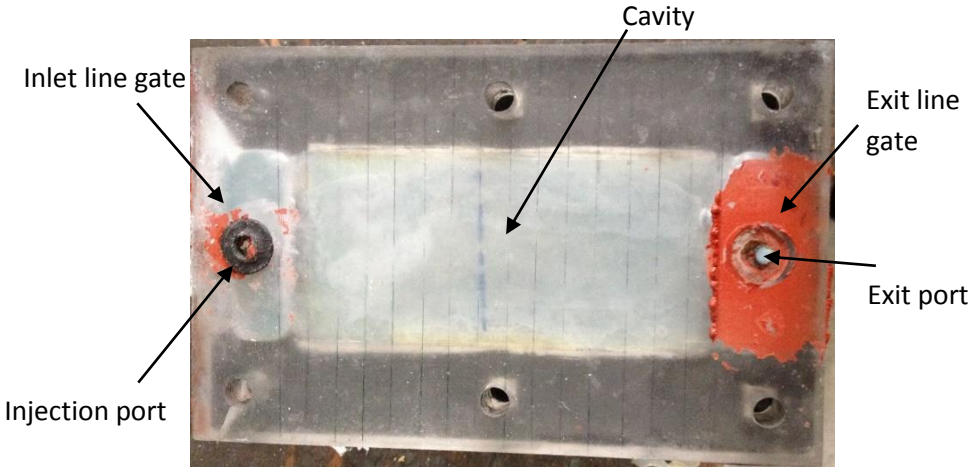

Figure 2.6 The image from the bottom of the mold, facing the transparent lower plate

Upper mold plate is positioned and clamped on the mold assembly with the help of a tensile test machine. The top plate is attached to the tensile machine, which can lower or raise the plate as desired. Furthermore, when the top plate is positioned in the mold assembly, it is held in place by the tensile test machine against any force (such as pressure force) developing in the mold during injection. Leakage of the resin during impregnation is prevented by sealing the mold with a mold gasket on the top plate. The upper mold plate and the mold gasket are shown in Figure 2.7.

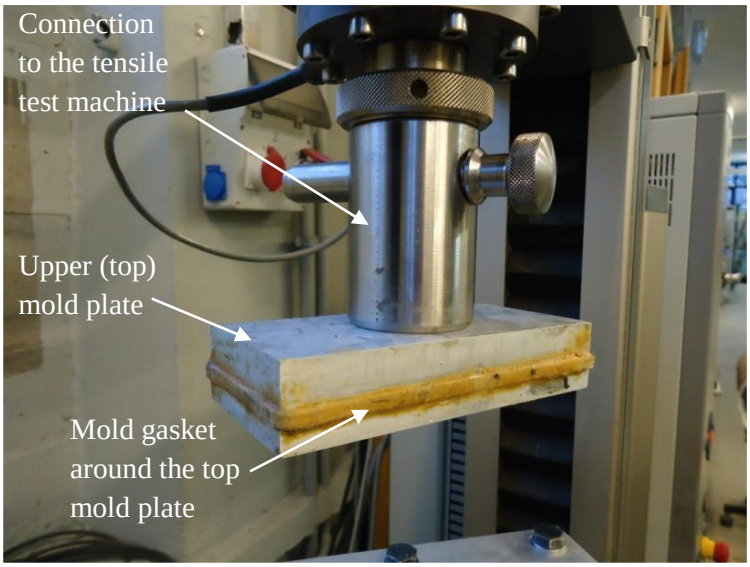

Figure 2.7 Upper mold plate and mold gasket

The full mold assembly is presented in Figure 2.8. The pressure of the particle resin suspension entering the mold is recorded using a pressure transducer, as shown. The mold sits on a pedestal. A nook (opening) below the mold (within the pedestal) houses a camera facing the transparent bottom mold plate, to record flow front progression.

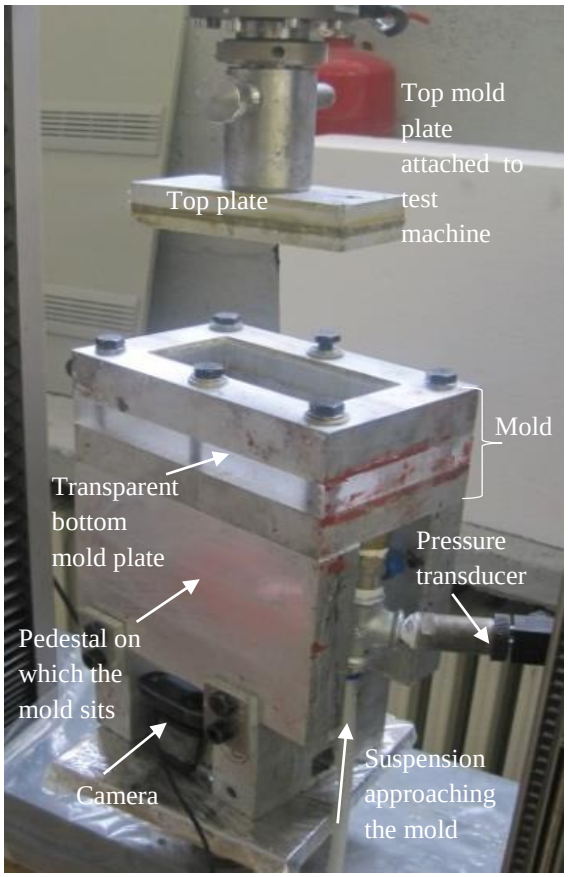

Figure 2.8 Mold assembly

2.5 Injection and Compression Set-up

A piston-cylinder set-up was designed and manufactured to achieve the injection of the suspension to the mold. Piston assembly consists of a nitrile butadiene rubber (NBR) gasket (K25, Kastas) with a diameter of 40 mm and a connector, which attaches the gasket to the actuator. Piston gasket and connector assembly is shown in Figure 2.9. A linear actuator (LA27, Linak) and a control unit move the piston and provide constant piston speed for injection. The actuator can apply a maximum thrust force 8000 N and 4000 N in push and pull applications, respectively. The suspension is poured in a steel cylinder and the piston pushes the suspension within the cylinder. The internal diameter and height of the cylinder are 40 mm and 300 mm, respectively.

The cylinder connects to the mold through general pneumatic pipes with the diameter of 10 mm that can withstand high pressure. Figure 2.10 shows the piston cylinder set-up.

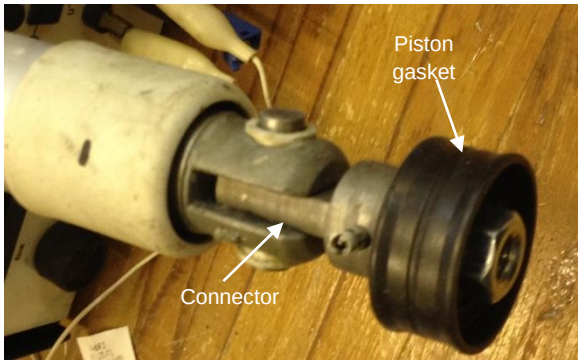

Figure 2.9 Piston gasket and Connector

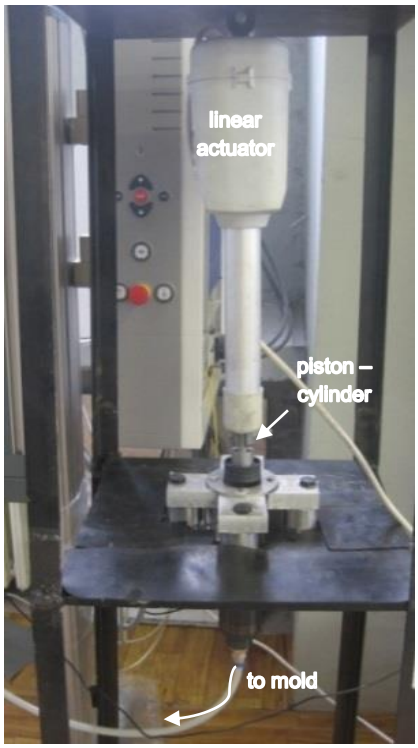

Figure 2.10 The injection system

The positioning of the top plate and the subsequent clamping is achieved by Zwick tensile testing machine (20 kN capacity) to which the top mold plate is fastened. The Zwick testing machine controls the closing speed of the top plate during the compression phase of CRTM process. Figure 2.11 and Figure 2.12 presents the Zwick tensile test machine to which the mold top plate is attached, and the user interface of this machine, respectively.

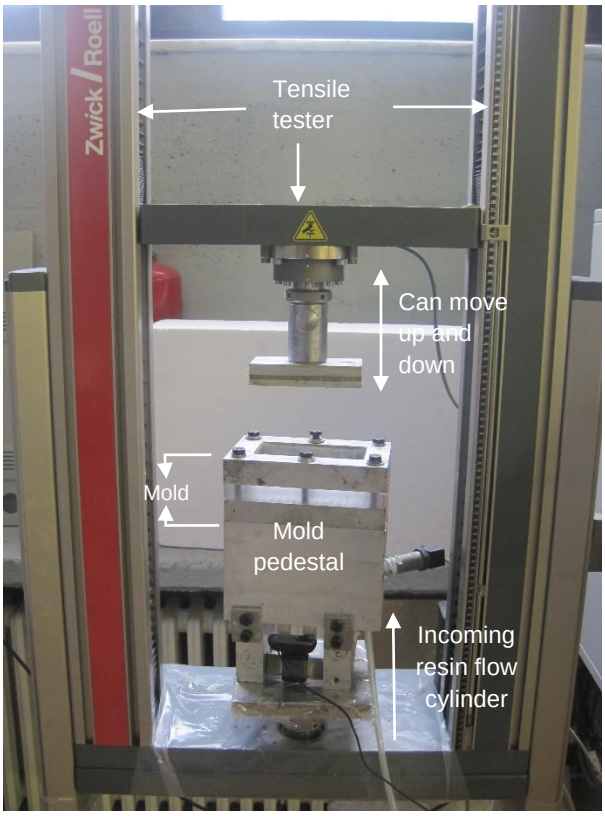

Figure 2.11 The Zwick tensile test machine

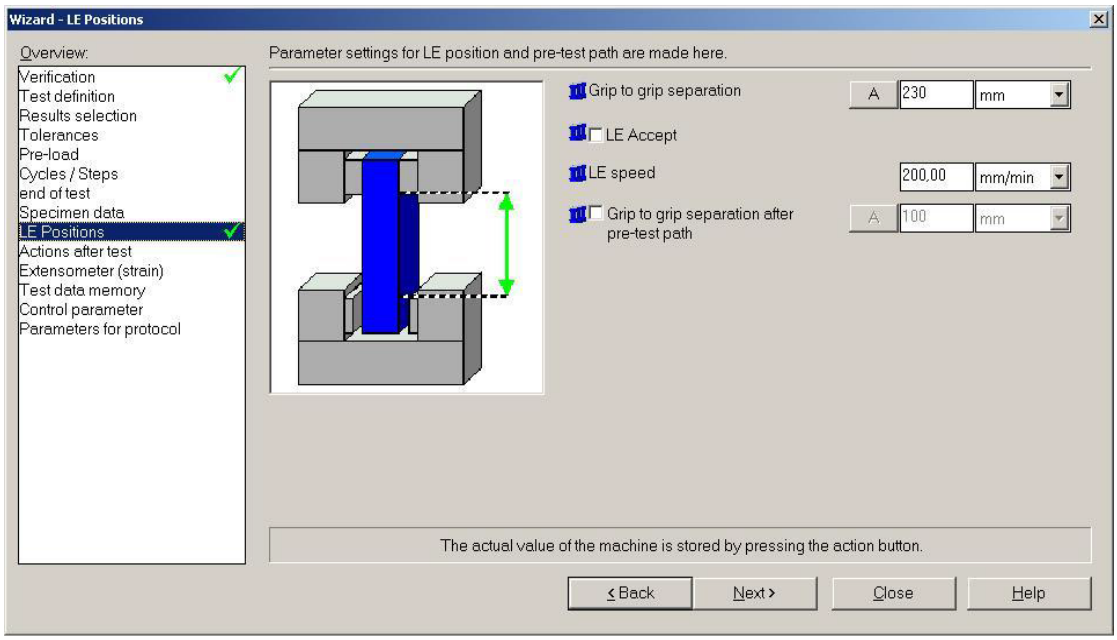

Figure 2.12 The user interface of Zwick Tensile Test Machine

2.6 Monitoring and Recording of Data during Composite Sample Production

A pressure transducer (Atek BT10-214-24BAR) is positioned below the injection port in inlet gate of the mold to measure the inlet resin pressure (Figure2.11) A camera is positioned below the lower mold plate to record the resin flow front progression during impregnation.

The linear actuator that moves the piston is equipped with an internal potentiometer so the piston position can be sensed using the output voltage of the potentiometer. The injection piston position and the piston speed are controlled, and the pressure is monitored and recorded using LabVIEW® Graphical Programming environment. The pressure data coming from the pressure transducer is also collected by the same package. As the data acquisition card, Arduino-UNO was used. Analogue voltage data from the sensors are captured by Arduino microcontroller and processed in the LabVIEW® Graphical Programming environment. An NPN Power Darlington Transistor (TIP 120) is used with the Arduino to drive motors. To maintain a constant actuator velocity, LabVIEW®

PID Toolbox was used. Figure 2.13 and Figure 2.14 present the graphical interface of LabVIEW ® and the whole set-up, respectively.

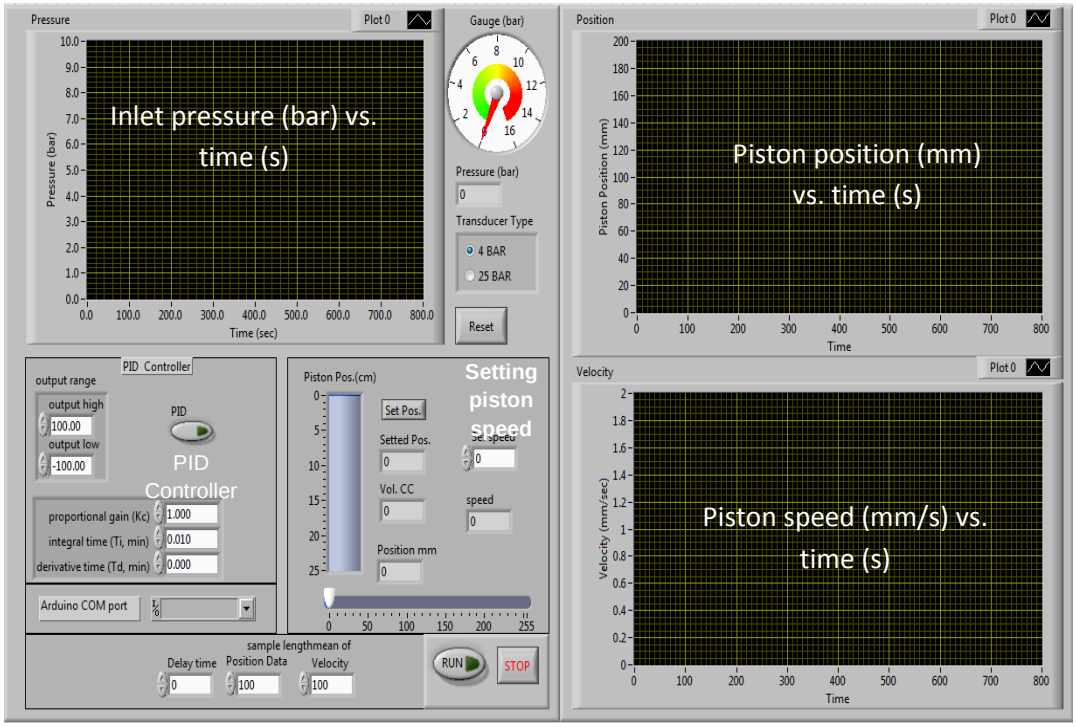

Figure 2.13 Image of the graphical interface of LabVIEW®

Figure 2.14 The whole set-up

2.7 Composite Sample Production Steps

2.7.1 Preparation of Particle Resin Suspension

The particles are mixed and dispersed in the resin using a three-blade marine propeller with diameter of 30 mm. The mixing operation is completed in two stages. In the first stage, particles are added to the resin in increments to prevent aggloremation. The mixing operation is preformed for 30 minutes at 560 rpm. The optimum mixing speed and duration were obtained by experimental trials. It was seen that at lower mixing speeds propeller could not break aggloramated particle clusters. Too high mixing speeds lead to the formation of air bubles and foaming in the suspension. This phenomenon is shown in Figure 2.15. In the second stage of mixing, the hardener is added to the resin-particle suspension and mixed for about 3 minutes at the same speed as before. In order to prevent swirling (formation of air bubles), the impeller was also mounted off center.

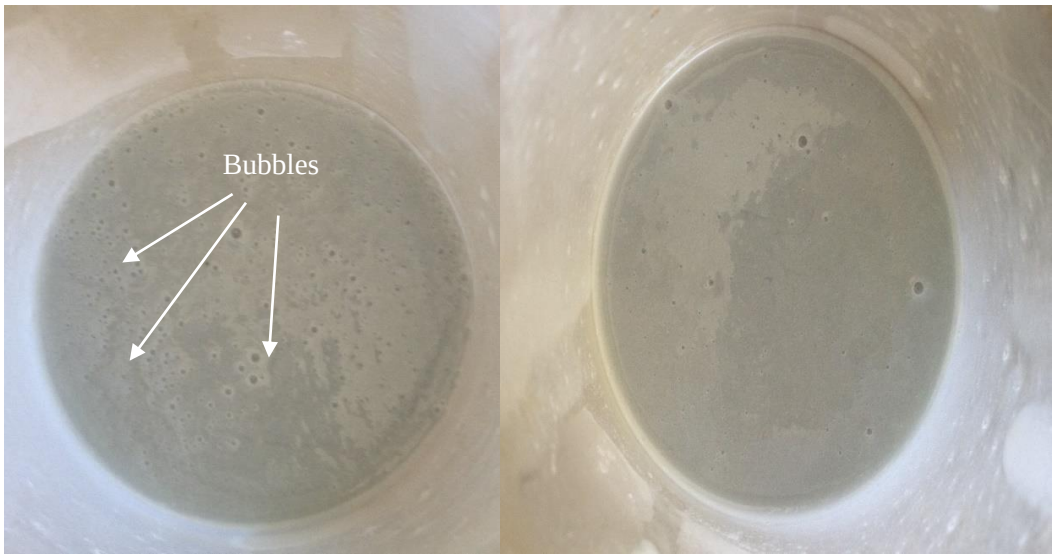

a .) **b .)**

Figure 2.15 Preparation of the particle-resin suspension a.) mixing at too high a speed (950 rpm) b.)mixing at a lower speed (560 rpm)

The volume of the suspensions that were used in all productions needed to be at least 250 cm^3. The required amount of particles for production is calculated according to the desired particle concentration in the suspension. In this study the production is carried out at three different particle concentrations (by volume) in the injected suspension. These are 20 %, 30 % and 40 % by volume. If the desired concentration is denoted as C_o, then

$$V_p = V_s\, C_o \tag{2.1}$$

$$m_p = \rho_p\, V_p \tag{2.2}$$

where V_p, V_s are the volume of particle and suspension, m_p and ρ_p are the mass of particles and true density of the particles, respectively.

The rest of the volume of suspension is composed of the volumes of the resin and the hardener, expressed as

$$V_h + V_r = V_s - V_p \tag{2.3}$$

where V_h, V_r are the volumes of hardener and resin, respectively.

The relative volumes of the hardener and the resin in the suspension can be found using the resin-hardener ratio of 100:30 by volume.

The suspension viscosities at different particle concentration has been measured. These will be presented later in the chapter.

2.7.2 Determination of Mold Top Plate Position during Injection in RTM and in CRTM

In all production, three layers of glass fiber mat are used as the fiber reinforcement. Layers are cut to the dimension of the cavity (150x70 mm) with a special fiber scissors that prevents dispersing of the fiber. Figure 2.16 shows an image of this scissor.

Figure 2.16 Image of the fiber scissor

The mold cavity thickness in each process is calculated based on the desired fiber volume fraction.

Before placing the fiber layers into the mold, they are weighed. This weight is used in the calculation of the cavity thickness that corresponds to a certain desired composite fiber volume fraction. For a design fiber volume fraction of v_{fo}, the required cavity thickness h is calculated with the following equations

Volume of fibers is related to the fiber mass by true fiber density, so:

$$V_{fiber} = \frac{m_{fiber}}{\rho_{fiber}} \tag{2.4}$$

where m_{fiber} and ρ_{fiber} are the mass of stacked fiber fabric layers and the true density of the glass fiber, respectively.

The volume of the mold cavity should be the same as the final composite volume, $V_{composite}$ and is calculated with respect to the desired fiber volume fraction.

$$V_{composite} = \frac{V_{fiber}}{v_{fo}} \tag{2.5}$$

where v_{fo} is the desired fiber volume fraction .

Since the composite volume is equal to the cavity volume, then

$$V_{composite} = A_c\, h \tag{2.6}$$

where A_c is the planar area of the cavity and h is the thickness of the cavity.
Substituting equations (2.4) and (2.6) in (2.5), h is obtained as

$$h = \frac{m_{fiber}}{\rho_{fiber}\, A_c\, v_f} \tag{2.7}$$

2.7.3 Fabric Lay-up, Preparation of Mold, Positioning of Mold

In order to produce a composite part with a uniform thickness, upper and lower mold plates are fixed on the Zwick tensile machine during impregnation. These plates must be parallel to each other. The position at which the top mold plate touches the bottom mold plate (the ‘‘zero’’ thickness position) is determined as follows. The top plate is lowered onto the bottom mold plate. When two plates touch each other, the sudden increase in interaction force is sensed by Zwick. The ‘‘zero thickness’’ position is set at this instant. Then the desired cavity thickness can be obtained by raising the top plate from this position.

The mold release (QZ5111, Huntsman) is applied to the inner surfaces of the upper and lower mold plates in order to demold the part easily after the resin cures. Figure 2.17 demonstrates a case in which the produced composite part could not be demolded properly, when the mold walls were not coated with the mold release.

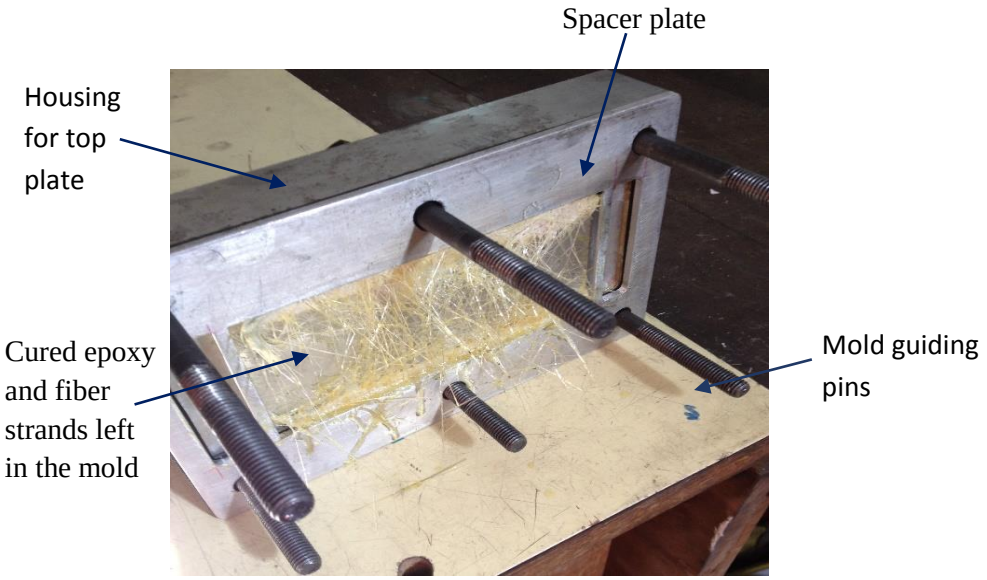

Figure 2.17 The mold cavity unsuccesfully demolded composite when mold release is not used

Presence of the mold release on the bottom transparent mold plate renders the camera view blurred. For clear visualization of flow front progression, 1% blue ink by volume is added to the resin-particle suspension during suspension preparation.

After cutting three layers of glass fiber mat, the layers are stacked up in the mold cavity carefully. A rubbery sealant is applied at the side walls to prevent the leakage of the suspension. Figure 2.18 presents a composite part after production, with the sealant on the edges.

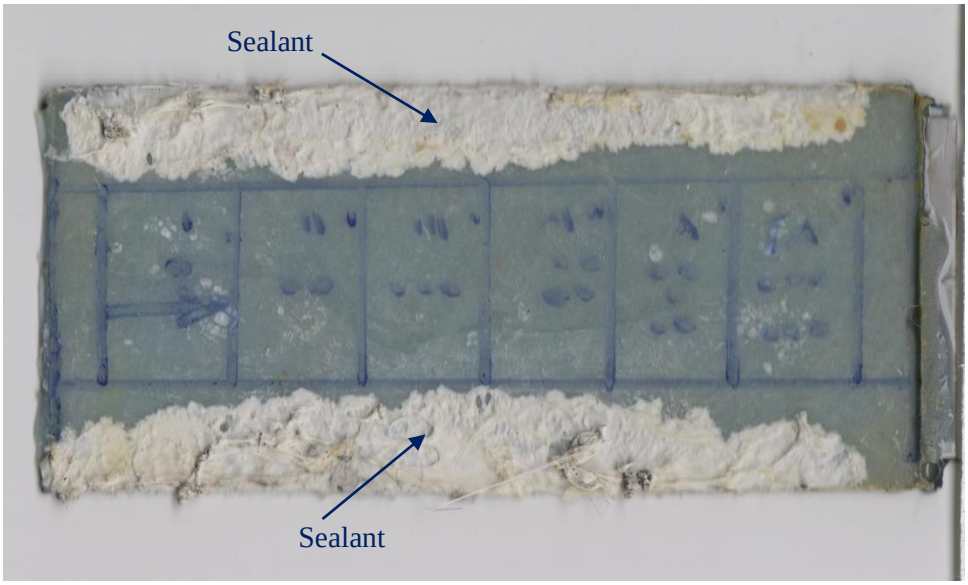

Figure 2.18 A produced sample with the sealant on its edges, after demolding

2.7.4 Resin Impregnation in RTM

After suspension is prepared, an appropriate amount is poured in the cylinder. Before injection, the air pockets in piping and connection need to be cleared. For this purpose, when the mold is open, the piston pushes the suspension in cylinder slowly, until the suspension fills the inlet gate. Then, the piston motion is stopped and the mold top plate is closed and the mold is clamped, ready for injection into the cavity. The injection of particle resin suspension is started by entering the appropriate command through LabVIEW® which signals the piston move. During injection, all the mold gates shown in Figure 2.19 are open. The particle resin suspension is injected through valve-1 and valve- 2. When the impregnation phase is completed, the excess particle resin suspension exists from valve-3.

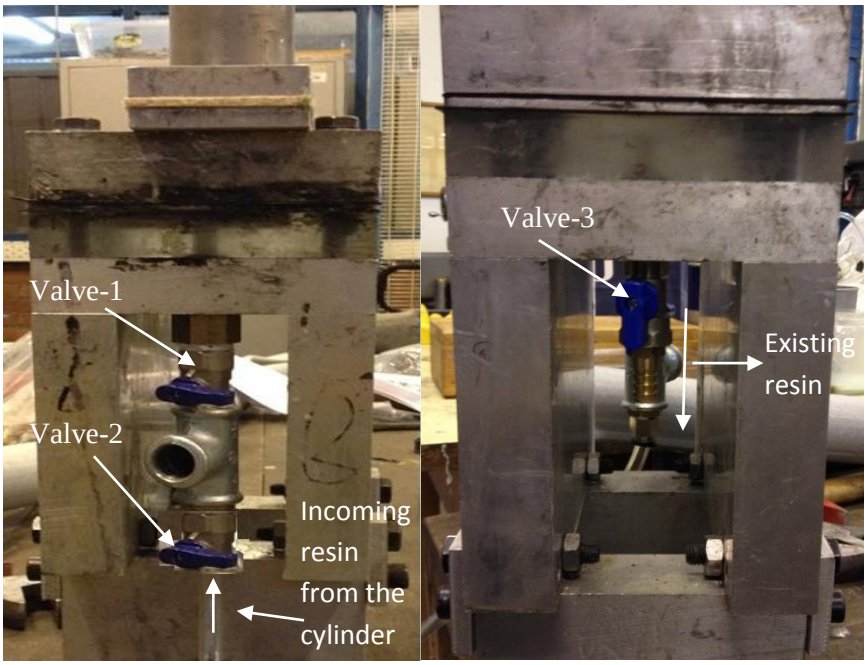

Figure 2.19 The valves regulating flow to and from the mold

During the process, piston speed and position of the piston are recorded in LabVIEW®. The flow front progression in the mold during injection is recorded via camera as is shown in Figure 2.20.

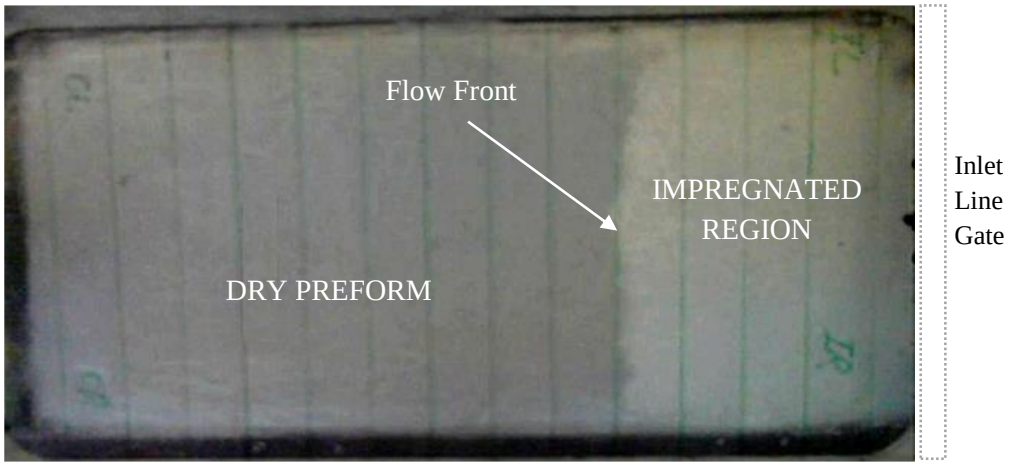

Figure 2.20 Snapshot of flow front progression in the mold cavity during injection

The completion of impregnation is observed from the camera. When the flow front reaches the end of the mold, the piston is stopped and then valve-2 is closed quickly

to prevent further movement of the suspension into the mold cavity. As the suspension reaches the mold end and exits from valve-3, valve-3 is also closed. Lastly, valve-1 is closed and the pressure transducer is dissembled from the mold and cleaned immediately with a thinner to avoid damage due to curing. The cylinder and piston are also cleaned immediately following injection.

There were some issues during the injection process. If higher than 20 % fiber volume fraction were used in RTM process, the injection pressure increased tremendously (up to 25 bars) even for small particle concentration in suspension, that overloaded the tensile test machine as clamping force increased accordingly. Extreme pressures could damage the mold and other equipment. The high flow pressures are also likely to cause leakage of the resin through the mold. All these issues are discussed in results in chapter 4.

2.7.5 Resin Impregnation in CRTM

In CRTM, the injection is performed at a low fiber volume fraction of the preform where the cavity thickness is high. The amount of suspension that is injected is equal to the matrix volume in the final composite.

The volume of the injected suspension, V_s , is then calculated as

$$V_s = V_{comp} \times (1 - v_{fo,final}) \tag{2.8}$$

where $v_{f,final}$ is the desired final fiber volume fraction of the composite and V_{comp} is the final volume of the composite calculated as

$$V_{comp} = h_f \times A_c \tag{2.9}$$

where h_f is the final desired thickness of the composite product (final cavity thickness at the end of the compression) and A_c is the planar area of the mold cavity.

Injection is performed partially; that is, the whole cavity is not filled during injection, as the filling will be completed in the compression stage. Figure 2.19 presents the impregnation stages.

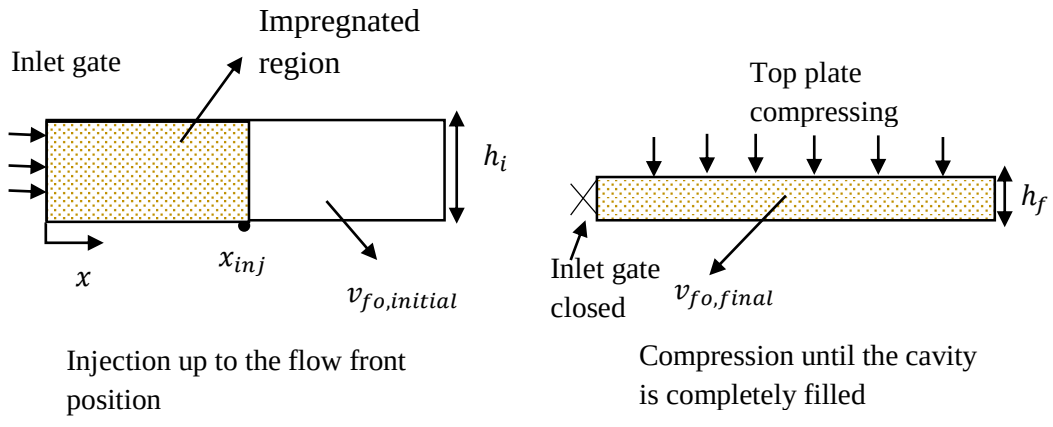

Figure 2.21 Impregnation in CRTM in injection and compression stages

Amount of suspension in the mold at the end of injection, V_s, is the same as the suspension volume in cavity throughout the compression stage.

The flow front position at which injection is stopped, x_{inj} is

$$x_{inj} = \frac{V_s}{w \times h_i \times (1 - v_{fo,initial})} \tag{2.10}$$

where $v_{fo,initial}$, h_i represent the initial fiber volume fraction, initial thickness during the injection phase, respectively, and w, the width of the mold cavity.

Note that $w \times h_i$ is the injection cross-sectional gate area in CRTM.

After the injection phase is completed, the piston is stopped and the inlet gate is closed. Then the upper mold is slowly lowered to compress the fiber preform pushing the

suspension towards the dry preform until the final thickness of the composite is reached. The compression is at constant speed, set through the tensile test machine. When the compression phase is finished, full impregnation is achieved.

2.7.6 Curing of the Resin and Demolding of the Composite Part

After resin impregnation is completed (in RTM or CRTM), the part is left in the mold to cure at room temperature. The chosen epoxy resin was suitable for room temperature cure (Table 2.1). The curing process is completed in the mold at 500 °C for 90 min and there is no post-cure of the part after demolding.

After curing in the mold, the whole mold is removed from the Zwick tensile machine and disassembled. The part is demolded during the disassembly. During the demolding, if one is not careful, the composite part may break (Figure 2.22).

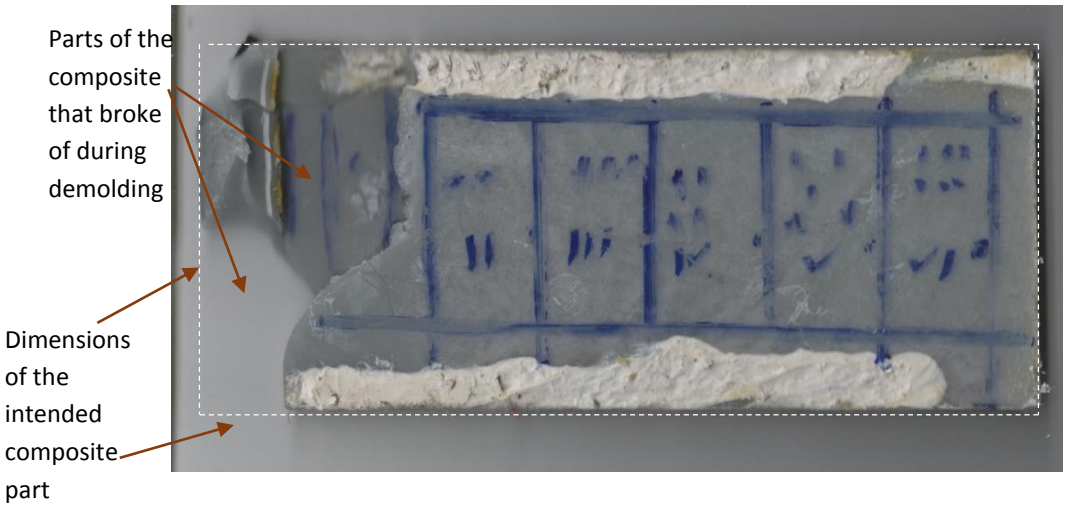

Figure 2.22 The breakage in the composite product

2.8 Characterization of Particle Distribution in Produced Composite Samples

The particle filler distribution along the flow length in produced composites is determined in order to study the effect of various processing parameters on the filler distribution. In this study, this characterization involves burning off the resin. A prior thermogravimetric analysis (TGA) of the resin was performed to determine the appropriate sintering temperature for the resin, at the Central Laboratory of METU. The result of this analysis is presented in Figure 2.23. According to the TGA analysis, it is found that burn-off of resin picks up at about 350 °C (yield temperature is 350 °C) and a 92 % mass loss is obtained at 650 °C. A series of experiments are performed to find appropriate time and temperature for complete elimination of the resin. It is found that the resin is completely burnt-off at 500 °C in 90 minutes. The mass loss in fiber reinforcement needs to be calculated at this sintering temperature of the resin. A series of burn-off tests were performed for only fiber reinforcement at 500 °C for 90 minutes. According to the ASTM D3171-99 8 [41] if the fiber mass loss during burn-off process in composites (for v_{fo} determination) is larger than 0.5 %, the fiber mass loss needs to be considered in calculations. The fiber mass loss at 500 °C for 90 minutes (the sintering condition) was found to be 3.9 % by volume, therefore, it was considered in calculation of particle volume fraction in the composite.

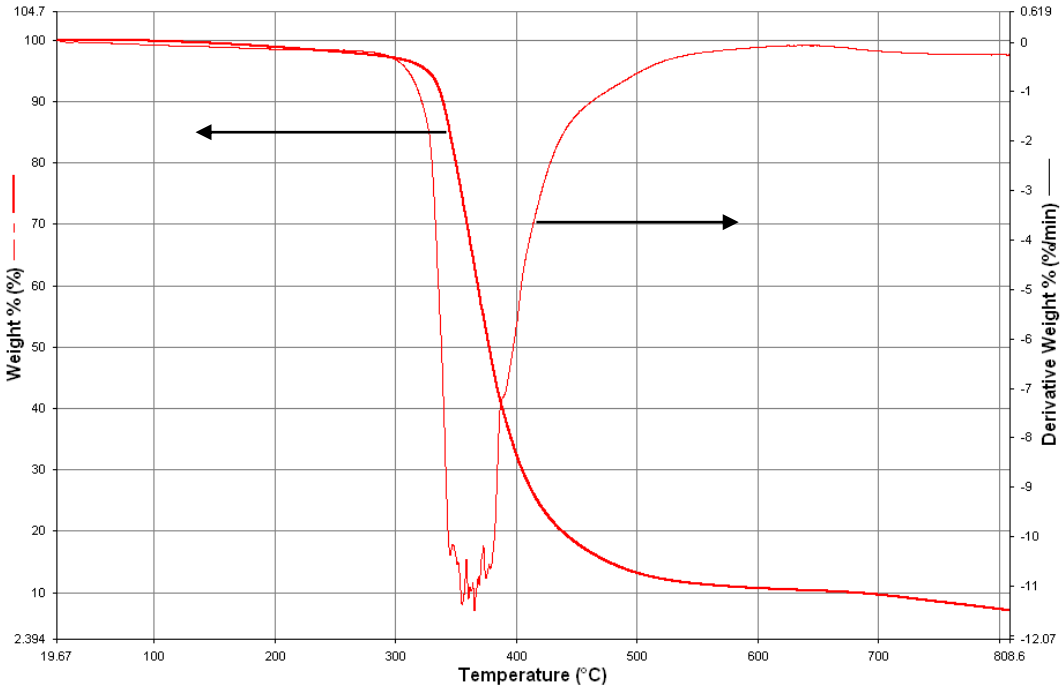

Figure 2.23 The result of TGA analysis for epoxy resin (Hexion MGS L160)

After composite specimens are produced, they are trimmed around the edges. Each composite is cut along marked lines using a band saw, into six identical rectangular samples. Figure 2.24 presents the cut six rectangular samples. By finding the filler content in each sample, the change (if any) in particle volume fraction along the flow direction can be obtained. The planar area of each cut sample is determined as follows. Each sample is scanned using scanner and the image is exported to AutoCAD®, and the planar area of the sample is found from image analysis. The thickness of each sample is found by averaging thickness measurements taken with a micrometer at three different locations on the sample. The volume of each cut sample, V_{sample} is then found by the product its planar area and its thickness.

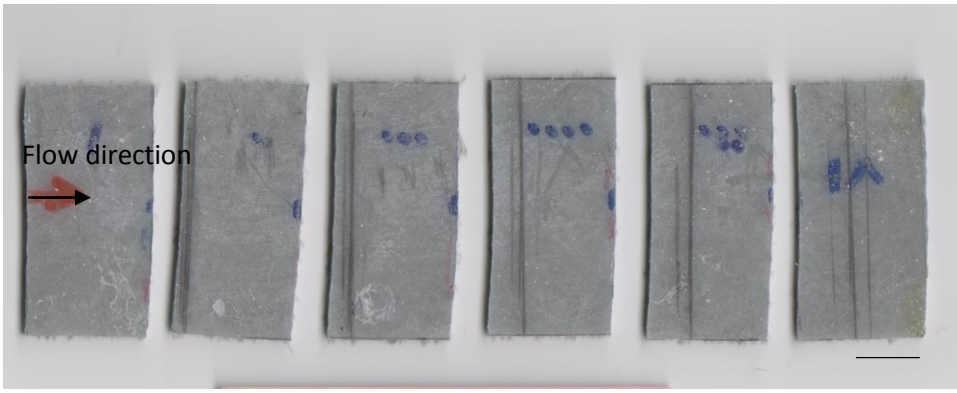

Figure 2.24 Image of the cut samples

For the sintering process, the samples are placed into a glass or ceramic container (Figure 2.25) that can withstand high temperatures.

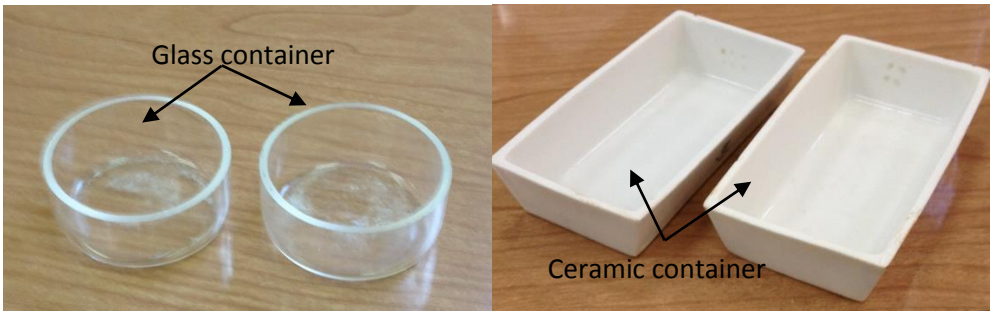

Figure 2.25 The glass and ceramic containers used for holding composite samples during sintering

The containers are weighed with and without cut composite samples to calculate the weight of each sample before sintering.

The samples are placed in the furnace as shown in Figure 2.26.

Figure 2.26 The composite samples that are to be sintered, placed in sintering furnace

After sintering, the samples are removed from the furnace. Figure 2.27 and Figure 2.28 present the sintered samples.

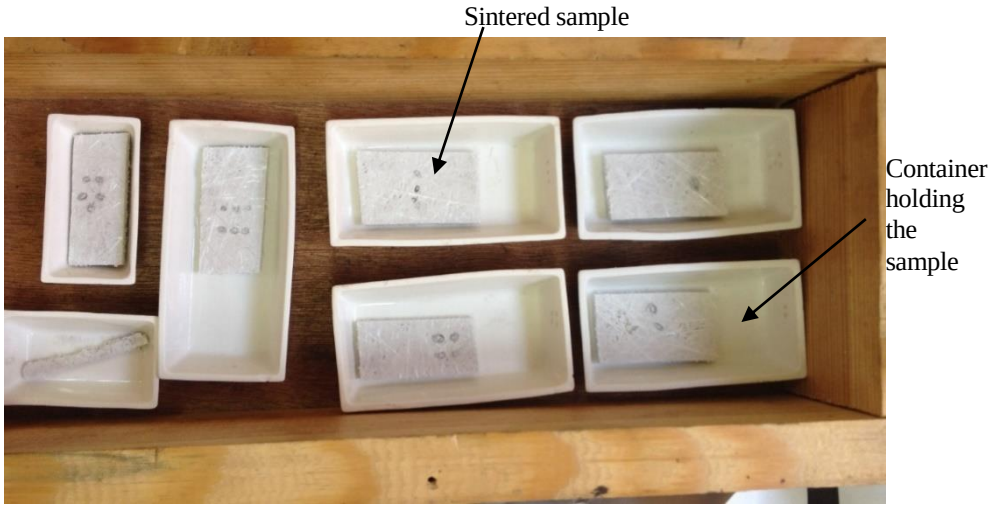

Figure 2.27 Sintered samples

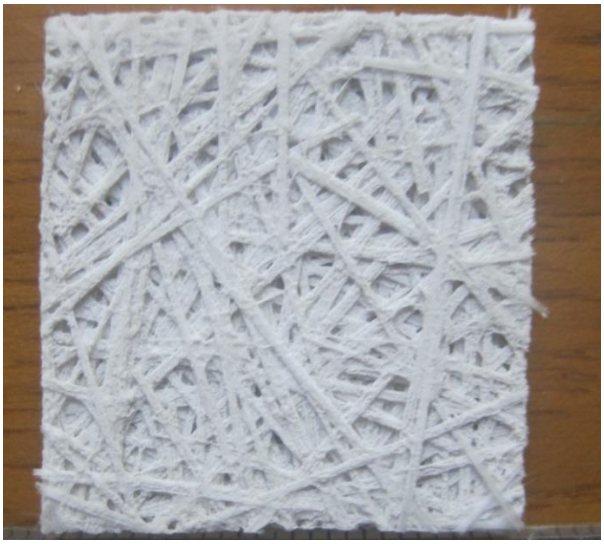

Figure 2.28 A close-up image of a sintered sample; resin is burnt-off, what remains is the fibers with particles

Each sintered sample is weighed with its container. The difference in mass before and after sintering (of the sample + its container) gives the sintered mass, m_{sint}. The mass of fibers, m_f in each sample before sintering is calculated as

$$m_f = m_{areal} \times A_{sample} \times n \tag{2.11}$$

where A_{sample} , m_{areal} are the planar area of each sample and the areal mass of glass fiber mat, respectively. n is the number of fabric layers used in composite production. m_{areal} is 450 g/m^2, and $n = 3$.

The mass of fibers in each sintered sample, m_{sf} is obtained as

$$m_{sf} = m_f \times 0.961 \tag{2.12}$$

by taking into account the 3.9 % fiber mass loss.

Since after sintering, the sample has only fibers and particles, the mass of the particles in each sample is found as

$$m_{particles} = m_{sint} - m_{sf} \tag{2.13}$$

The volume of the particles in each sample, $V_{particles}$ is found as

$$V_{particles} = \frac{m_{particles}}{\rho_{particles}} \tag{2.14}$$

where $\rho_{particles}$ is true density of the glass fillers (2.5 g/cm^3). Then, the particle volume fraction $v_{f,particle}$ in each sample is obtained as

$$v_{f,particle} = \frac{V_{particles}}{V_{sample}} \tag{2.15}$$

The fiber volume fraction of each sample cut from the produced composite is found as

$$v_{fo,i} = \frac{m_f}{\rho_f \times V_{sample}} \tag{2.16}$$

The fiber volume fraction of the composite is found as the average of all cut sample values.

$$v_{fo,i} = \sum_{1}^{6} v_{fo,i} \tag{2.17}$$

2.9 Determination of Permeability of Fiber Reinforcement

The permeability of the fiber reinforcement plays a significant role in the composite production. It affects main process parameters such as injection pressure and suspension velocity. The determination of permeability is an important part of process design by flow modeling [42]. In this study, the permeability of fiber reinforcement was measured by a series of experiments in which fiber preformis impregnated with neat epoxy resin (no particle fillers). These experiments involved injection into fiber preforms at 20 % and 30 % fiber volume fraction. Three layers of glass fiber fabric was cut and placed into the mold. To achieve 20 % and 30 % fiber volume fraction, the required cavity thickness of the mold was calculated using equation (2.7). The injection was performed (as in production of composite samples) at constant injection speed. Pressure and flow front progression in cavity were recorded as explained before.

For a constant 1-D injection velocity u, the continuity equation becomes

$$u = \frac{\partial u}{\partial x} = 0 \tag{2.18}$$

where x is the flow front progression direction, rendering the velocity everywhere in flow domain constant.

For constant neat resin viscosity, the pressure distribution in the impregnated region is linear as shown through Darcy's Law [43]

$$u = -\frac{K}{\mu}\frac{dp}{dx} = constant \tag{2.19}$$

where K is the preform permeability, μ neat resin viscosity and $\frac{dp}{dx}$ the constant pressure gradient.

Since,

$$\frac{dp}{dx} = constant \tag{2.20}$$

$$p = Ax + B \tag{2.21}$$

where A, B are constants.

In the flow, at inlet gate

$$(x = 0), p = p_{inlet} \tag{2.22}$$

At the flow front ,

$$\left(x = x_{front}\right), p = 0 \text{ (atmospheric)} \tag{2.23}$$

Then, variation of p within the impregnated region is found as

$$p(x) = p_{inlet} - \frac{p_{inlet}}{x_{front}}\, x \tag{2.24}$$

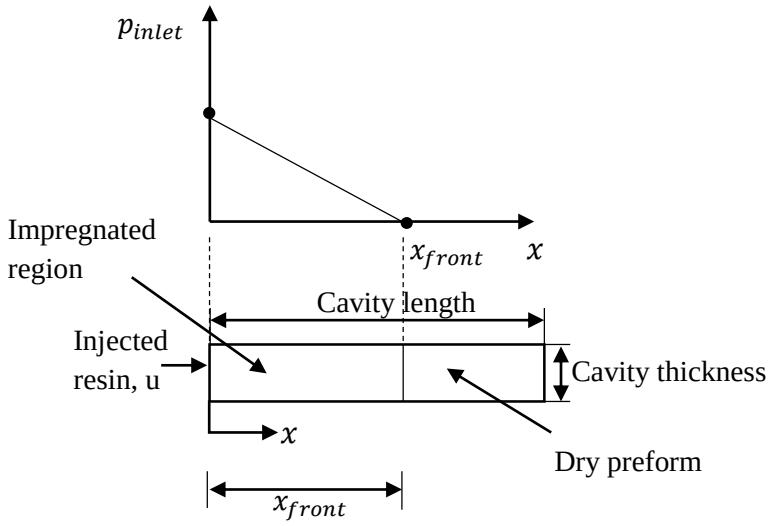

Figure 2.29 Pressure distribution in impregnated preform for neat resin injection at a time instant

Then at any instant during the impregnation , the permeability of the preform can be obtained as follows. At any time instant,

$$\frac{dp}{dx} = -\frac{p_{inlet}}{x_{front}} \tag{2.25}$$

From Darcy's Law

$$K = \frac{\mu u}{\left(-\frac{dp}{dx}\right)} = \frac{\mu u x_{front}}{(p_{inlet})} \tag{2.26}$$

Note that per definition of Darcy's Law, the velocity u is superficial. That is , it is the volumetric flow rate of the (neat) resin per cross-sectional area of the cavity,ie.

$$u = \frac{Q}{A} = \frac{Q}{hw} \tag{2.27}$$

The actual velocity through the fibers during impregnation is

$$u_{actual} = \frac{u}{\varepsilon} \tag{2.28}$$

The permeability data will be used in modeling the impregnation processto simulate the production experiments.

2.10 Determination of Viscosity of Particle Resin Suspension

The particle-resin suspension viscosity varies with the particle concentration. The viscosity of the particle resin suspensions was measured at room temperature with a rheometer (TA Instruments ARES Rheometer) in the Rheological Characterization Unit of Central Labarotory at METU. The results of the viscosity measurements will be given in Chapter 4.

CHAPTER 3

MATHEMATICAL MODEL AND NUMERICAL IMPLEMENTATION OF PARTICLE FILLED RESIN IMPREGNATION

In this chapter, particle –filled resin impregnation model is presented for two liquid molding techniques that are of interest Resin Transfer Molding (RTM) and Compression Resin Transfer Molding (CRTM). The numerical implementation of the presented model and its solution achieved by the using commercial software, Comsol Multiphysics ®.

For modeling the flow, a previously developed Darcy flow based macroscopic model coupled with particle filtration in used [17].

The current study contributes to particle-filled resin impregnation model development by obtaining

- a suitable filtration kinetics model
- An appropriate suspension viscosity model,

based on experimental data

3.1 Modeling of Particle-Filled Resin Impregnation in RTM

The impregnation model is based on flow through porous media and particle filtration in a continuously evolving flow domain with a free surface. Resin impregnation is depicted in Figure 3.1. The fibrous preform forms the porous medium into which the suspension penetrates.

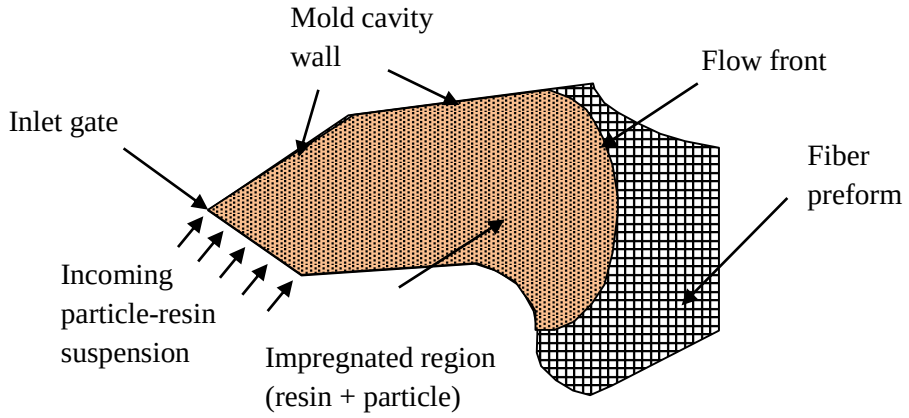

(Inside an irregular shaped mold cavity)

Figure 3.1 The depiction of 2-D impregnation of a fiber preform with particle-resin suspension

For impregnation, a Darcy-based macroscopic approach is used and the following assumptions [24,44,45] are made

- The resin flow is incompressible,
- Inertial effects are negligible,
- The flow is isothermal with the curing taking effect after the mold filled,
- The suspension fluid (resin + particle) is Newtonian,
- The relative velocity between the particles and the resin in the suspension is zero.

3.1.1 Conservation of Mass

The mass conservation of particle-filled, incompressible resin during the impregnation is shown on an infinitesimal control volume in Figure 3.2. The mass conservation presented for three species on this control volume. These species are particles suspended in the resin, the neat resin and the filtered particles that get stuck to the preform. Each species will be studied in this section.

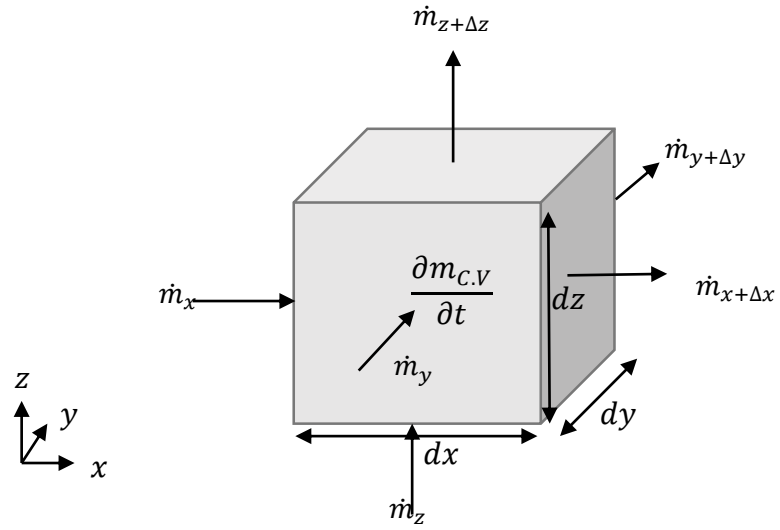

Figure 3.2 Flow domain control volume for the derivation of conservation equations in RTM

Conservation of mass of particles in the suspension is given by

$$\dot{m}_{in} - \dot{m}_{out} - \dot{m}_{lost} = \dot{m}_{stored} \tag{3.1}$$

$\dot{m}_{lost}$ does not represent a physical mass loss in particles. It is present to quantify the amount of particles that are filtered onto the fiber preform.

From equation (3.1), and using the control volume of Figure 3.2, the conservation of particles in the suspension can be found as

$$\frac{\partial(\varepsilon C)}{\partial t} + \nabla.\{\vec{V}'\varepsilon C\} = -\frac{\dot{m}_{lost}}{\forall_o \rho_p} \tag{3.2}$$

where C is the particle concentration in the injected suspension (volume of particles in the suspension per volume of the suspension) , ε is the domain porosity, ρ_p is the particle density, $\vec{V}'$ is the actual velocity of particles in suspension and $\forall_o$ is the volume of the control volume.

The mass conservation of neat resin yields

$$\dot{m}_{in} - \dot{m}_{out} = \dot{m}_{stored} \tag{3.3}$$

Equation (3.3) can be put into the below form

$$\frac{\partial[\varepsilon(1-C)]}{\partial t} + \nabla.\{\vec{V}'\varepsilon(1-C)\} = 0 \tag{3.4}$$

where $\vec{V}'$ is the actual velocity of the polymer (particle and resin velocities are the same)

The specific particle deposit, which is the volume of filtered particle per volume of the mold cavity is expressed as σ. Then the conservation of filtered particles can be expressed as

$$\frac{\partial\sigma}{\partial t} = -\frac{\dot{m}_{lost}}{\forall_o \rho_p} \tag{3.5}$$

where $\dot{m}_{lost}$ is the mass rate of particles filtered onto the preform from the suspension.

Substituting the equation (3.5) into equation (3.2) yields the conservation equation for particle fillers

$$\frac{\partial(\varepsilon C)}{\partial t} + \nabla.\{\vec{V}'\varepsilon C\} = -\frac{\partial \sigma}{\partial t} \tag{3.6}$$

The domain porosity is defined based on the porosity of fiber preform in the cavity, as well as filtered particles, as

$$\varepsilon = \varepsilon_0 - \sigma \tag{3.7}$$

Likewise solids volume fraction is defined as

$$v_f = v_{f0} + \sigma \tag{3.8}$$

where v_f is the fiber volume fraction. Note that

$$\varepsilon = 1 - v_f \tag{3.9}$$

Differentiating equation (3.7) yields

$$\frac{\partial \varepsilon}{\partial t} = -\frac{\partial \sigma}{\partial t} \tag{3.10}$$

Combining equation (3.10) and (3.6) yields

$$\frac{\partial[\varepsilon(1-C)]}{\partial t} + \nabla.\{\vec{V}'\varepsilon C\} = 0 \tag{3.11}$$

Substituting (3.11) into equation (3.4) yields the bulk continuity equation as

$$\nabla.\{\vec{V}'\varepsilon(1-C)\} + \nabla.\{\vec{V}'\varepsilon C\} = \nabla.(\vec{V}'\varepsilon) \tag{3.12}$$

The superficial velocity is related to the actual velocity

$$\vec{V}' = \frac{\vec{V}}{\varepsilon} \tag{3.13}$$

Then, the continuity equation becomes

$$\nabla.\vec{V} = 0 \tag{3.14}$$

The details of this model can be found in [19]

3.1.2 Filtration Kinetics

The filtration of particles can be expressed in most general form, as [46–48]

$$\frac{\partial\sigma}{\partial t} = \alpha VC \tag{3.15}$$

Here, the time rate of increase in particle deposit filtration rate is related to the volume flux of the particles in the suspension by a proportionality constant α, which is called the filtration coefficient.

As the particle filtration takes place in the filter medium, the clogging of the preform pores results in increase in actual suspension velocity due to the reduction of porosity of medium. Filtration can proceed indefinitely; some filtered particles may be sheared back into the suspension flow. So equation (3.15) can be modified as

$$\frac{\partial \sigma}{\partial t} = \alpha V C - \beta \sigma \tag{3.16}$$

The second term on the right expresses the reintroduction of a portion of filtered particles back into the suspension flow, β is the detachment coefficient.

When a clogging stage is reached, the filtration rate becomes zero. Specifying the ultimate specific particle at this instant as σ_u, equation (3.16) becomes

$$\frac{\partial \sigma}{\partial t} = \alpha V C - \beta \sigma_u = 0 \tag{3.17}$$

σ_u denotes the maximum amount of particles that can be filtered.

Equation (3.17) can be rewritten as

$$\frac{\partial \sigma}{\partial t} = \alpha V C \left(1 - \frac{\sigma}{\sigma_u}\right) \tag{3.18}$$

When the particle filtration takes place in the fiber preform, the microstructure of the medium changes with it. This change in the porous medium, in turn, affects the particle deposition rate. Filtration coefficient of the particle deposition is a time dependent local function as deposition increases with time and varies spatially [35]. It is also an empirical parameter. In general α can be expressed as

$$\alpha = \alpha_0 F(\sigma) \tag{3.19}$$

where α_0 is the initial value of α and $F(\sigma)$ is the deposition rate that is a function of σ. In equation (3.18) for a constant α value, the term in the parenthesis $\left(1 - \frac{\sigma}{\sigma_u}\right)$ can be considered as a form of the deposition rate function, $F(\sigma)$.

In literature, a number of empirical expressions of $F(\sigma)$ has been suggested. $F(\sigma)$ can be a certain order, polynomial function. Bai and Tien [35] investigated the particle deposition rate and the extent of deposition with the effluent concentration history. They compared numerical results with experimental applications. They found that the filtration rate (or filtration quality) could increase then decrease or vice versa with time and a polynomial function $F(\sigma)$ of appropriate order could capture such features

$F(\sigma)$ can be expressed as a third order polynomial function of σ as

$$F(\sigma) = 1 + k_1\sigma + k_2\sigma^2 \tag{3.20}$$

where k_1 and k_2 are empirical model constants.

Then the filtration coefficient can be expressed as

$$\alpha = \alpha_0(1 + k_1\sigma + k_2\sigma^2) \tag{3.21}$$

By using filtration coefficient equation (equation (3.21)) and the particle filtration equation (equation (3.15)), the final form of filtration equation that is used in this study is expressed as

$$\frac{\partial\sigma}{\partial t} = \alpha_0 VC(1 + k_1\sigma + k_2\sigma^2) \tag{3.22}$$

3.1.3 Equation of Motion: Darcy Flow

In modeling resin impregnation, Darcy's Law [43] for flow through porous media is frequently used as the equation of motion. Darcy's law relates flow velocity to the flow pressure drop through porous medium permeability and viscosity [17,18]. For quasi-steady resin flow through fiber preform Darcy law expressed as

$$\vec{V} = -\frac{1}{\mu}\left(\underline{\underline{K}} \cdot \nabla p\right) \tag{3.23}$$

where $\vec{V}$ is superficial flow velocity vector, μ is the fluid (particle filled suspension) viscosity, ∇p is the flow pressure gradient and $\underline{\underline{K}}$ is the permeability tensor.

Permeability designates the relative ease with which the resin flows through the fiber preform[42] and it is a property of the porous medium (fiber preform). The permeability is a tensor for multi-dimensional flow.

$$\underline{\underline{K}} = \begin{bmatrix} K_{xx} & K_{xy} & K_{xz} \\ K_{xy} & K_{yy} & K_{yz} \\ K_{xz} & K_{yz} & K_{zz} \end{bmatrix} \tag{3.24}$$

An element K_{ij} in the tensor refers to the permeability that induces flow in *i* direction due to the pressure gradient in *j* direction.

If the principle permeability axes of the preform coincide with the coordinate axes so permeability becomes a diagonal tensor.

3.1.4 Permeability of Filtered Fiber Preform

As a result of particle filtration, specific surface area of the fiber preform pores changes locally and this leads to a decrease in the porosity of preform. In order to model the change in specific surface area of the preform pores due to filtration, several assumptions are made. The fiber diameter is assumed to be much larger than the particle filler diameter; the fiber preform is assumed to be composed of cylindrical fibers and capillaries; the particle fillers filtered into fiber preform are assumed to be distributed evenly, forming a uniform layer around the fiber.

A model that relates the change in permeability to the change in specific deposit had been proposed as [17]

$$K = K_0 \left[\left(\frac{\varepsilon}{\varepsilon_0} \right) \left(\frac{1-\varepsilon}{1-\varepsilon_0} \right)^{-2} \right]^{a_2} \tag{3.25}$$

based on Kozeny-Carman relation. Here, K_0 is the permeability of the fiber preform (without any particle deposit) and a_2 is an empirical constant based on the process conditions. In the current model a_2 is taken as 1.

3.1.5 Viscosity model for Particle Resin Suspension

The particle-resin suspension viscosity depends on particle loading in the suspension strongly and this dependence is expressed as following, using the model in [49]

$$\mu = \mu_0 \left(1 - \frac{C}{A} \right)^{-B} \tag{3.26}$$

where, μ_o is the neat resin viscosity and A and B are empirical model constants.

The viscosity change takes place at a constant shear rate. In this study, the resin viscosity is assumed Newtonian which means that the effect of shear dependence is small due to the very low viscosity of the resin. Variation of viscosity with respect to temperature and time is neglected.

It is possible to replace this model with other models, specific to the type of particle-resin suspension used in the process.

3.1.6 Mathematical Problem Statement and Boundary Conditions

The four unknowns in suspension impregnation in RTM are the flow pressure (p), the velocity ($\vec{V}$), particle concentration (C) and the specific particle deposit (σ). They are determined by solving the four equations: Continuity (equation (3.14)), Darcy's Law (equation (3.23)), the particle conservation (equation (3.6)) and the filtration kinetic equation (equation (3.22)).

The boundary and initial conditions are presented in Figure 3.3. The shown cavity corresponds to an irregular shaped mold for 2-D flow.

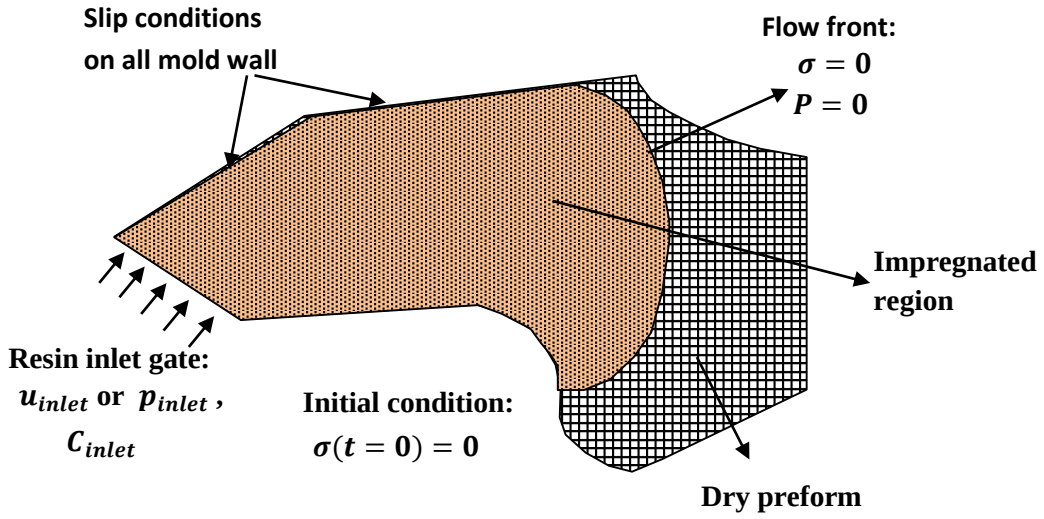

Figure 3.3 Initial and boundary conditions in RTM

There is no flow across the solid boundaries (mold walls). At the inlet, either the injection velocity or the injection pressure can be specified. The particle concentration in the injected suspension at the gate is specified. The pressure at the flow front is zero gage (atmospheric) due to air vents at the mold exit. Initially; there is no particle deposit in the cavity.

3.2 Modeling of Particle Resin Impregnation in CRTM

CRTM is comprised of injection and compression stages. The injection stage of CRTM is same as the injection of RTM process however, in this study injection phase is not carried out until the mold is filled. The fiber volume fraction at this stage is much lower than that in RTM.

3.2.1 Injection Stage

The model for the injection stage is the same as that for RTM. Equations (equation (3.14), equation (3.23), equation (3.6) and equation (3.22)) are used along with boundary and initial conditions given in Figure 3.3, to solve for the unknowns.

3.2.2 Compression Stage

3.2.2.1 Conservation of Mass

In compression stage,

- no injection,
- flow by movement of top plate only (in z-direction)

The conservation equations reflect the change in flow domain due to compression.

The conservation of mass of particles can be shown to be [19]

$$\frac{\partial(\varepsilon C)}{\partial t} + \nabla.\left\{\varepsilon C\vec{V}'\right\} + \frac{\partial(\sigma)}{\partial t} = (\varepsilon C + \sigma)\frac{U_z}{H} \tag{3.27}$$

where U_z is the constant downward closing speed on the top mold plate, and H is the instantaneous cavity gap thickness.

Similarly the continuity equation is [19]

$$\nabla.\left\{\vec{V}\right\} = -\frac{U_z}{H} \tag{3.28}$$

It must be noted that in compression stage, unlike the injection stage, the fiber volume fraction and the preform porosity do not remain constant, i.e. $v_{f0} \neq$ constant and $\varepsilon_0 \neq$ constant.

3.2.2.2 Filtration Kinetics

The filtration model in compression is the same model outlined in section 3.1.2

3.2.2.3 Equation of Motion: Darcy's Law

The formulation of Darcy's Law through equation (3.23) [32,50] is valid in compression stage as well.

3.2.2.4 Permeability of Filtered Fiber Model

The permeability model (equation (3.25)) is valid in compression stage as well.

In RTM, K_0 is constant since the fiber preform does not go through any changes. However, the porosity of the fibrous medium is changed under compression, the fiber volume fraction continuously increases. Therefore, the preform permeability must be a function of fiber preform porosity

$$K_0 = f(\varepsilon_0) \tag{3.29}$$

3.2.2.5 Viscosity of Model

The viscosity model of equation (3.26) is valid for compression.

3.2.2.6 Mathematical Statement and Boundary Conditions

The four unknowns in suspension impregnation in compression phase of CRTM are the flow pressure (p), the velocity ($\vec{V}$), particle concentration (C) and the specific particle deposit (σ). They are determined by solving the four equations: Continuity (equation (3.28)), Darcy's Law (equation (3.23)), the particle conservation (equation (3.27)) and the filtration kinetic equation (equation (3.22)).

The boundary and initial conditions are presented in Figure 3.4.

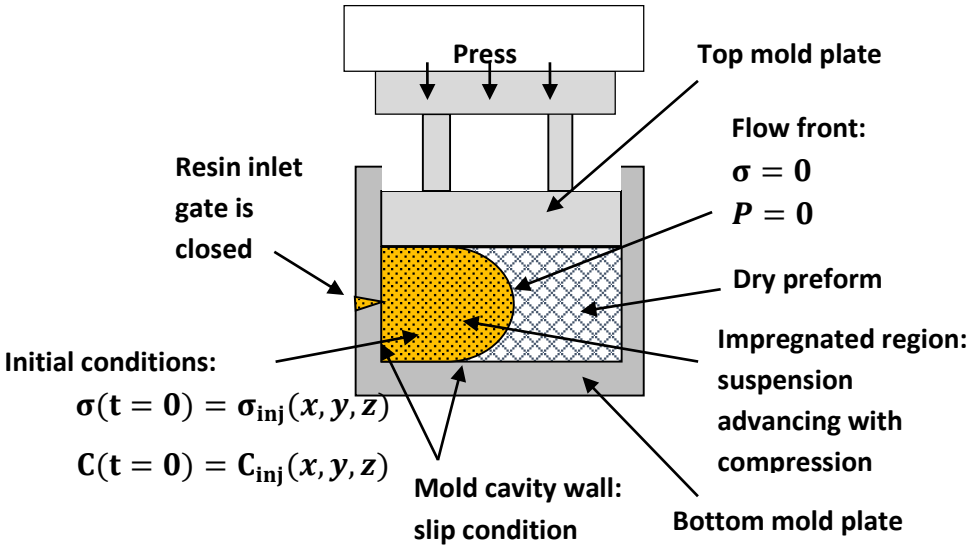

Figure 3.4 Boundary and initial conditions in CRTM

During the solution of compression phase, boundary conditions are similar to those in the injection phase however, there is not injection at the gate; the movement of suspension is due to compression alone. Since the end of the injection phase is the initial condition of the compression phase, the particle concentration in the suspension (C) and specific particle deposit (σ) at the end of the injection stage are given as the initial stage of the compression phase.

3.3 Numerical Implementation and Solution

The numerical of the presented model for RTM and CRTM and their solution are performed on COMSOL Multiphysics® commercial software. In this package, a variety of physic-based systems can be modeled and in applications such as electrical, mechanical, fluid flow, chemical applications [51]. For this study Comsol Multiphysics® version 4.3 has been employed. The governing equations are solved using its " time dependent" DIRECT (UMFPACK) solver.

The following application modes are used for the implementation and solution of the impregnation of RTM and CRTM processes

- Darcy's Law application mode in the Chemical Engineering Module
- Partial differential equation (PDE) mode in the Comsol Multiphysics Module
- Level Set Method in the Chemical Engineering Module (used to track the flow front)
- Deformed mesh mode (Arbitrary Lagrangian Eulerian Method) in the Comsol Multiphysics Module (only used for the compression phase of CRTM process)

Darcy's Law application mode in Chemical Engineering module enables the creation of a mathematical model which is suitable for modeling flow through porous media by combining Darcy's Law (equation (3.23)) and continuity equation (equation (3.14) for RTM, equation (3.28) for CRTM). Boundary conditions for Darcy's Law and continuity equation are specified in this mode.

Partial differential equation (PDE) mode in the Comsol Multiphysics Module is used for solving the filtration equation (equation (3.22)) and particle conservation equation (equation (3.6) for RTM and equation (3.27) for CRTM). The two PDE's are created separately: A general partial differential form is adapted to these equations by defining the proper constants in the built-in partial differential form. Initial and boundary conditions, for specific particle deposit (σ) and particle concentration (C) are defined in this mode.

Since the impregnation phase of RTM and CRTM processes involve a free surface (flow front), the movement of this free surface is tracked by the Level Set Method in the Chemical Engineering Module. In this method, the interface is depicted by a certain level or isocontour of a globally defined function, the level set function ϕ. This is a step function whose value alternates between 0 and 1. The dry preform region in cavity has a ϕ value of 0; the impregnated region have a value of 1.The transition from 0 to 1 occurs at the across the interface. Level set function is taken as 0.5 at the interface of the two regions. Level set function is simply connected in the solution domain. To avoid numerical problems due to the step change its value from 0 to 1, a transition region is employed.

The equation governing the level set function is

$$\frac{\partial \phi}{\partial t} + \vec{V}' \cdot \nabla \phi = \gamma \nabla \cdot \left(\epsilon \nabla \phi - \phi(1-\phi) \frac{\nabla \phi}{|\nabla \phi|} \right) \tag{3.30}$$

The thickness of the transition region is controlled by ϵ and the right hand side of the equation is a diffusion term. The left hand side of the equation depicts correction of ϕ.

Arbitrary Lagrangian Eulerian (ALE) method is used only in the solution of compression phase of CRTM, which handles the change of the mold cavity volume due to compression. The top plate closing speed, U_z, is imposed with this method.

CHAPTER 4

RESULTS AND DISCUSSION

4.1 Viscosity of Glass Particle-Filled Epoxy Resin

The viscosity of the prepared suspensions was measured at room temperature with a rheometer (TA Instruments ARES Rheometer) in the Rheological Characterization Unit of Central Laboratory at METU. Figure 4.1 depicts the viscosity of the prepared neat resin suspension (hardener + resin) and 10 %, 20 %, 30 %, 40 % particle concentrations suspensions according to shear rates.

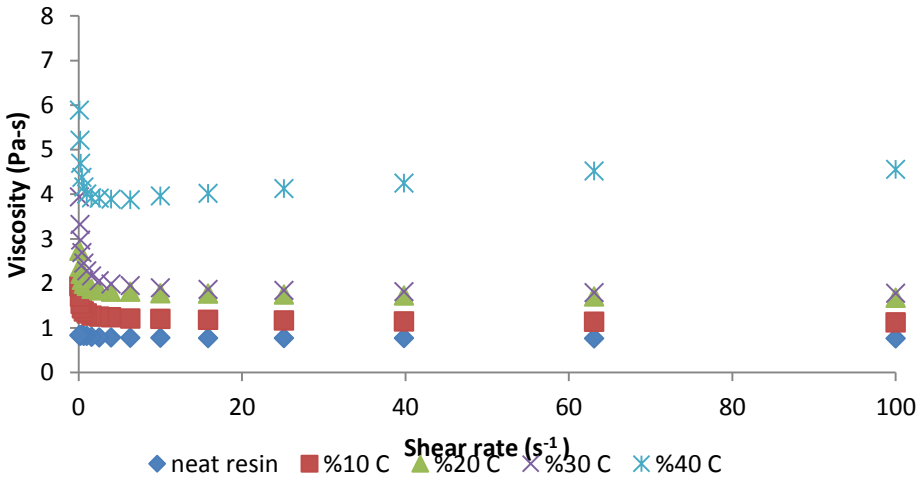

Figure 4.1 The results of the viscosity of the suspension for neat resin, 10 %, 20 %, 30 %, 40 % particle concentration

The viscosities of the suspensions which have 20 % and 30 % concentration data are too close to each other so other samples of these suspensions were measured again. The results are shown in Figure.4.2.

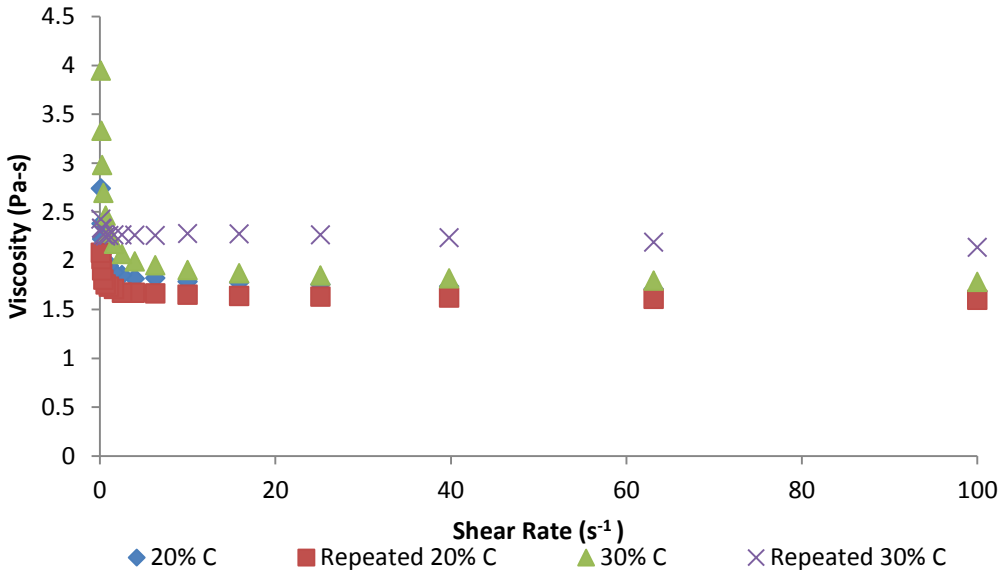

Figure 4.2 The repeated result for viscosity of the 20 % and 30 % particle concentration suspensions.

The viscosities of the samples 20 % concentration match each other. However, there is a difference in the viscosities of the samples with 30 % concentration. Thus, a second order polynomial is fitted to the data of neat resin, 10 %, 20 %, 40 % concentration that is shown in Figure 4.3, and the viscosity of 30 % particle concentration is then estimated with respect to this polynomial function. Typical shear rates in experiments were estimated to be higher than 100 s^{-1}. Viscosity measurements show that there is little change in viscosity values beyond 63 s^{-1}. Therefore, viscosity measurements of 100 s^{-1} shear rate are taken as on the viscosity of the corresponding suspension.

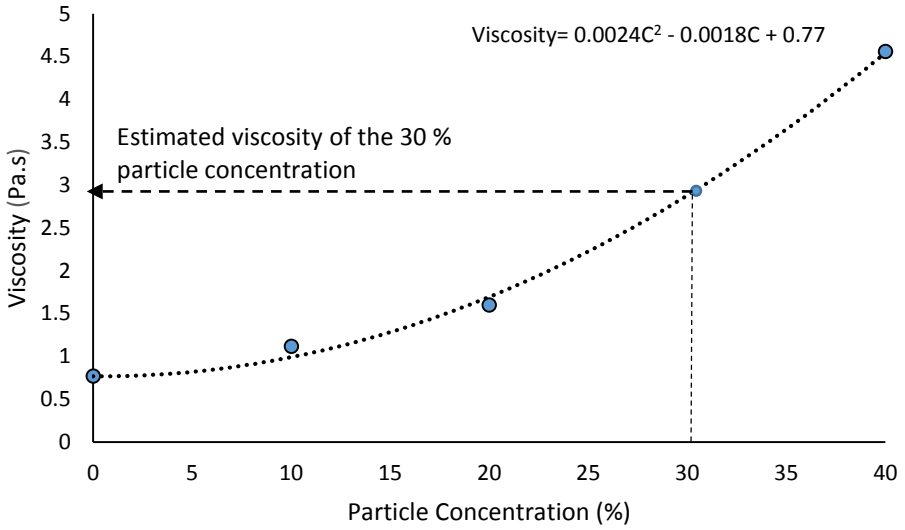

Figure 4.3 Determination viscosity of 30% concentration suspension from existing data

According to the Figure 4.3 the estimated viscosity of the 30 % concentration is 2.88 Pa-s at 100 s^{-1} shear rate.

Table 4.1 presents the measured viscosities of the prepared neat resin suspensions (hardener +resin) and with 10 %, 20 %, 30 %, 40 % particle concentrations at 100 s^{-1} shear rate.

Table 4.1 The viscosity of the glass particle epoxy resin suspensions

Particle concentration (%) by volume	Viscosity (Pa.s) at 100 s^{-1} shear rate
0 (Neat Resin)	0.77
10	1.12
20	1.6
30	2.88
40	4.56

When the experimental data is fitted to the viscosity model of equation (3.26) using nonlinear least square method, the constants A and B in that equation are found as 1.40 and 5.30, respectively, and the model is

$$\mu = \mu_0 \left(1 - \frac{c}{1.40}\right)^{-5.30} \tag{4.1}$$

Figure 4.4 presents the results of the viscosity measurements.

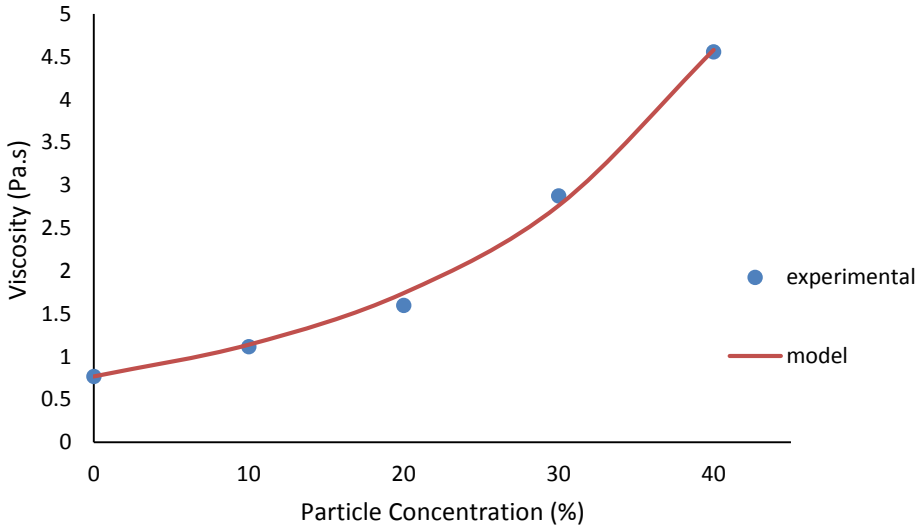

Figure 4.4 The suspension viscosity measurements and viscosity model

4.2 Determination of Permeability

The permeability of fiber reinforcement was measured by a series of experiments in which the fiber preform was impregnated at constant injection rate in a closed mold by neat resin, at 20 % and 30 % fiber volume fraction. The details of measurement were explained in Chapter 2.

The flow front progression result of the 20 % and 30 % fiber volume fraction-time permeability experiments are presented in Figure 4.4. Flow front position, x_{front} can be expressed as a function of time and this relation is obtained by fitting an appropriate polynomial data . The differentiation of $x_{front}(t)$ gives the flow front velocity, which is also the actual velocity everywhere within the impregnated region, at that instant

$$u_{front} = \frac{dx_{front}}{dt} = u_{actual} \tag{4.2}$$

The corresponding $x_{front}(t)$ and actual velocity, $u_{actual}(t)$ for 20 % fiber volume fraction experiment are

$$x_{front} = 0.0006t^3 + 0.0017t^2 + 4.3494t \quad mm \tag{4.3.a}$$

$$u_{actual} = \frac{dx_{front}}{dt} = 0.0018t^2 + 0.0034t + 4.3994 \quad mm/s \tag{4.3.b}$$

and for the 30 % fiber volume fraction experiment,

$$x_{front} = -0.0014t^3 + 0.0959t^2 + 2.8764t \quad mm \tag{4.4.a}$$

$$u_{actual} = \frac{dx(flow\ front)}{dt} = -0.0042t^2 + 0.1918t + 2.8764 \quad mm/s \tag{4.4.b}$$

Although u_{actual} is found as a function of time, the velocities exhibit little variation with respect to time, as expected for constant piston injection speed.

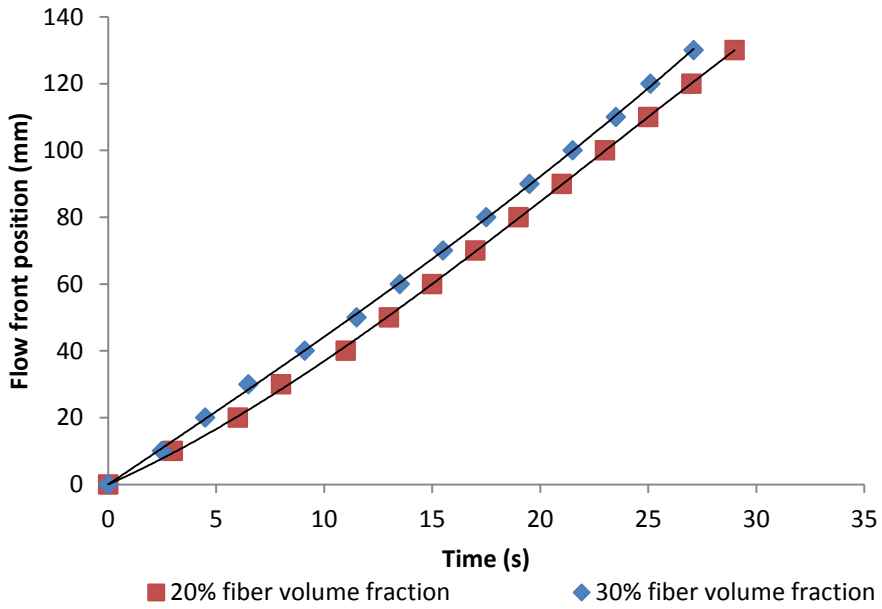

Figure 4.5 Flow front progression during the impregnation of fiber preforms with neat resin at 20 % and 30 % fiber volume fraction

Permeability is determined by using equation (2.20) given in Chapter 2. The pressure gradient is obtained using the recorded inlet pressure.

Actual and superficial velocities, the pressure gradient and calculated permeabilities for the 20 % and 30 % fiber volume fraction are presented in Tables 4.2 and 4.3 respectively. Calculated permeability values in Table 4.2 and 4.3 are determined through equation (2.20).

Table 4.2 The results of permeability experiment for 20% fiber volume fraction fiber preform ($v_{fo} = 0.20$)

Flow front location from the inlet, x_{front} (mm)	Time (s)	Inlet pressure, P_{inlet} (10^5.Pa)	Pressure gradient, $-\frac{dP}{dx} = \frac{P_{inlet}}{x_{front}}$ (Pa/mm x 10^{-5})	Actual flow front velocity, u_{actual} (mm/s)	Resin viscosity, μ (Pa.s)	Superficial flow front velocity, u (mm/s) $u = u_{actual}(1 - v_f)$	Permeability, K^* (m^2x10^{-11})
10	15	0.24	0.024	3.414	0.77	2.7312	87.626
20	18	0.3	0.015	3.876	0.77	3.1008	159.174
30	20	0.41	0.0136	4.142	0.77	3.3136	186.693
40	23	0.45	0.0112	4.478	0.77	3.5824	245.195
50	25	0.66	0.0132	4.66	0.77	3.728	217.466
60	27	0.87	0.0145	4.8084	0.77	3.84672	204.274
70	29	0.99	0.0141	4.9232	0.77	3.93856	214.430
80	31	1.28	0.016	5.004	0.77	4.00352	192.669
90	33	1.38	0.0153	5.052	0.77	4.0416	202.958
100	35	1.68	0.0168	5.066	0.77	4.0528	185.753
110	37	1.76	0.016	5.046	0.77	4.03712	194.286
120	39	2.18	0.0182	4.99	0.77	3.99456	169.310
130	41	2.5	0.0193	4.91	0.77	3.92512	157.160

$K(v_{fo} = 20\,\%) = 1.85x10^{-9}$

Table 4.3 The results of permeability experiment for 30% fiber volume fraction fiber preform($v_{fo} = 0.30$)

Flow front location from the inlet, x_{front} (mm)	Time (s)	Inlet pressure, P_{inlet} (10^5.Pa)	Pressure gradient, $-\frac{dP}{dx} = \frac{P_{inlet}}{x}$ (Pa/mm x 10^{-5})	Actual flow front velocity, u_{actual} (mm/s)	Resin viscosity, μ (Pa.s)	Superficial flow front velocity, u (mm/s) $u = u_{actual}(1 - v_f)$	Permeability, K^* (m^2x10^{-11})
10	30	0.7	0.07	4.3691	0.77	3.0584	33.642
20	32	1.17	0.0585	4.4011	0.77	3.0808	40.550
30	34	1.56	0.052	4.4475	0.77	3.1132	46.100
40	36.6	2.1	0.0525	4.5293	0.77	3.1705	46.501
50	39	2.7	0.054	4.6265	0.77	3.2385	46.179
60	41	3.4	0.0566	4.7233	0.77	3.3063	44.927
70	43	4.3	0.0614	4.8345	0.77	3.3851	42.420
80	45	5.07	0.0633	4.9601	0.77	3.4721	42.185
90	47	6.19	0.0687	5.1005	0.77	3.5701	39.969
100	49	7.15	0.0715	5.2545	0.77	3.6781	39.611
110	51	7.7	0.07	5.4233	0.77	3.7963	41.759
120	52.6	8.2	0.0683	5.5687	0.77	3.8981	43.925
130	54.6	8.9	0.0684	5.7634	0.77	4.0334	45.376

$K(v_{fo} = 30\ \%) = 0.42x10^{-9}$

The preform permeability at each fiber volume fraction is taken as the average of the values of in Tables 4.2 and 4.3. These are found as 1.85x10^{-9} m^2 and 0.42x10^{-9} m^2 for 20 % and 30 % fiber volume fraction, respectively.

Using experimental data that was obtained, the permeability is presented as a function of preform porosity. In this study, in order to simulate compression resin transfer molding where the porosity of the fibrous medium is changed during the compression phase, preform permeability as a function of porosity must be known. It is difficult to fit an appropriate function with 2 data points. However, in literature, similar function fits to experimental permeability data here often used experimental function [31].

Figure 4.6 presents the exponential function fit to the experimentally obtained permeability data.

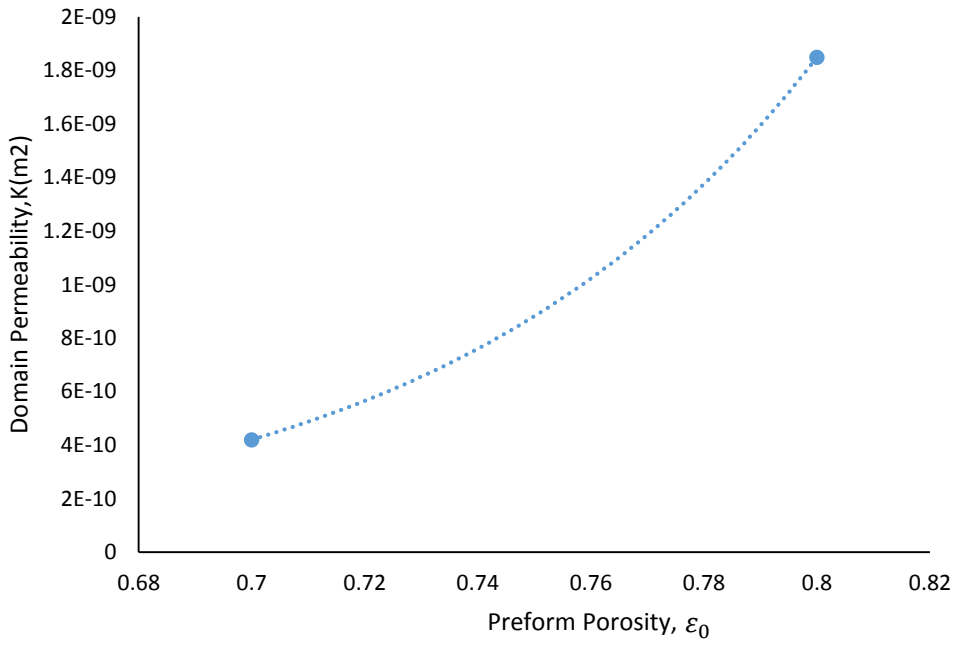

Figure 4.6 Domain permeability vs porosity

The preform permeability is expressed as

$$K = 1x10^{-14}e^{14.817(1-v_f)} \tag{4.5}$$

4.3 Experimental Results for RTM and CRTM of Particle Filled Continuous Fiber Reinforced Composites

In order to investigate the effect of parameters on the particle distribution along the composite length, series of experiments were performed. Table 4.4 depicts types and values of constant process parameters used in each process.

Table 4.4 Process parameters that were kept the same in all experiments

Constant Process Parameters	Value
Mold Cavity Dimensions	150mm (length)x70 mm (width)
Particle Filler Type	Spherical glass particle (20μm) (Microperl 050-20-215)
Fiber Reinforcement	Glass chopped strand mat
Resin	Epoxy resin (Hexion MGS L160)

Table 4.5 shows the process parameters (whose effects on the particle distribution in the resulting composite, were investigated). The values in which they were varied are also given.

Table 4.5 Process parameters that were varied (whose effect on particle distribution were sought)

Varied Process Parameter	Target Values of the Varied Parameter
Injection Piston Speed (mm/s)	0.05-1
Particle Concentration in Injected Resin (% vol)	20 %, 30 %, 40 %
Final Composite Fiber Volume Fraction	20 %-30 %
Process type	RTM / CRTM

Table 4.6 Production of Composite Samples for Assessing the Effect of Process Parameters on Particle Distribution within the Composite

Exp. No	Process Type	Design fiber volume fraction v_{fo} (%)	Actual fiber volume fraction v_{fo} (%)	Inlet Particle Concentration, C_o (%)	Injection speed (mm/s)
1	RTM	20	20±1	20	0.18
2	RTM	20	21±0.5	30	0.06
3	RTM	20	20±0.2	30	0.48
4	RTM	20	20±0.2	20	0.61
5	RTM	20	18±0.4	40	0.3
6	CRTM	30	23±0.4	30	0.3
7	CRTM	30	22±0.3	40	0.24
8	CRTM	30	27±0.7	20	0.44
9	CRTM	30	26±1.4	30	0.37

Nine samples, produced by these experiments, are analyzed to understand the effect of each process parameters on particle distribution in the composite. Final fiber volume fraction and injection speed are different from their desired values. The reasons for the difference will discussed in coming sections

There were also many additional experiments that were carried out to produce additional samples using RTM and CRTM processes. They are not included in Table 4.6. In each of these experiments, certain issues arised that prevented successful production of samples. For instance, for 30 % fiber volume fraction injection in RTM, the inlet pressure increased substantially (up to 23 bars) and Zwick Tensile Testing

machine was overloaded. Therefore, clamping force was not enough to hold the mold assembly at the desired thickness and the desired fiber volume fraction. As a result of high pressure, suspension leaked from the mold. Because of these issues, injection at 30 % fiber volume fraction in RTM was not attempted again. The leakage isssue arose in several other experiments due to increased pressures or due to the failure in proper closing/clamping of the mold. The fiber preform moving in cavity was an issue that occured during the impregnation phase, which caused uneven (undesired) impregnation. In two CRTM experiments, the preform could not be impregnated properly the unimpregnation of the fiber preform.

4.3.1 Experimental Results for RTM of Particle Filled Continuous Fiber Reinforced Composite

4.3.1.1 Effect of injection speed on the particle distribution in the composite

Two composite specimens were produced by RTM where each had 20 % particle concentration in injected resin and 20 % fiber volume fraction, while the injection speeds were different in order to isolate the effect of injection speed on the resulting particle distribution in the composite. Experimental conditions are shown in Table.4.7.

Table 4.7 Production of Composite Samples for Assesing the Effect of Injection Speed on Particle Distribution within the Composite

Sample Label	Experiment No.*	Process Type	Design fiber volume fraction v_{fo} (%)	Actual (obtained) fiber volume fraction v_{fo} (%)	Inlet Particle Concentration C_o (%)	Injection Speed (mm/s)
Lo_Speed	1	RTM	20	20±1	20	0.18
Hi_Speed	4	RTM	20	20±0.2	20	0.61

*per Table 4.6

The flow front progression result for are presented in Figure 4.7. Best lines have been fitted to the data; the slope of the trend lines gives the average flow front velocity in each case. The different piston injection speeds reflect directly on th flow front speeds.

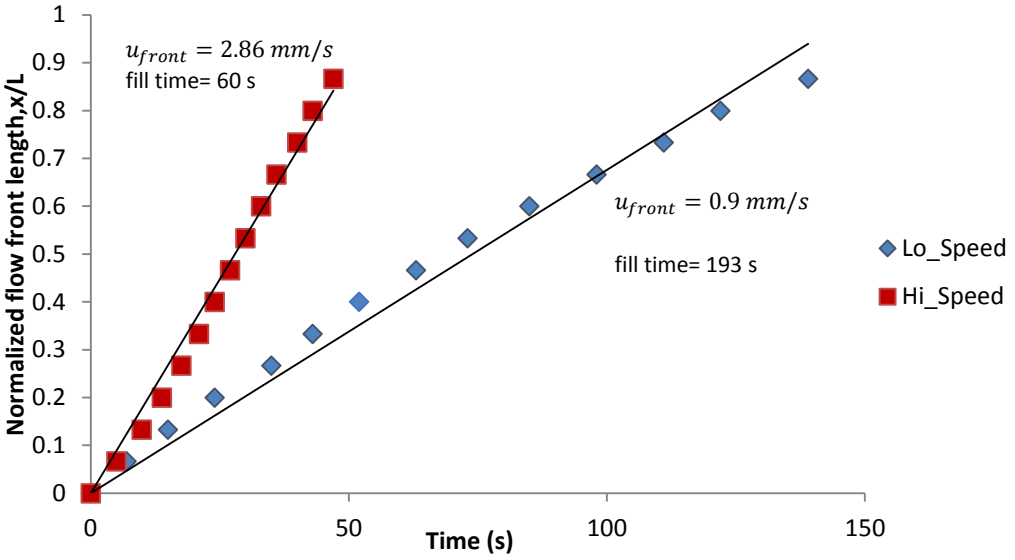

Figure 4.7 Flow front progression in RTM, for the effect of injection speed. (Flow front position normalized by cavity length, L)($v_{fo} = 20\ \%$)

The variation of pressure with recorded by the pressure sensor below the inlet line gate of the mold is presented in Figure 4.8. The difference of the injection speeds affects the inlet pressure, P_{inlet} significantly as seen. Everything else being the same, the high flow velcocity increases the injection pressure significantly. There is also substential difference between the fill times.

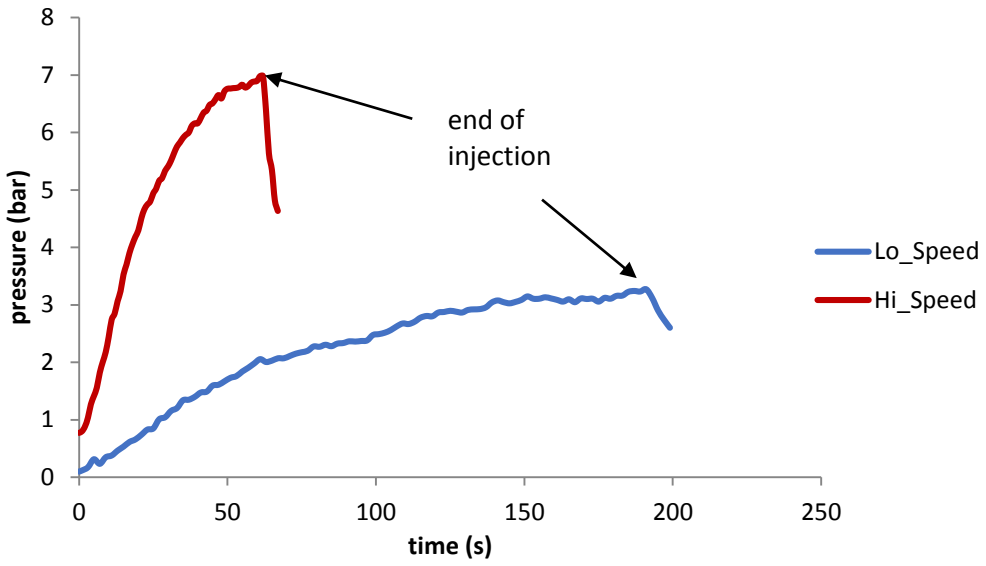

Figure 4.8 Variation of inlet pressure with time in RTM, for the effect of injection speed ($v_{fo} = 20$ %)

Particle volume fraction distributions along the composite specimens produced at different injection speeds are shown in Figure 4.9. The particle volume fraction distributions followed nearly the same trend with very little deviation. It is concluded that the particle volume fraction distribution in composite is not affected by the injection speed. However, the injection speed affects the inlet pressure variation tremendeously.

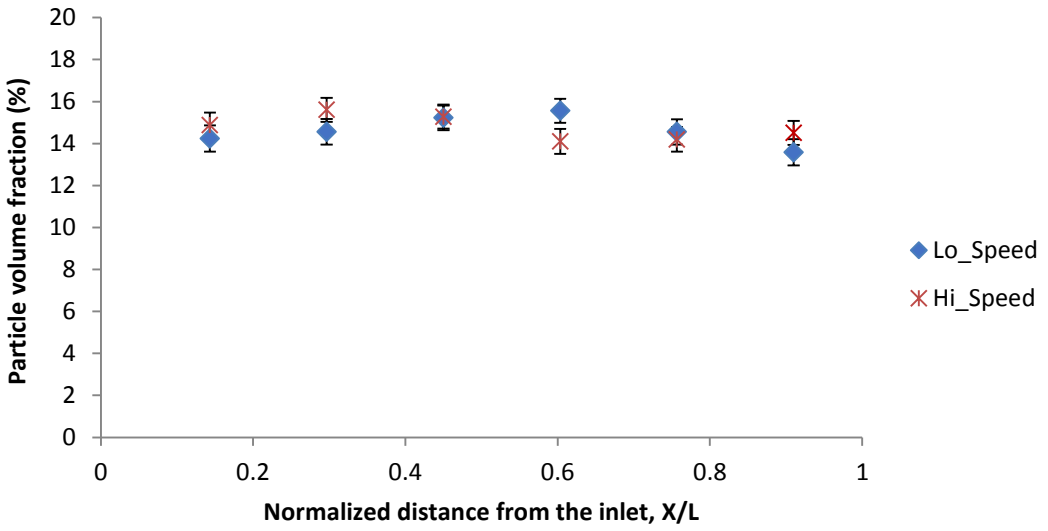

Figure 4.9 Particle volume fraction distributions along the composites, produced at different injection speeds at 20 % fiber volume fraction (distance along composite is along flow length and is normalized by the composite length, L)

The effect of injection speed on particle distribution was also investigated at 30 % particle concentration. The experimental conditions are presented in Table 4.8.

Table 4.8 Production of Composite Samples for Assesing the Effect of Injection Speed on Particle Distribution within the Composite

Sample Label	Experiment No.*	Process Type	Design fiber volume fraction v_{fo} (%)	Actual (obtained) fiber volume fraction v_{fo} (%)	Inlet Particle Concentration, C_o (%)	Injection Speed (mm/s)
Lo_Speed	2	RTM	20	21±1	30	0.06
Hi_Speed	3	RTM	20	20±0.2	30	0.48

*per Table 4.6

Figure 4.10 presents the flow front progression. There is more deviation from linerity of front progression, in this case. The difference between the injection speeds can be seen in the different slopes of the flow front positions.

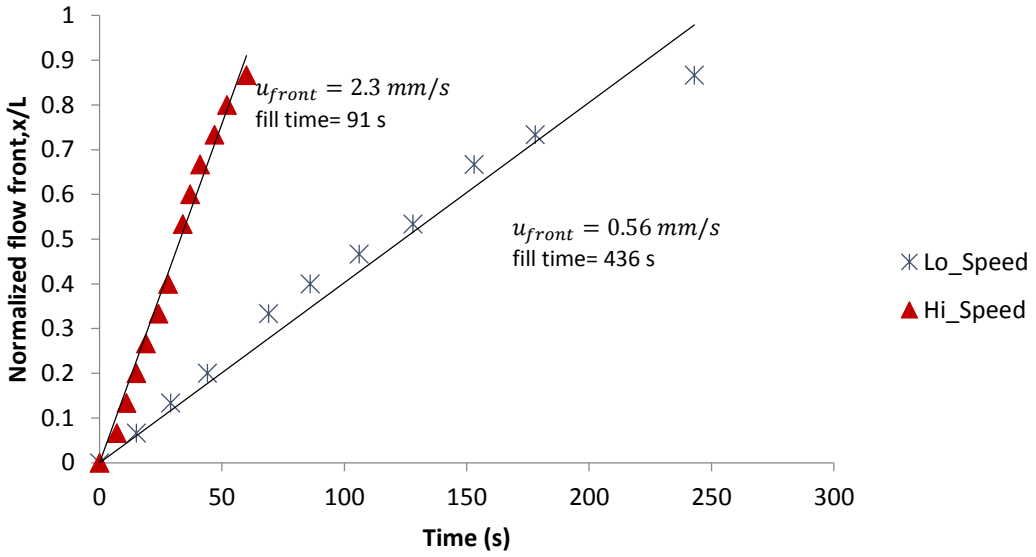

Figure 4.10 Flow front progression in RTM, for the effect of injection speed. (Flow front position normalized by cavity length, L)($v_{fo} = 20\ \%$)

Figure 4.11 presents the variation of inlet pressure with time. The high injection speed again results in high inlet pressure .

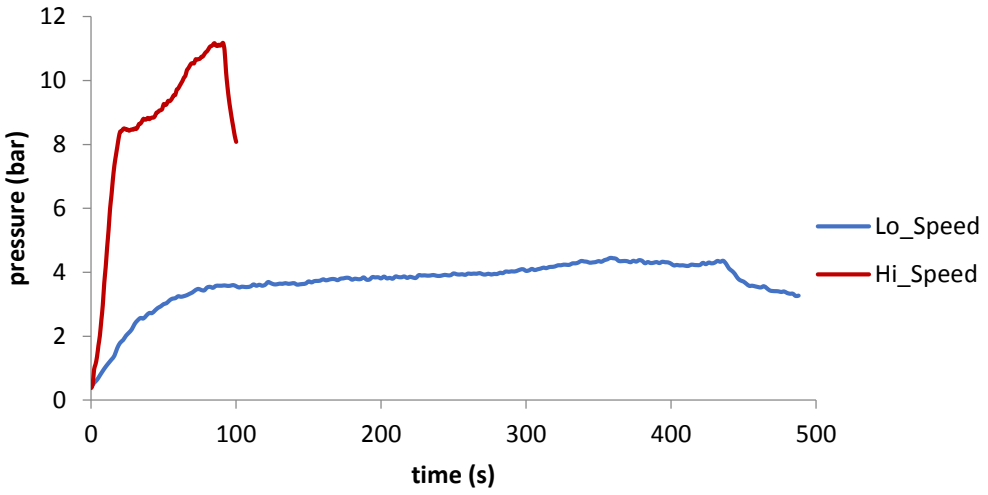

Figure 4.11 Variation of inlet pressure with time in RTM, for the effect of injection speed ($v_{fo} = 20$ %)

Particle volume fraction distributions along these two composite specimens produced at different injection speed are shown in Figure 4.12.

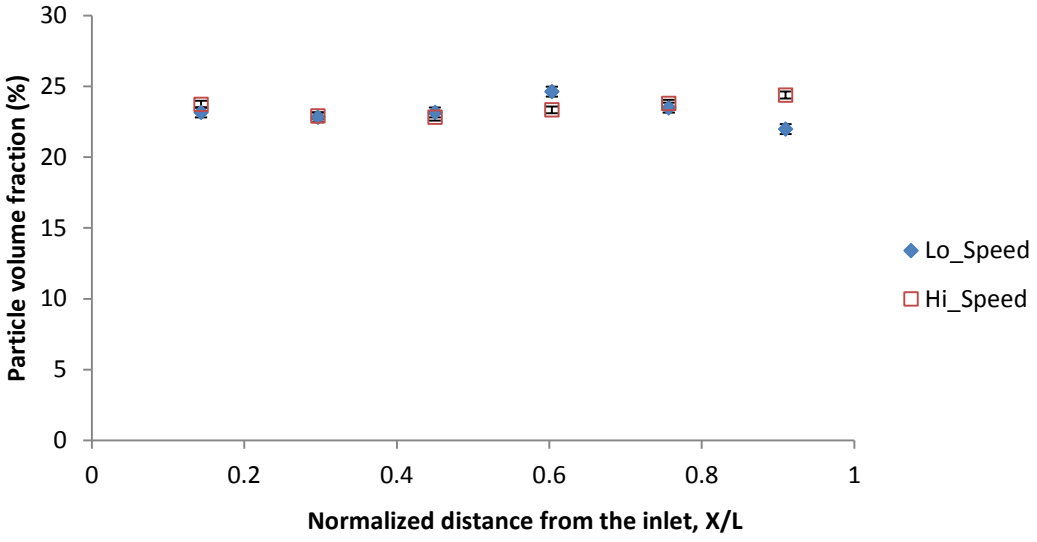

Figure 4.12 Particle volume fraction distributions along the composites, produced at different injection speeds at 20 % fiber volume fraction (distance along composite is along flow length and is normalized by the composite length, L)

The particle distribution shows a slight U-profile in the Hi_Speed sample whereas in the Lo_Speed sample there is slight S trend. The particle volume of fractions still have little variation in these two experiments and are fairly close in value for these two experiments. As before, the particle volume fraction along the composite specimens are not affected by the injection speed.

Since injection speed is not an effective parameter, it will not be taken into account in analyses involving the effect of other processing parameters on particle distribution in composite.

4.3.1.2 Effect of particle filler concentration in injected particle-resin suspension on the particle distribution in the composite

Three composite specimens were produced to study the effect of suspension particle concentration on particle distribution in composites. Their production settings are given in Table 4.9.

Table 4.9 Production of Composite Samples for Assesing the Effect of Particle Concentration in the Injected Particle-Resin Suspension on Particle Distribution within the Composite

Sample Label	Experiment No.*	Process Type	Design fiber volume fraction v_{fo} (%)	Actual (obtained) fiber volume fraction v_{fo} (%)	Inlet Particle Concentration, C_o (%)
Lo_Particle	4	RTM	20	20±0.2	20
Med_Particle	3	RTM	20	20±0.2	30
Hi_Particle	5	RTM	20	18±0.4	40

*per Table 4.6

The flow front progression and the variation of inlet pressure with time are presented for these three experiments in Figure 4.13 and Figure 4.14, respectively. The injection speeds were different as seen in Figure 4.13, however, as was shown before, the speed is not affecting the particle distribution in the composite. The differences in pressure profile (Figure 4.14) are due to not only injection speed but also due to different suspension viscosities at different particle concentration. For instance, Lo_Particle and Med_Particle production here similiar, yet the pressure rise in Med_Particle production is substentially larger (maximum pressure 12 bars) than in Lo_Particle production (maximum pressure 6 bars).

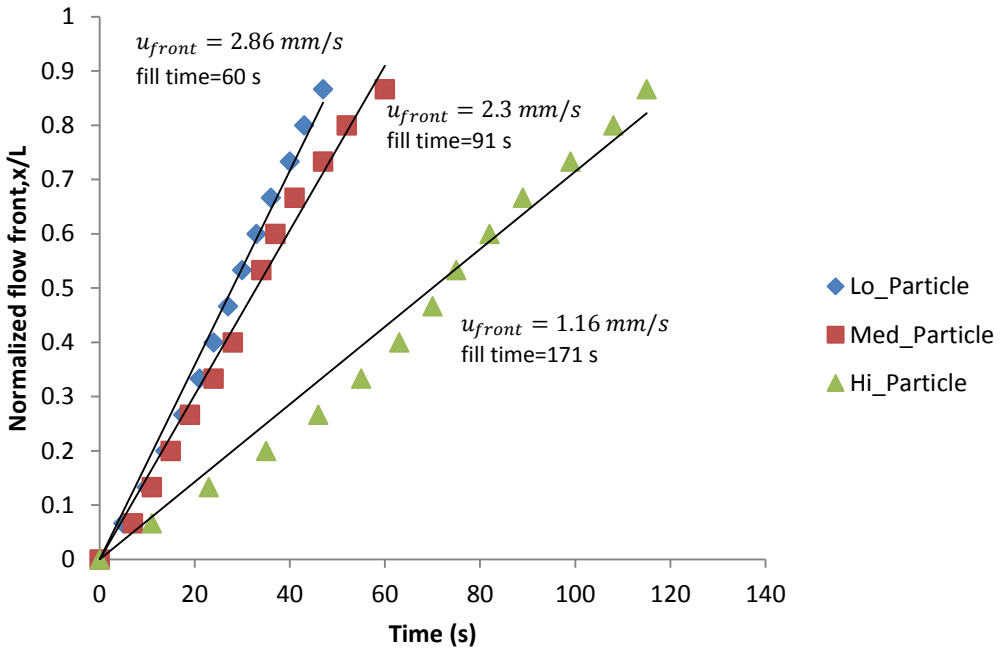

Figure 4.13 Flow front progression in RTM, for the effect of particle concentrationin injected particle-resin suspension. (Flow front position normalized by cavity length, L)($v_{fo} = 20\ \%$)

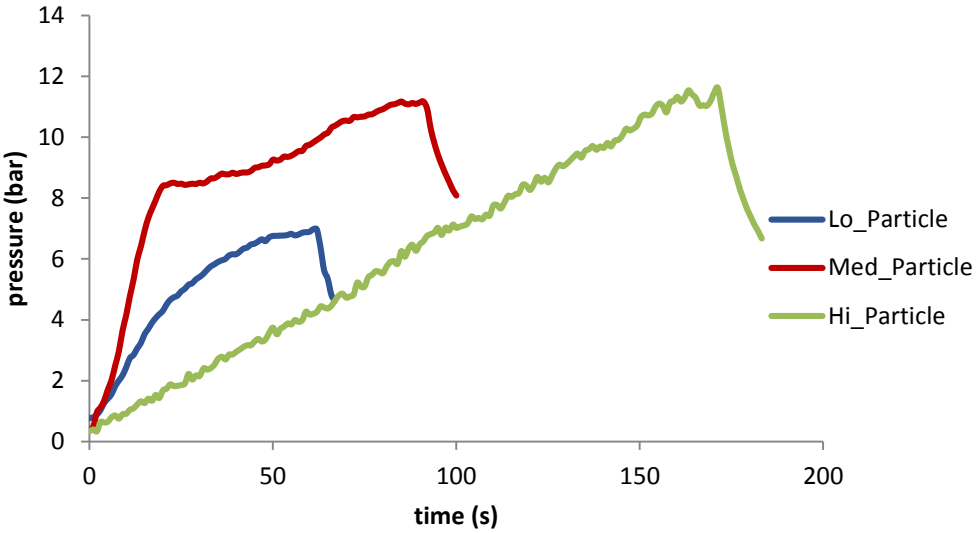

Figure 4.14 Variation of inlet pressure with time in RTM, for the effect of particle concentration in injected particle-resin suspension ($v_{fo} = 20$ %)

Particle volume fraction distribustions along the composite specimens are presented in Figure 4.15.

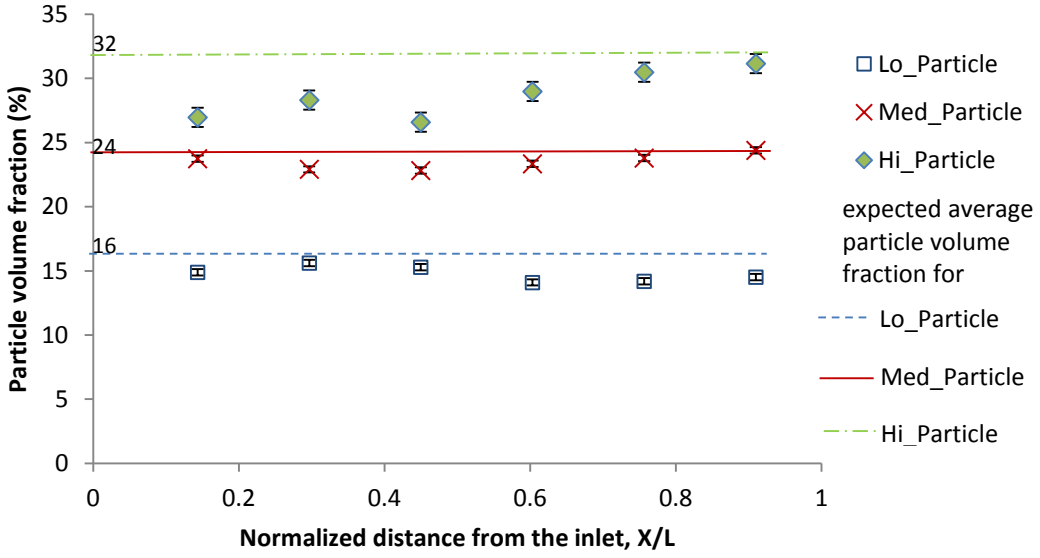

Figure 4.15 Particle volume fraction distributions along the composites, produced at different particle concentration in injected particle-resin suspension at 20 % fiber volume fraction (distance along composite is along flow length and is normalized by the composite length, L)

A small change is observed in the particle volume fraction with a slight alternating trend (increase/decrease/increase for 20 % and 40 %, decrease/increase for 30 % particle concentration) in all samples. As the particle concentration in the injected suspension increases, the variation in particle volume fraction distribution along the composite length increases. The maximum variation in particle volume fraction is 4.5 % at the highest particle concentration, the maximum variation in particle volume fraction is 1 % at the lowest concentration.

When conservation of particle filler mass in the composite is considered, the expected average particle volume fraction along the composite can be found through

$$\bar{v}_{f,particle} = C_0(1 - v_{f0}) \tag{4.6}$$

for a zero-porosity composite assumption. v_{f0} is taken as the actual fiber volume fraction in this equation. Based on equation (4.6), the expected average of particle volume fractions in the three composite samples are 16 % for 20 % particle concentration, 24 % for 30 % particle concentration and 32 % for 40 % particle concentration. These average values are shown in Figure 4.15. The experimentally determined values are only slightly below the expected values.

4.3.2 Experimental Results for CRTM of Particle Filled Continuous Fiber Reinforced Composites

As the injection speed was found as an effective parameter on the particle distribution along the composite in the previous section, it will not taken into account for the analyses involving the effect of other process parameters on particle distribution in CRTM productions.

In CRTM, injection was performed at low fiber volume fraction until about 75 % of the preform in cavity was impregnated. The mold closing speed is 0.05 mm/s for all CRTM experiments.

The effect of suspension particle concentration on particle distribution along the composite part are investigated for the two composite samples shown in Figure 4.10.

The significant difference between the design composite fiber volume fraction and the actual fiber volume fractions becomes from the deviation of the mold setup according to compression phase.

Table 4.10 Production of Composite Samples for Assesing the Effect of Particle Concentration in the Injected Particle-Resin Suspension on Particle Distribution within the Composite, in CRTM for $v_{fo} = 23 - 24$ %

Sample Label	Experiment No.*	Process Type	Fiber volume fraction during injection, $v_{f0,initial}$ (%)	Design fiber volume fraction (after compression) v_{f0} (%)	Actual (obtained) fiber volume fraction of compression v_{f0} (%)	Inlet Particle Concentration, C_0 (%)	Top mold plate closing speed, (mm/s)
Lo_Particle	6	CRTM	16	30	23±0.4	30	0.05
Hi_Particle	7	CRTM	16	30	22±0.3	40	0.05

*per Table 4.6

The non-dimensionalized flow front progression with time during the molding of the composite specimens is presented in Figure 4.16. At the begining of impregnation (up to 17 s), the flow front progression is similar for both experiments due to the same fiber volume fraction (16 %) and the similar piston injection speeds. Then, the fronts fork slightly, with slower velocity for high particle concentration production. The fill time for low particle concentration production is about 53 s whereas for high particle concentration is about 73 s for injection phase . The time lag between the two phases of

CRTM process is due to the practical aspect of preparing the mold/set-up for compression.

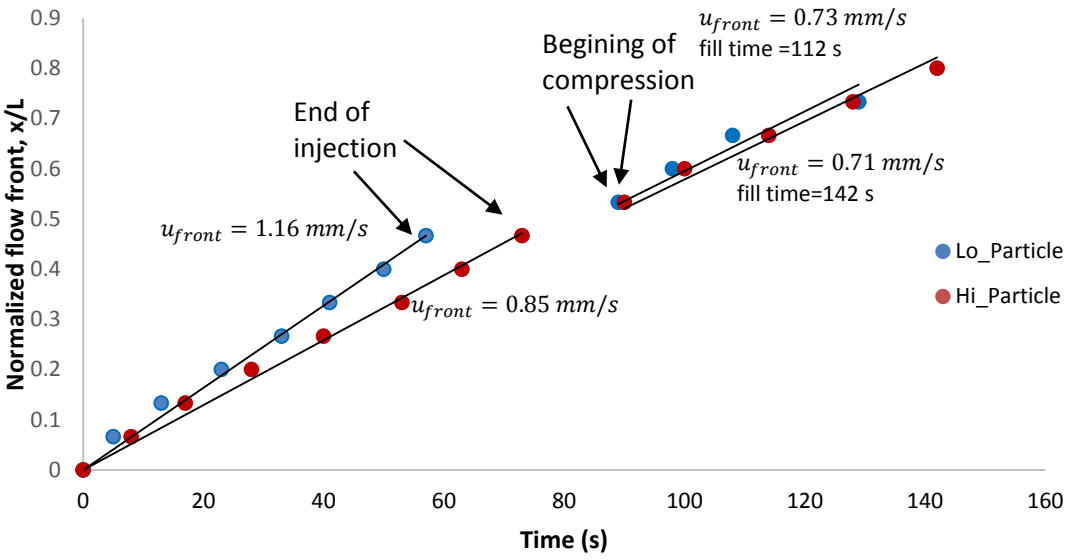

Figure 4.16 Flow front progression in CRTM, for the effect of particle concentration in injected particle-resin suspension. (Flow front position normalized by cavity length, L) ($v_{fo} = 23 - 24\%$)

The variation of inlet pressure during the process is shown in Figure 4.17. The slopes of variation of pressure during the injection phase are same for both experiments due to the similiar flow front speeds. In compression stage, for high particle concentration production, the maximum inlet pressure during the compression phase is significantly higher (14.6 bar) than that in low particle concentration production (8.8 bar) due to the higher particle resin suspension viscosity. Note that injection port is closed during compression, therefore rise in pressure at inlet is a result of pressurization due to compression, alone.

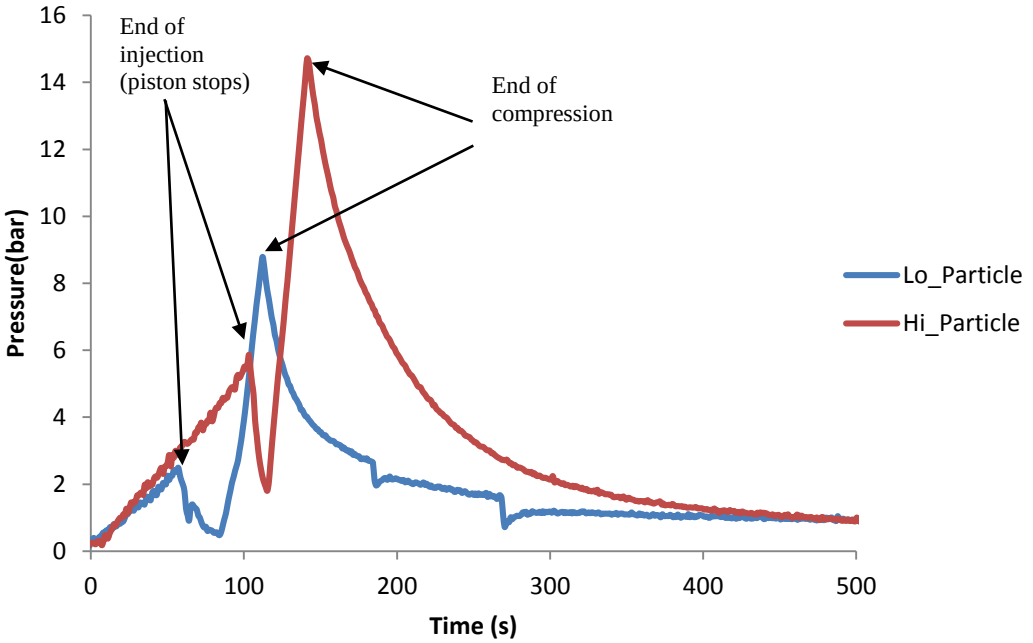

Figure 4.17 Variation of inlet pressure with time in CRTM, for the effect of particle concentration in injected particle-resin suspension ($v_{fo} = 23 - 24$ %)

Figure 4.18 presents the particle volume distributions along the composite sample. For Hi_Particle sample, the particle content along the flow path first increases and then decreases in an alternating pattern centering around a value of 33 % particle volume fraction. The maximum particle volume fraction is 36 % and is observed near the middle of composite. For the other sample, there is a clear increase along flow path in composite reaching 30 % with a slight in the end to 25 %. The expected average particle volume fraction in the Lo_Particle and Hi_Particle composites are 23 % and 31 %, respectively.

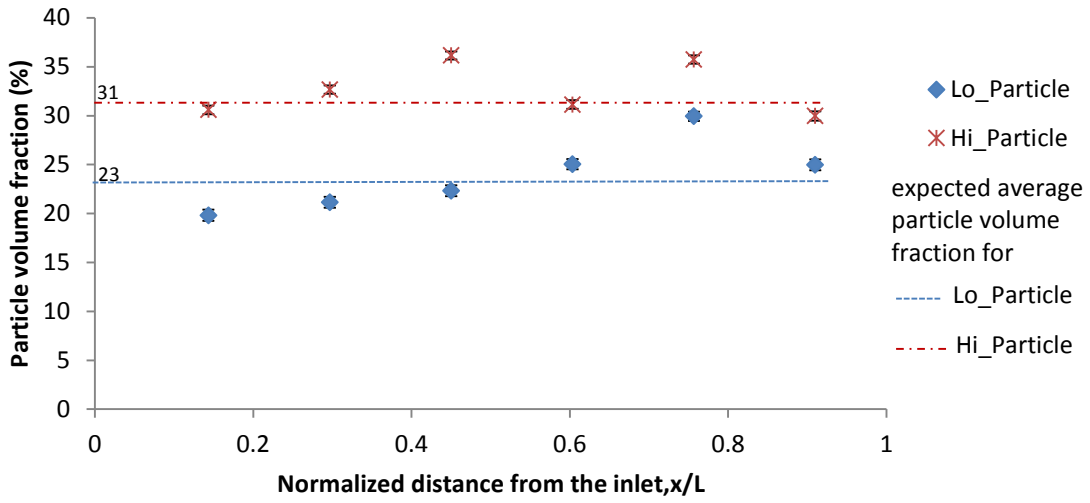

Figure 4.18 Particle volume fraction distributions along the composites, produced at different particle concentration in injected particle-resin suspension ($v_{fo} = 23 - 24$ %) (distance along composite is along flow length and is normalized by the composite length, L)

The effect of particle concentration on the particle distribution along the composite length in CRTM is investigated for two samples which have 26-27 % fiber volume fractions. Table 4.11 depicts the production data of these samples.

Table 4.11 Production of Composite Samples for Assesing the Effect of Particle Concentration in the Injected Particle-Resin Suspension on Particle Distribution within the Composite, in CRTM, for ($v_{fo} = 26 - 27$ %)

Sample Label	Experiment No.*	Process Type	Fiber volume fraction during injection, $v_{f0,initial}$ (%)	Design fiber volume fraction v_{fo} (%)	Actual (obtained) fiber volume fraction v_{f0} (%)	Inlet Particle Concentration C_0 (%)	Top mold closing speed, (mm/s)
Lo_Particle	8	CRTM	16	30	27±0.7	20	0.05
Hi_Particle	9	CRTM	16	30	26±1.4	30	0.05

*per Table 4.6

Figure 4.19 presents the flow front progression in production of these two samples. The injection speed for Lo_Particle sample production is higher so the injection phase

is completed sooner than at for Hi_particle sample production. Despite the higher injection speed for Lo_Particle sample, the slope of the inlet pressure at injection phase in both experiments are close to each other, as indicated in Figure 4.20, since in the Lo_Particle sample production, the viscosity of suspension is lower. On the other hand there is significant difference between maximum pressures in compression phase, where a pressure around 6 bars for low particle concentration part is observed, the maximum pressure is around 9.5 bar for the high particle concentration part. Such a difference is expected since the two production involved different viscosities, where the closing speed were the same. Figure 4.21 presents the particle distribution along the composite for these two samples. For the Lo_Particle sample, the maximum and the minimum volume fractions are 16.6 % and 13 %, respectively, which indicates same (but not much variation) along the composite product. For the Hi_Particle sample, at the inlet and outlet of the sample the particle volume fraction is close to the expected value 22.35 % (for zero porosity assumption) however around the middle of sample, particle volume fraction reaches a maximum value (26.92 %). The particle distribution can not be uniform-though the change is not too high. Furthermore, there is some " increasing particle content " along the composite trend.

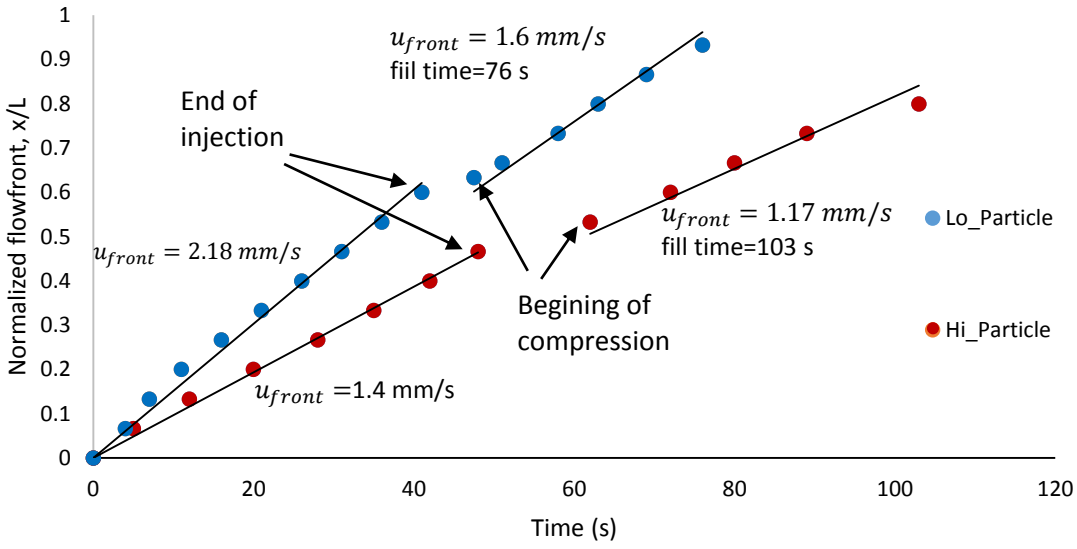

Figure 4.19 Flow front progression in CRTM, for the effect of particle concentration in injected particle-resin suspension. (Flow front position normalized by cavity length, L)($v_{fo} = 26 - 27$ %)

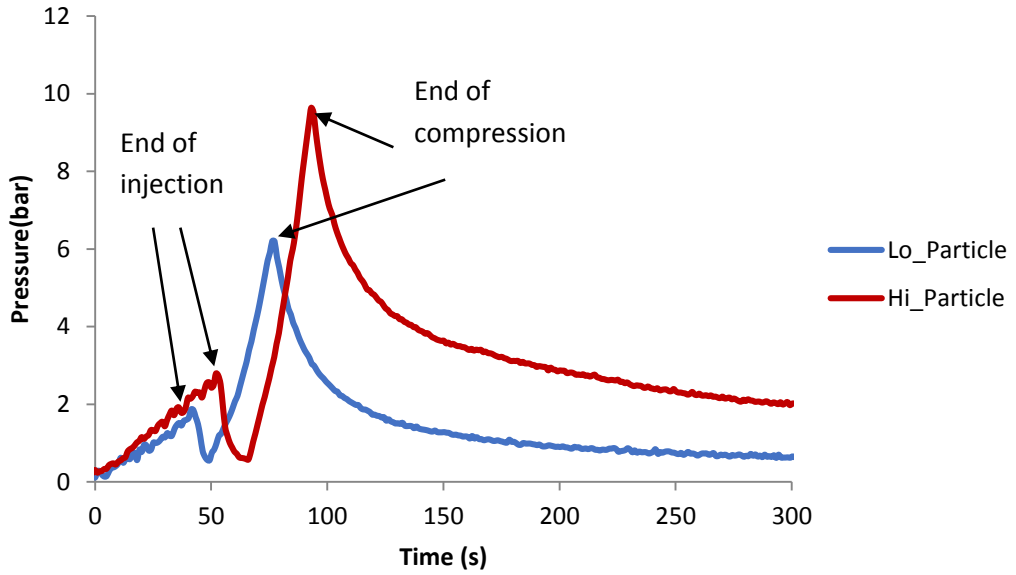

Figure 4.20 Variation of inlet pressure with time in CRTM, for the effect of particle concentration in injected particle-resin suspension ($v_{fo} = 26 - 27$ %)

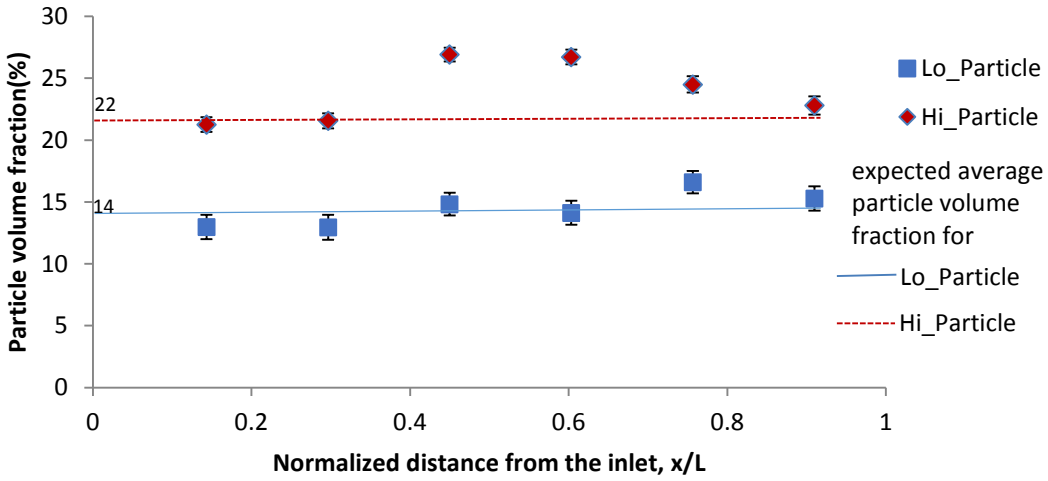

Figure 4.21 Particle volume fraction distributions along the composites, produced at different particle concentration in injected particle-resin suspension ($v_{fo} = 26 - 27\%$) (distance along composite is along flow length and is normalized by the composite length, L)

4.4 Comparison of RTM and CRTM process

In order to understand the effect of process type on particle distribution in composite, two composite samples that have 30 % particle concentration each in injected suspension and around 20 % fiber volume fraction have been produced using RTM and CRTM. The experimental conditions are presented in Table 4.12.

Table 4.12 Processing Specifications of Samples Produced to Study the Effect of Process Type on the Particle Distribution within the Composite

Sample Label	Experiment No.*	Process Type	Design fiber volume fraction v_{fo} (%)	Actual (obtained) fiber volume fraction v_{fo} (%)	Inlet Particle Concentration, C_o (%)
RTM	3	RTM	20	20±0.2	30
CRTM	6	CRTM	30	23±0.4	30

*per Table 4.6

Figure 4.22 presents the flow front progression during the production of these two samples. In CRTM since there are two stages, flow front speed in each stage of CRTM differs with respect to injection speed and compression speed.

In the RTM experiment , although the piston speed was set to a constant value of 0.9 mm/s (to yield a constant suspension velocity in the mold), the piston velocity dropped to 0.48 mm/s when the suspension filled 1/3rd the cavity, and remained at this value for the remainder of the injection process. However, this effect was not as apparent in the suspension flow front. The suspension flow front remained nearly uniform throughout the molding and its position with respect to time has been expressed by capturing the front position along the center of the cavity. Although there is a slight

decrease in the velocity when the piston speed drops, this effect is not directly apparent in the Figure 4.22. The flow front speed reduces slightly, picks up speed and finally reduces once more towards the end of injection. The overall trend is nearly linear indicating a roughly constant flow front velocity.

The variation of inlet pressure with time for RTM and CRTM samples are shown in Figure 4.23. The effect of piston speed variation during impregnation of the RTM sample is apparent on the inlet pressure where the pressure increase rate drops as the piston speed drops. The pressure sensor on the inlet side of the mold shows a larger pressure rise during compression, when compared to injection phase of CRTM. However, the choice of compression speed also influences the pressure of compression. The maximum pressure for RTM is around 11 bars while for CRTM maximum pressure of injection is 2.26 bars and maximum pressure of compression phase 8.79 bars.

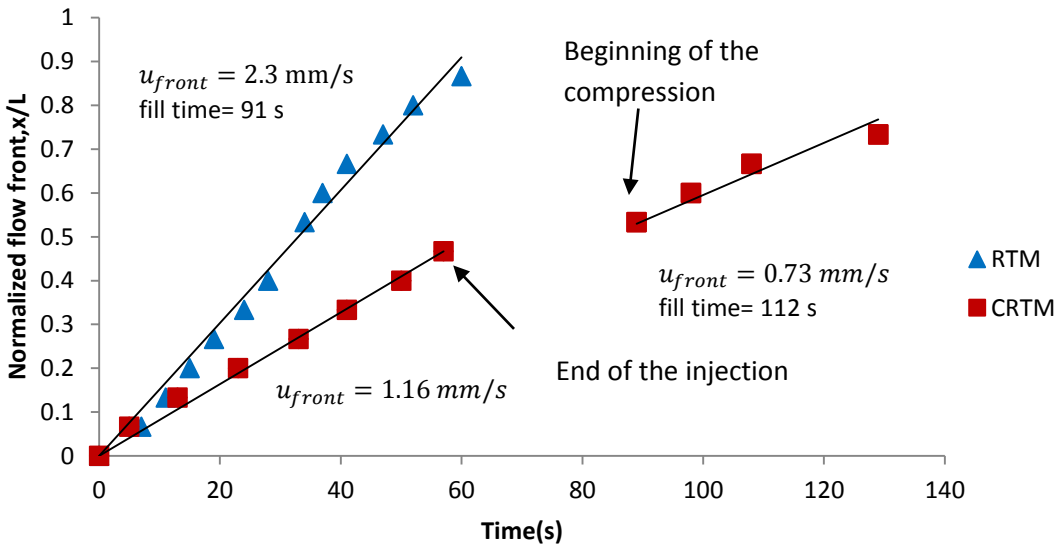

Figure 4.22 Flow front progression with time for RTM and CRTM samples (flow front position normalized by cavity length, L)

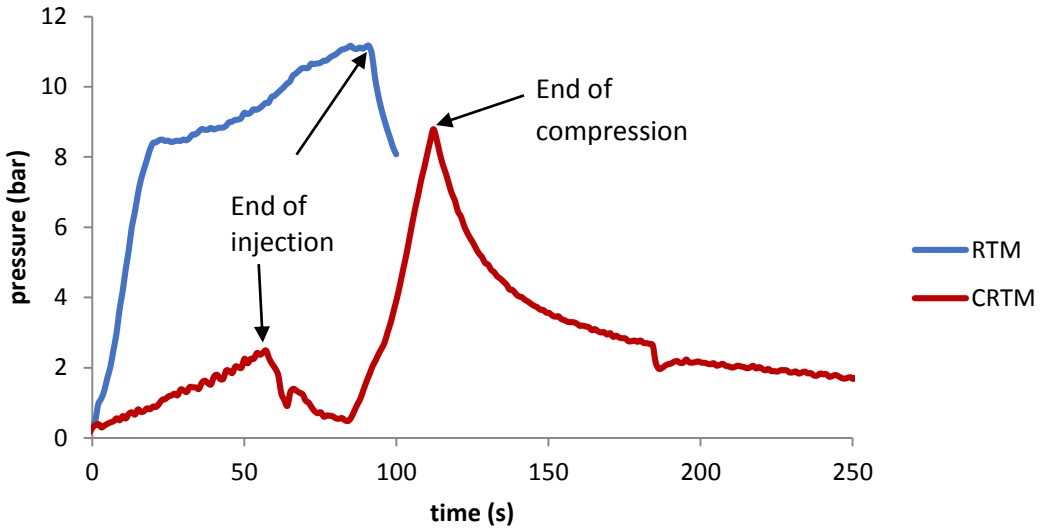

Figure 4.23 Variation of inlet pressure with time for RTM and CRTM samples

Figure 4.24 presents the particle filler volume fraction distributions along the two composite specimens. In RTM, the filler volume fraction exhibits little change, centering around 23 %. The filler content decreases very slightly at mid-composite followed by a slight increase at the end. With respect to the particle filler concentration in the injected resin (30 %) and the porosity of the cavity (80 % - fiber volume fraction in the composite is 20 %), the expected value for a uniform particle distribution is 24 %; which is only slightly above the obtained values. For the CRTM sample there is a clear increase in particle content with the particle volume fraction reaching 30% and following by a decrease to 25 % which is higher than the expected particle content (23%).

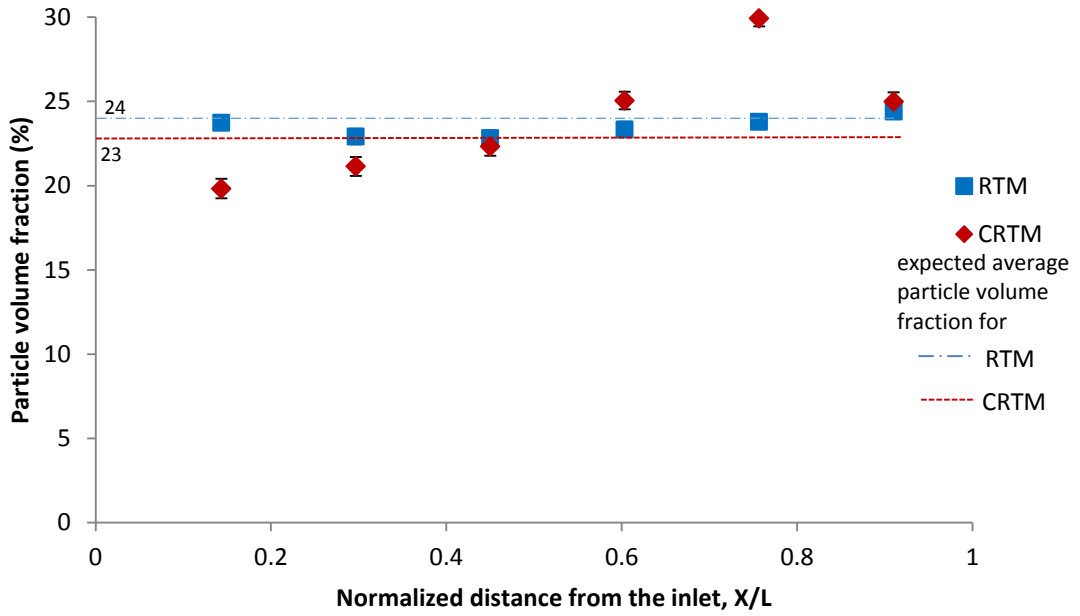

Figure 4.24 Particle filler volume fraction distributions along RTM and CRTM composite specimens (distance along composite normalized by composite length, L)

4.5 Results for Modeling of Impregnation in RTM and CRTM of Particle-Filled, Continuous Fiber Reinforced Composites

In this section, the production experiments for RTM and CRTM simulated using the flow model and numerical implementation given in Chapter 3. As mentioned before the used flow model for particle-filled impregnation developed previously. In this study, an appropriate particle filtration model for the investigated process is sought form of

$$\frac{\partial \sigma}{\partial t} = \alpha V C \qquad (3.15)$$

where

$$\alpha = \alpha_0(1 + k_1\sigma + k_2\sigma^2) \quad (3.21)$$

Specifically, an appropriate model for filtration coefficient is to be found.

The average filtration coefficient α_0 and the constants k_1 and k_2 will be determined based on experiments.

4.5.1 Determination of appropriate α_0, k_1 and k_2 of filtration coefficient in RTM

Since, in general, the specific particle deposit, σ, is a very small value (10^{-2} or less) the variations in k_1 and k_2 values when k_1 and k_2 values do not have significant effect on the overall particle distribution levels for any α_0 value. In order to find a proper range for each constant simulations have been performed by changing one of the constants while others were kept constant. Table 4.13 shows the experiment that was simulated for assessing the effect of values of k_1 on the particle volume fraction distribution in the composite. In numerical simulations, the particle volume fractions of a location in composite is expressed the sum of particles in suspension and the filtered particles:

$$v_{f,particle} = \varepsilon C + \sigma \quad (4.7)$$

Figure 4.25 presents the effect of different values of k_1 on the particle volume fraction in composite. Change in k_1 does not yield a significant difference in the particle volume fraction distribution except when its value reaches 100. In this value, the particle volume fraction decreases near the injection gate of composite sample.

Table 4.13 Simulation conditions for assessing the effect of k_1 values on the particle volume fraction $(\varepsilon C + \sigma)$ distribution in composite

Simulated Experiment	Simulation Label	α_0	k_1	k_2
C_o=20%, $v_{fo} = 20\ \%$, $u_{front} = 2.86\ mm/s$ RTM- Exp. 4*	Sim.1	0.5	1	1
	Sim.2	0.5	10	1
	Sim.3	0.5	100	1

*per Table 4.6

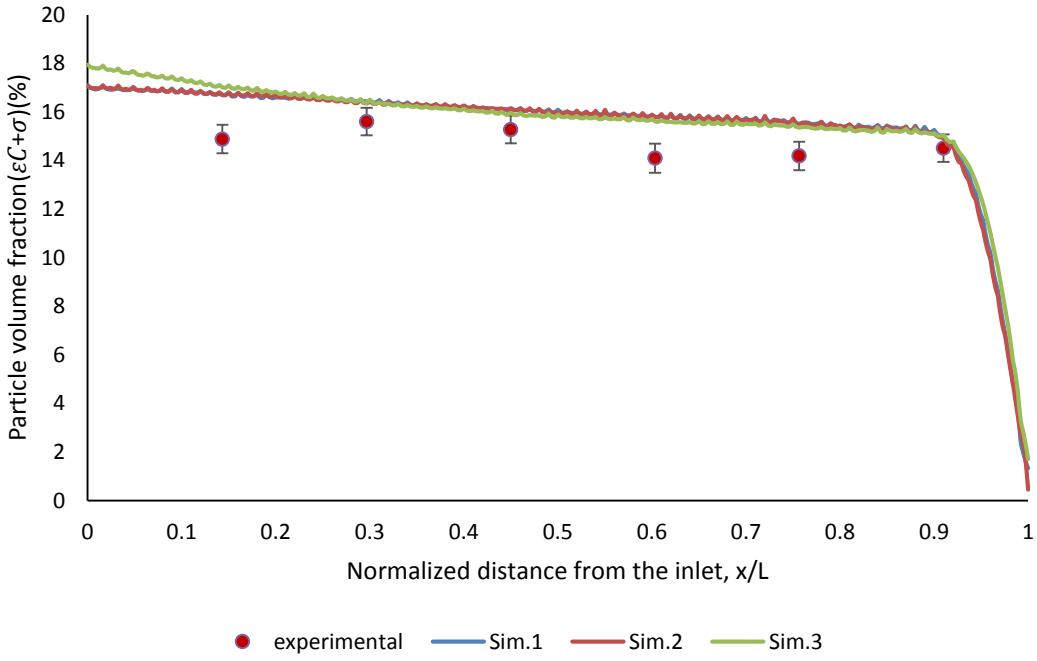

Figure 4.25 The effect of k_1 in filtration coefficient model on the particle volume fraction distribution in composite

The effect of k_2 is not apparent until its value reaches 10000 as shown in Figure 4.26. Conditions of experiment, which were simulated when studying the effect of values of k_2 on the particle volume fraction distribution in composite is given in Table 4.14.

Table 4.14 Simulation conditions for assessing the effect of k_2 values on the particle volume fraction ($\varepsilon C + \sigma$)

Simulated experiment	Simulation Label	α_0	k_1	k_2
C_o=30 %, v_{fo} = 21 % , $u_{front} = 0.56\ mm/s$ RTM- Exp. 2*	Sim.4	0.5	1	1
	Sim.5	0.5	1	10
	Sim.6	0.5	1	100
	Sim.7	0.5	1	1000
	Sim.8	0.5	1	10000

*per Table 4.6

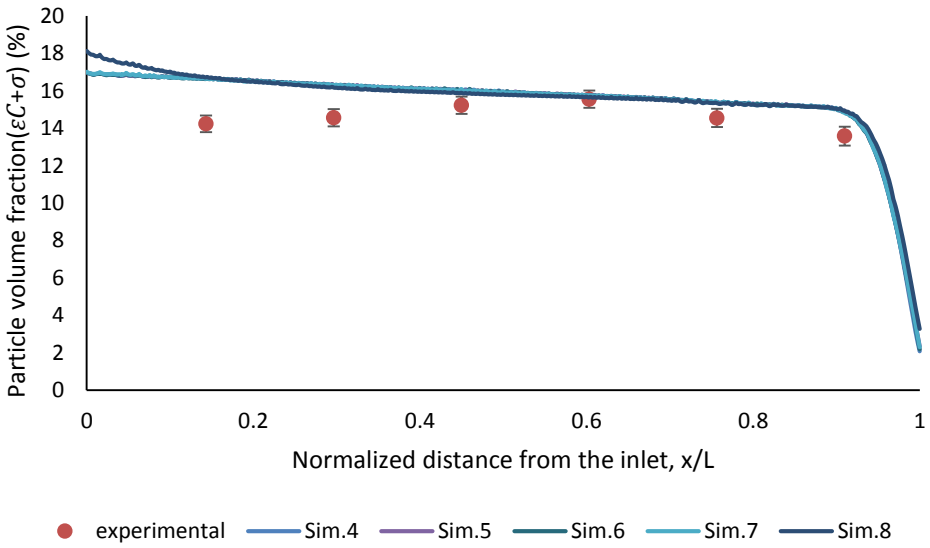

Figure 4.26 The effect of k_2 in filtration coefficient model on the particle volume fraction distribution in composite

The parabolic change in the particle volume fraction does not appear in Figure 4.26 and Figure 4.25 due to the small value of the unchanged constant.

The negative values of k_1 show a uniform particle distribution trend at any k_2 and α_0 values. Table 4.15 presents the simulation conditions for assessing the effect of negative value of k_1 on the particle volume fraction. These simulations is presented in Figure 4.26.

Table 4.15 Simulation conditions for assesing the effect of negative k_1 on the total particle volume fraction ($\varepsilon C + \sigma$)

Simulated Experiment	Simulation Label	α_0	k_1	k_2
C_o= 20 %, v_{fo} = 20 % $u_{front} = 2.86\ mm/s$ RTM-Exp. 4*	Sim.9	0.5	-1000	-100000
	Sim.10	0.5	-10000	100
	Sim.11	0.5	-10000	-100000

*per Table 4.6

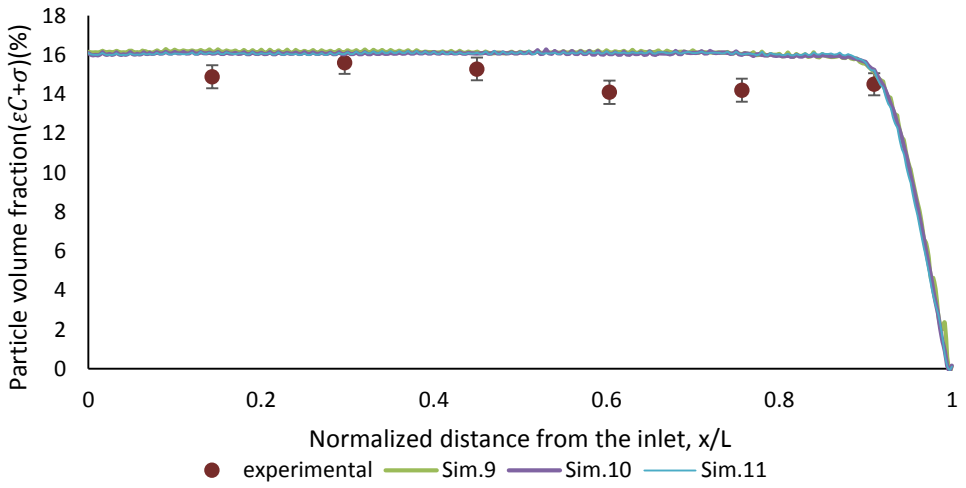

Figure 4.27 The effect of negative k_1 on the particle volume fraction distribution in the composite

Same results of effect of negative k_1 simulation based on different experiment is presented in Figure 4.28. Simulation conditions of these results are shown in Table 4.16.

Table 4.16 Simulation conditions for assessing the effect of negative k_1 on the total particle volume fraction ($\varepsilon C + \sigma$)

Simulated experiment	Simulation Label	α_0	k_1	k_2
C_o=30%, $v_{fo} = 20$ % , $u_{front} = 2.3\ mm/s$ RTM-Exp.3*	Sim.12	0.1	-500	-20000
	Sim.13	0.2	-500	20000
	Sim.14	0.5	-500	-20000
	Sim.15	1	-500	-20000

*per Table 4.6

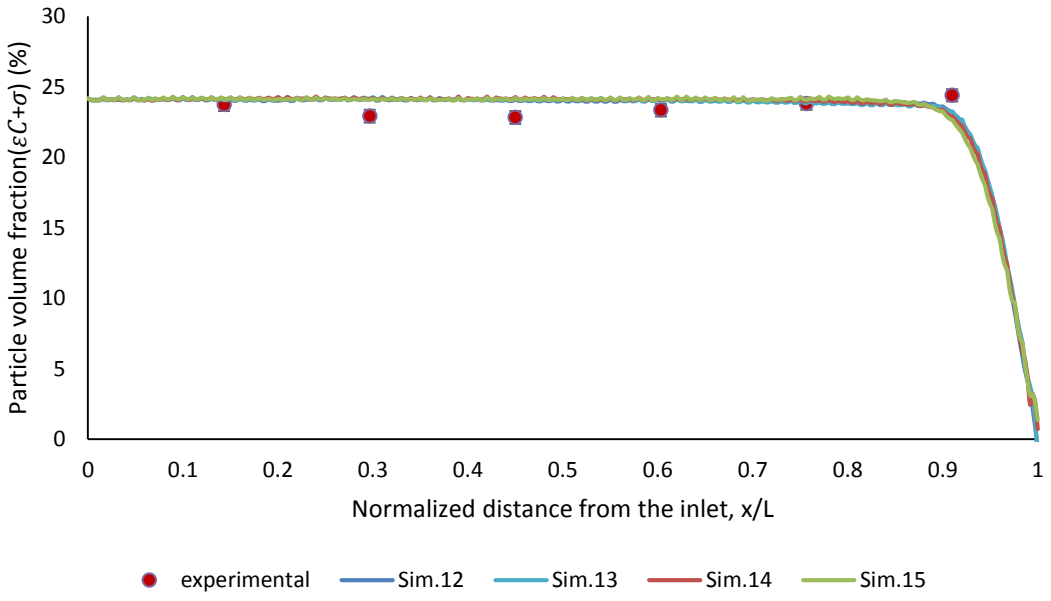

Figure 4.28 The effect of negative k_1 on the total particle volume fraction

In order to find the effect of α_0 at particle distribution trend other constants were kept same and several simulation were done for different values of α_0. Three of them are presented in Figure 4.29. Simulation conditions of them are shown in Table 4.17.

Table 4.17 Simulation conditions for assesing the effect of α_0 on the total particle volume fraction ($\varepsilon C + \sigma$)

Simulated Experiment	Simulation Label	α_0	k_1	k_2
C_o=30%,$v_{fo} = 21\ \%$, $u_{front} = 0.56\ mm/s$ RTM-Exp. 2*	Sim.16	0.2	500	-10000
	Sim.17	0.4	500	-10000
	Sim.18	0.5	500	-10000

*per Table 4.6

As it shown in Figure 4.29 for lower value of α_0 decreasing in particle distribution trend starts closer to the inlet gate and also the trend becomes more linear for smaller value α_0. In Figure 4.29 particle volume fraction trend starts to decrease around 0.3, 0.5 and 0.6 normalized distance from the inlet for α_0=0.2 , 0.5 and 0.6 , respectively.

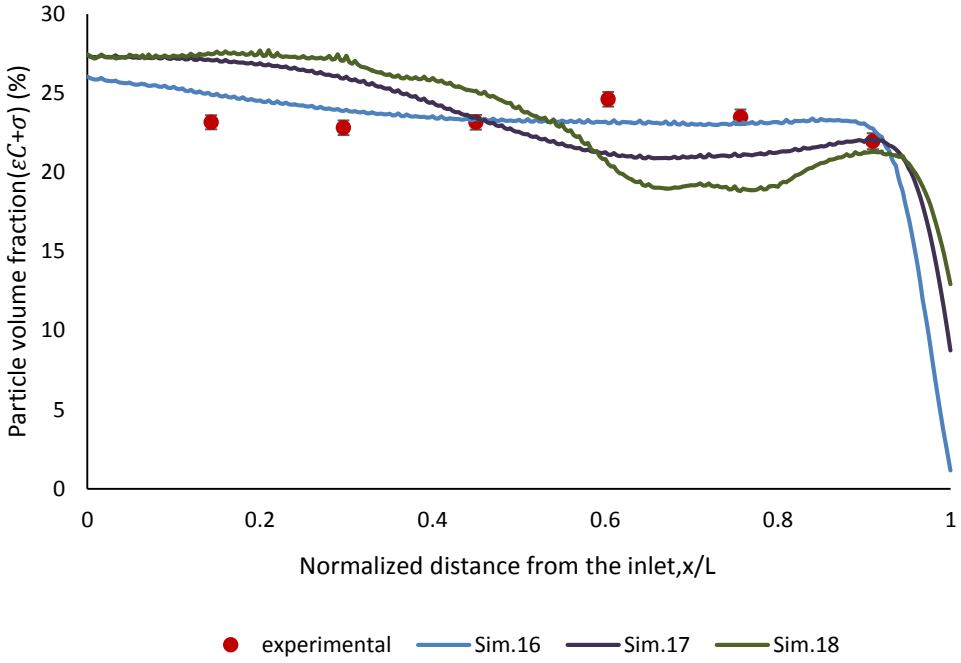

Figure 4.29 The effect of a_0 on the total particle volume fraction

In order to find accurate results, more simulations were performed using the model constants that were selected within the range that had been found before. Experimental conditions that are simulated given in Table 4.18.

Table 4.18 Simulation conditions for finding appropriate α_0, k_1 and k_2 on the particle volume fraction ($\varepsilon C + \sigma$)

Simulated experiment	Simulation Label	α_0	k_1	k_2
C_o=20%, v_{fo} =20 (%) u_{front} =2.86mm/s RTM-Exp.4 *	Sim.19	0.5	500	-11000
	Sim.20	0.5	500	-20000
	Sim.21	0.5	400	-11000
	Sim.22	0.5	400	-20000
C_o=30%,v_{fo} =20 (%) u_{front} =2.3 mm/s RTM-Exp. 3*	Sim.23	0.2	500	-10000
	Sim.24	0.2	700	-10000
	Sim.25	0.2	500	-20000
C_o=40%, v_{fo} = 18(%) u_{front} =0.95 mm/s RTM-Exp. 5*	Sim.26	0.2	500	-10000
	Sim.27	0.2	700	-10000
	Sim.28	0.2	500	-20000

*per Table 4.6

Figure 4.30, 4.31 and 4.32 represent the simulation results along with experimental data for particle distribution along the composite part at different injected suspension particle concentrations.

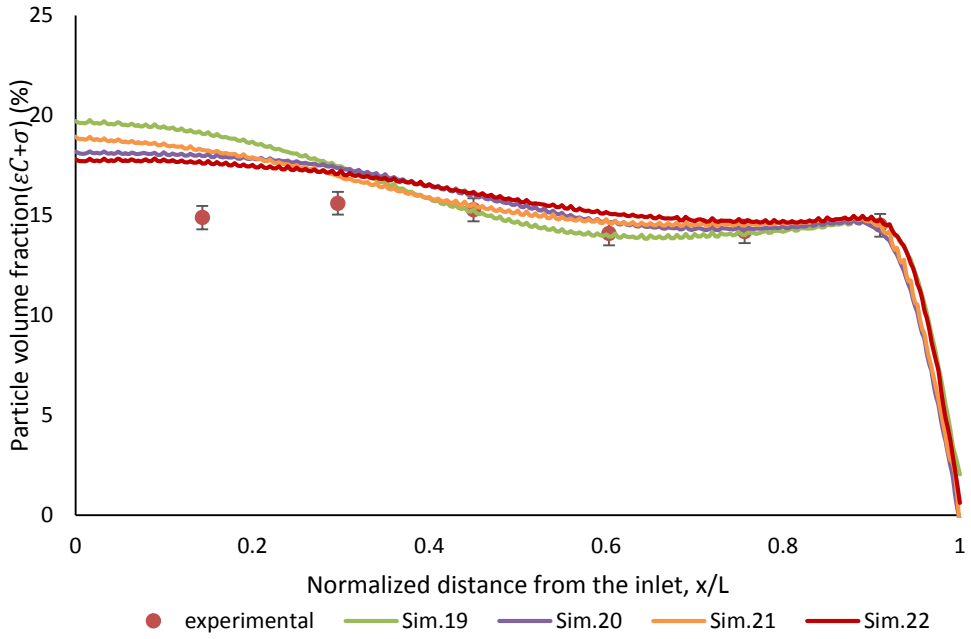

Figure 4.30 Simulation results for particle filler volume fraction distributions along the composite specimens for experiment: 20% particle concentration in suspension and 20 % fiber volume fraction

For 20 % particle concentration (Figure 4.30), the experimental trend shows a decrease around 0.45 normalized distance from the inlet. To meet this decrease for this experiment α_0 was selected 0.5. To approach the experimental particle distribution trend, several simulations were performed using different values of k_1 and k_2 per Table 4.18. In Figure 4.30, the comparison between Sim.19 and Sim.20 also Sim.21 and Sim.22 shows the effect of k_2 on the particle distribution in composite. As a result of these comparison when k_2 decreases (-11000 to -20000), particle volume fraction increases at the beginning of the composite, however there is also a reduction on the particle volume fraction after the middle of the composite.

The simulation result for the experiment that has 30 % suspension particle concentration and 20 % fiber volume fraction is presented in Figure 4.31. In order to obtain approximately uniform simulation trend α_0 selected 0.2. Several simulations were performed at this α_0 value using different values of k_1 and k_2. As a result of comparison between Sim.23 and Sim.24, the little change in k_1 (where one of them is

500, the other is 700) does not affect significantly the particle distribution in composite.

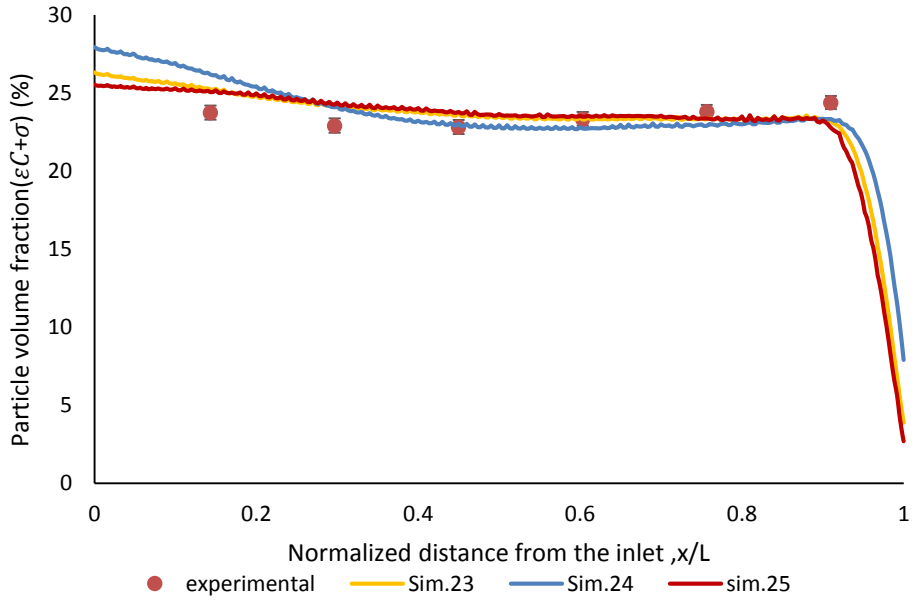

Figure 4.31 Simulation results for particle filler volume fraction distributions along the composite specimens for experiment: 30 % particle concentration in suspension and 20% fiber volume fraction

The simulation result for the experiment that has 40 % suspension particle concentration and 18 % fiber volume fraction is presented in Figure 4.32. According to the experimental conditions, the average particle volume fraction along the composite should be around 33 % (equation 4.6) however, the maximum experimentally determined particle volume fraction was around 30 %. As a result, there was more difference which result in high error between simulation and experimental results.

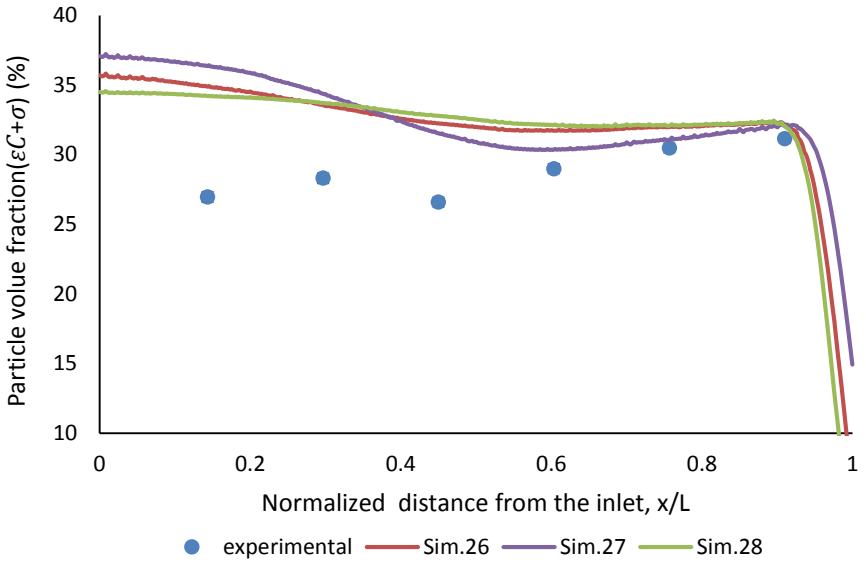

Figure 4.32 Simulation results for particle filler volume fraction distributions along the composite specimens for experiment: 40 % particle concentration in suspension and 18 % fiber volume fraction

Simulations also shows that positive k_1 (values higher than 10^2) and negative k_2 (values less than -10^4) result in first a decrease then an increase in particle distribution trends (Figure 4.30, 4.31, 4.32). The same trends were also shown by Tien et al. [48] with using positive $k_1$and negative k_2 constants.

In order to find best fit between experimental and simulation results, error sum of squares were calculated in each run and the smallest error sum case was chosen on the best fit. The errors are based on the difference between the experimental and numerical result.

$$SSE = \sum_{i=1}^{\#\ of\ exp.\ data} (1 - \frac{v_{f,particle,sim,i}}{v_{f,particle,exp,i}})^2 \qquad (4.8)$$

Sum of error squares were calculated for each case and the results are shown in Table 4.19.

Table 4.19 The sum of square of errors (SSE) between the simulations and experimental results for RTM simulations

Simulation Label	α_0	k_1	k_2	SSE
Sim.19	0.5	500	-11000	0.094
Sim.20	0.5	500	-20000	0.060
Sim.21	0.5	400	-11000	0.062
Sim.22	0.5	400	-20000	0.061
Sim.23	0.2	500	-10000	0.012
Sim.24	0.2	700	-10000	0.017
Sim.25	0.2	500	-20000	0.011
Sim.26	0.2	500	-10000	0.18
Sim.27	0.2	700	-10000	0.20
Sim.28	0.2	500	-20000	0.17

According to the Figures 4.30, 4.31, 4.32, a positive k_1 and a negative k_2 result in first a decrease and then an increase in particle distribution trends. The particle volume of fractions near to the inlet of the sample are sensitive to the values of both k_1 and k_2. If k_2 is kept constant, by increasing k_1, the particle volume fraction near the inlet will increase. For constant k_1, by decreasing k_2, the differences between the maximum and the minimum values of particle volume fraction in composite will be decrease. However, the value of k_1 and k_2 do not show a significant effect on the particle volume of fraction at the end of the composite.

From SSE analysis selected as $\boldsymbol{\alpha_0}$, $\boldsymbol{k_1}$ and $\boldsymbol{k_2}$, are shown in Table 4.20. According to the simulation results, the selected model constants in filtration coefficient yield good agreement with the experimental results.

Table 4.20 The selected model constants for RTM based on SSE analysis

Model Constants	C_o=20 % (Sim.20)	C_o=30 % (Sim.25)	C_o=40 % (Sim.28)
$\boldsymbol{\alpha_0}$	0.5	0.2	0.2
$\boldsymbol{k_1}$	500	500	500
$\boldsymbol{k_2}$	-20000	-20000	-20000

Figure 4.33, 4.37, 4.41 present the comparison of experimental and numerical particle volume fraction distributions along the flow direction in the composite. Numerical simulations have been done using the proper model constants, which were given in Table 4.20. The numerical results yield in a good agreement with the experimental result.

The particle volume fractions of a location in composite was obtained with the sum of particles in suspension and the filtered particles through the equation (4.7).

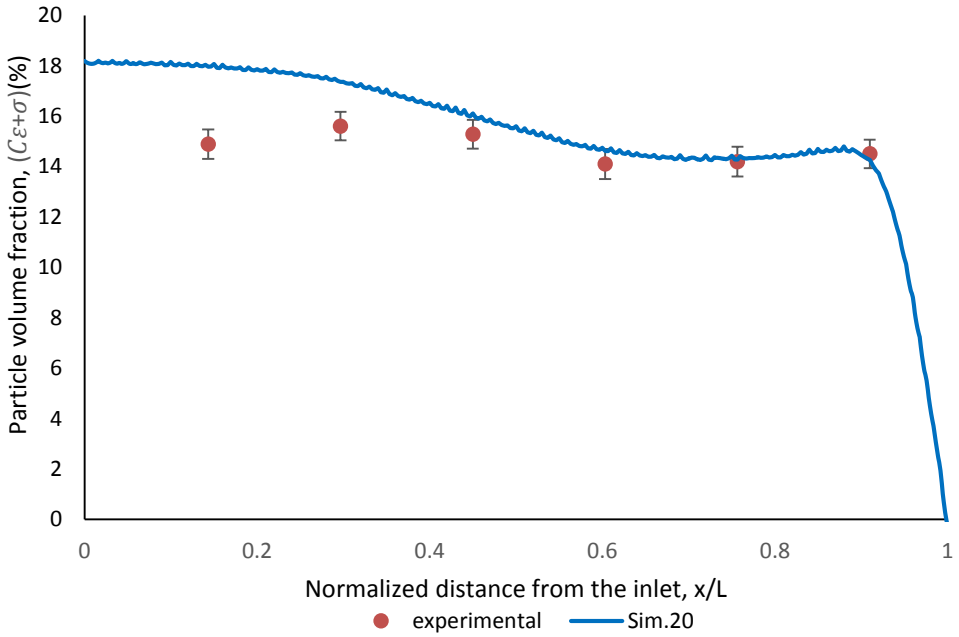

Figure 4.33 Comparison of experimental and numerical particle volume fraction distributions along the flow direction in the composite for experiment (20 % particle concentration and fiber volume fraction)

According to result in Figure 4.33, the specific particle deposit, porosity and particle concentration along the flow direction results are shown in Figure 4.34, Figure4.35, Figure 4.36, respectively.

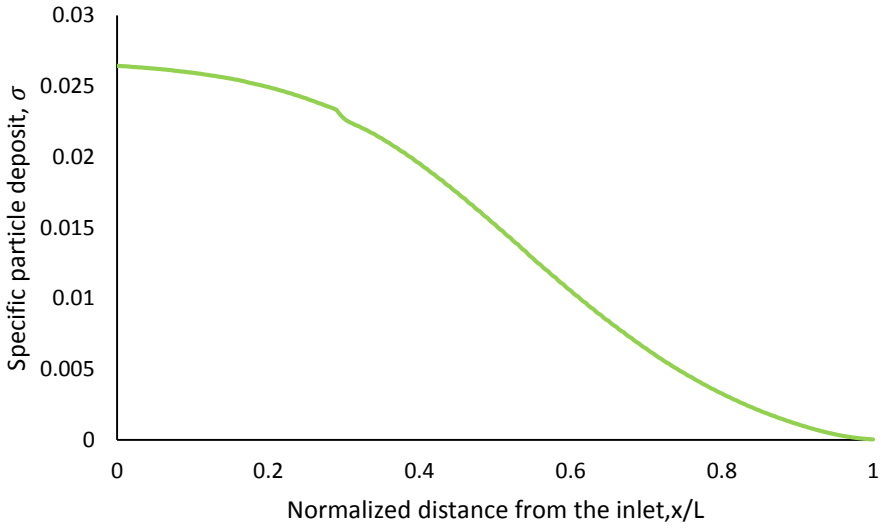

Figure 4.34 Specific particle deposit along the flow direction for Sim.20

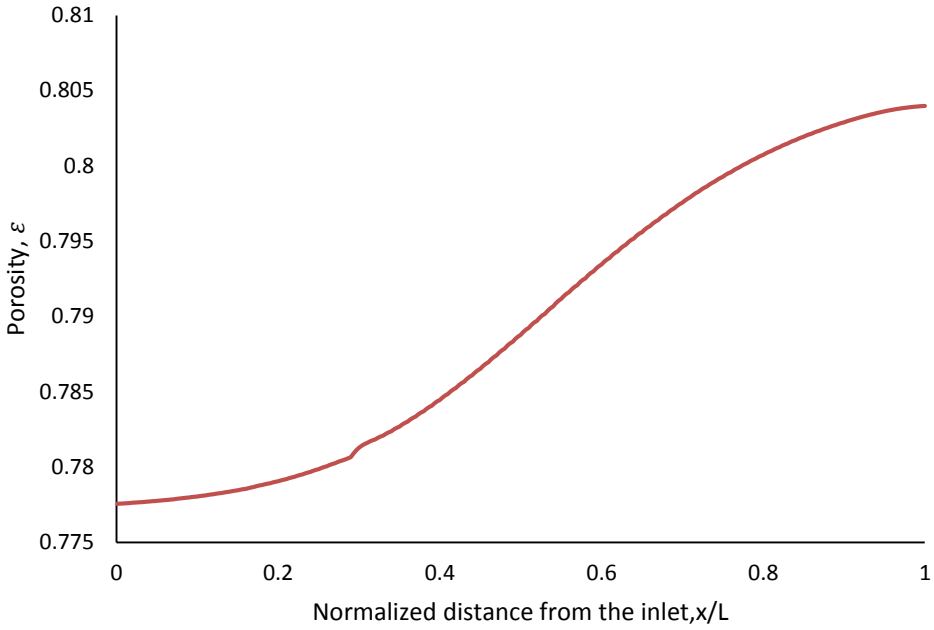

Figure 4.35 Porosity along the flow direction for Sim.20

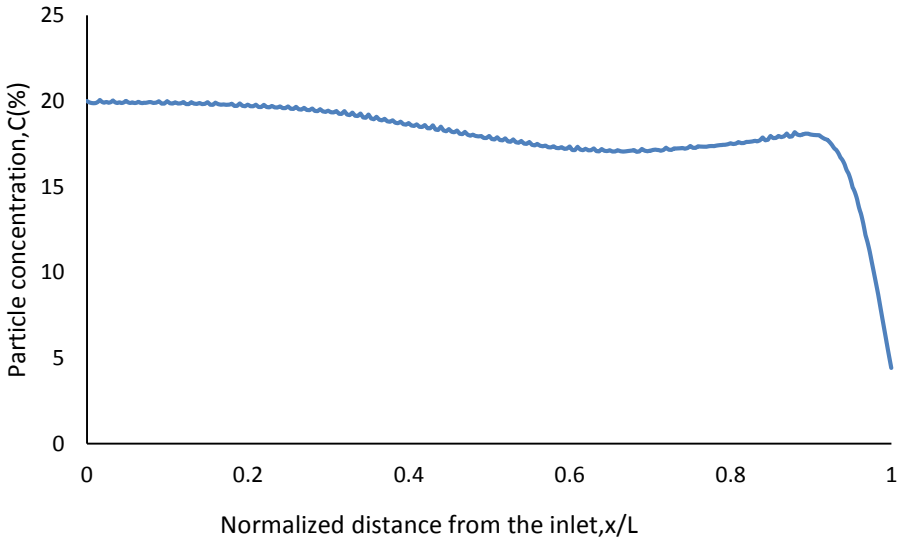

Figure 4.36 Particle concentration along the flow direction for Sim.20

According to result in Figure 4.37, the specific particle deposit, porosity and particle concentration along the flow direction results are shown in Figure 4.38, Figure 4.39, Figure 4.40, respectively.

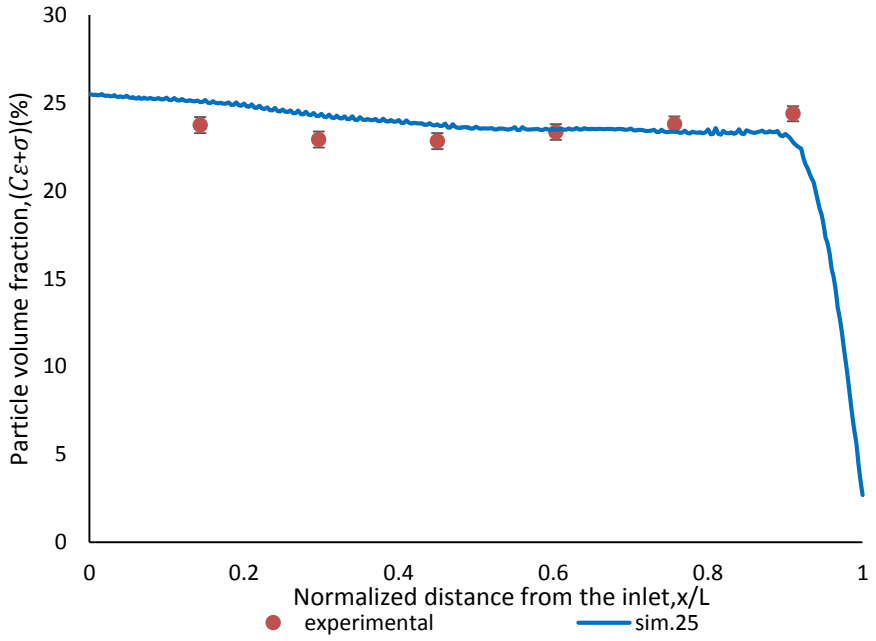

Figure 4.37 Comparison of experimental and numerical particle volume fraction distributions along the flow direction in the composite for experiment : 30% particle concentration and 20% fiber volume fraction

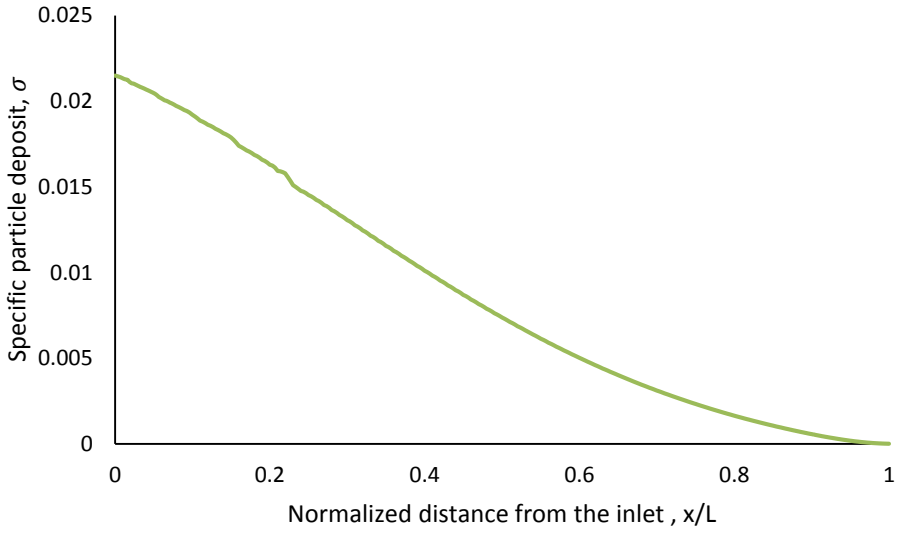

Figure 4.38 Specific particle deposit along the flow direction for Sim.25

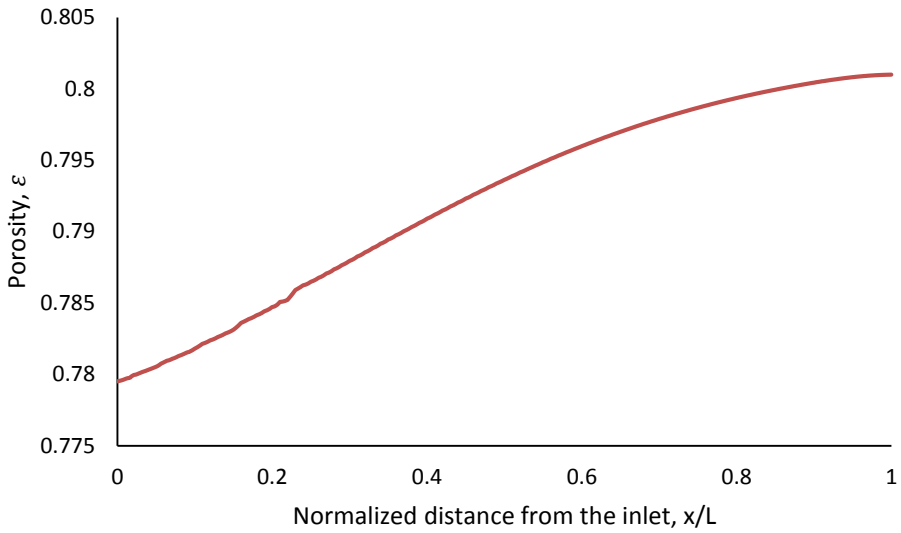

Figure 4.39 Porosity along the flow direction for Sim.25

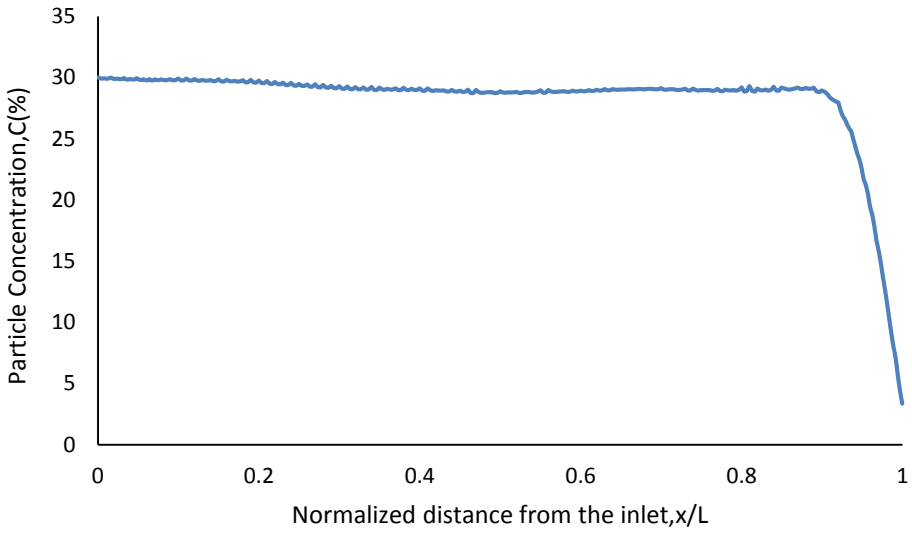

Figure 4.40 Particle concentration along the flow direction for Sim.25

According to result in Figure 4.41, the specific particle deposit, porosity and particle concentration along the flow direction results are shown in Figure 4.42, Figure 4.43, Figure 4.44, respectively.

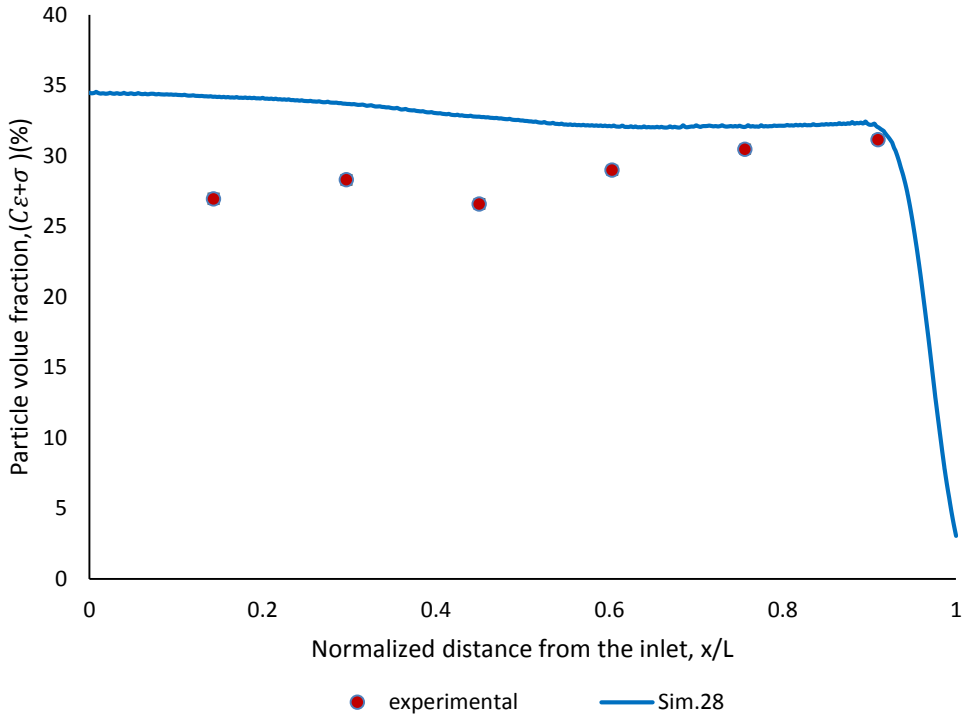

Figure 4.41 Comparison of experimental and numerical particle volume fraction distributions along the flow direction in the composite for for experiment which has 40% particle concentration and 18% fiber volume fraction

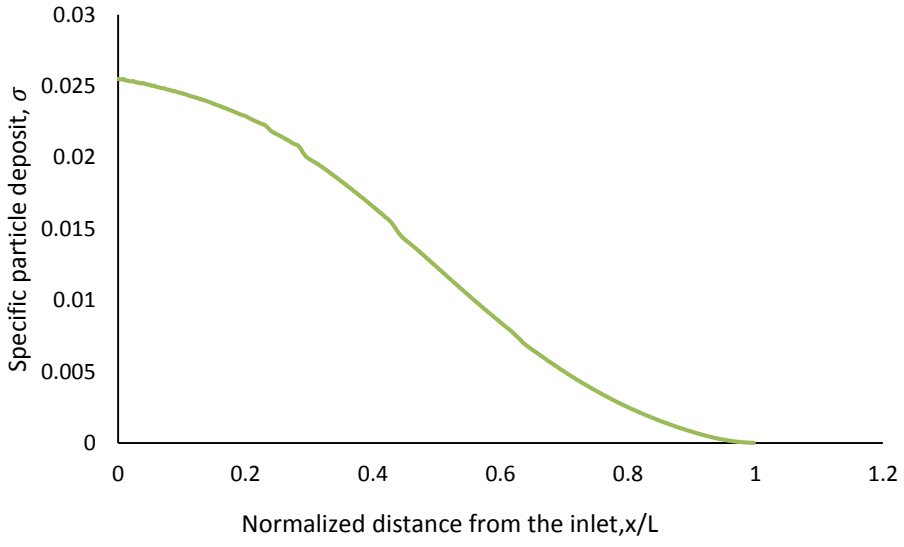

Figure 4.42 Specific particle deposit along the flow direction for Sim.28

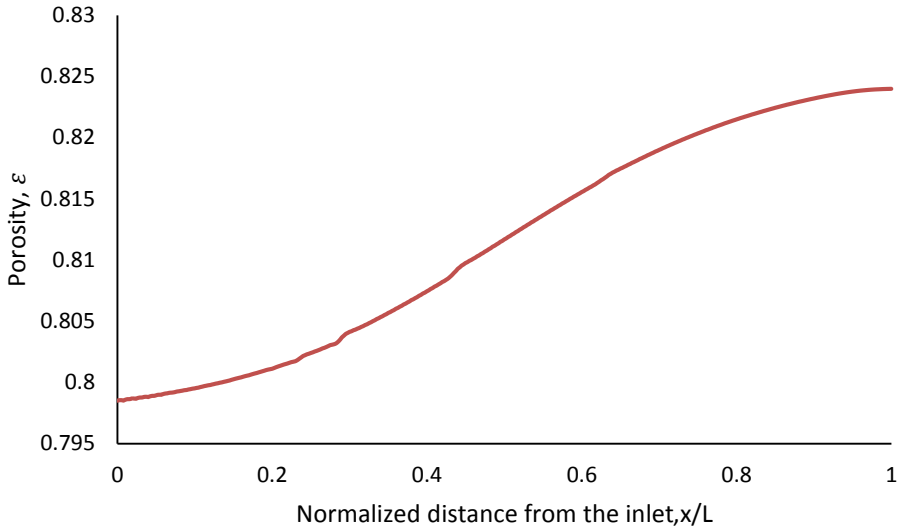

Figure 4.43 Porosity along the flow direction for Sim.28

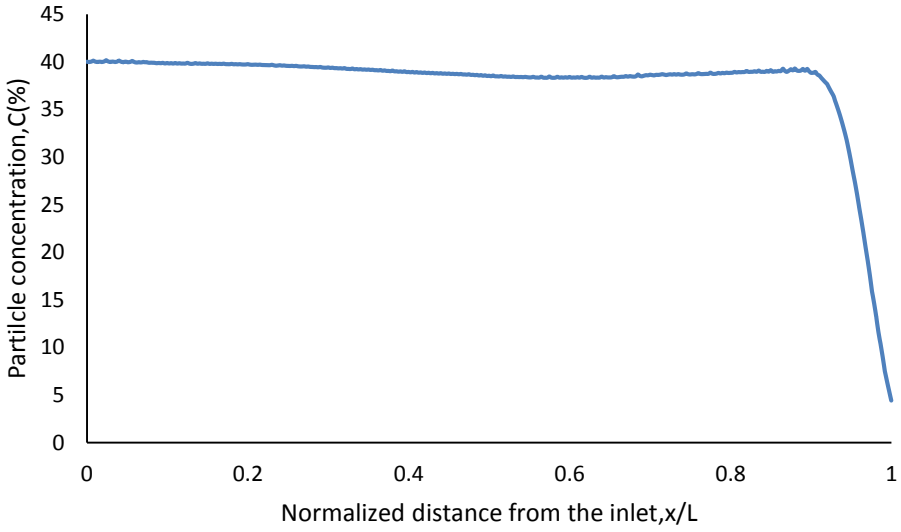

Figure 4.44 Particle concentration along the flow direction for Sim.28

As expected, the specific particle deposition is inversely proportional to the domain porosity in all results.

The particle concentration at the beginning of simulation starts with the particle concentration in injected suspension as expected. The change in the particle concentration then depends on the specific particle deposit that varies with the filtration coefficient constant.

4.5.2 Determination of appropriate α_0, k_1 and k_2 for filtration coefficient in CRTM

In CRTM, several simulations were performed to find the proper range of the filtration coefficient model constants. As a result of RTM simulations: Change in k_1 does not yield a significant difference in the particle volume fraction distribution except when its value reaches 100, the effect of k_2 is not apparent until its value reaches 10000. Therefore, in CRTM simulations the range of constants starts with the range of constant results in RTM simulations. Table 4.21 presents simulation parameters and the experiment condition which were simulated.

Table 4.21 Simulation parameters and experimental conditions that are simulated for filtration model constants determination in CRTM

Conditions of experiment that is simulated	Simulation Label	Injection phase			Compression phase		
		$\boldsymbol{\alpha_0}$	$\boldsymbol{k_1}$	$\boldsymbol{k_2}$	$\boldsymbol{\alpha_0}$	$\boldsymbol{k_1}$	$\boldsymbol{k_2}$
C_o=20(%) v_{fo} =27(%) $v_{fo,initial}$ =16(%) CRTM-Exp.8*	Sim.37	0.5	500	-2*10^4	0.5	500	-2*10^4
	Sim.38	0.5	500	-2*10^4	0.1	500	-2*10^4
	Sim.39	0.5	500	-2*10^4	0.1	1000	2*10^4
	Sim.40	0.5	500	-2*10^4	0.1	1000	-2*10^4
	Sim.41	0.5	500	-2*10^4	0.1	-500	2*10^4
	Sim.42	1	500	-2*10^4	1	500	-2*10^4
	Sim.43	1	500	-2*10^4	0.5	500	-2*10^4
	Sim.44	0.1	500	-2*10^4	0.1	500	-2*10^4
	Sim.45	0.1	500	-2*10^4	0.5	500	-2*10^4

*per Table 4.6

Figure 4.45, Figure 4.46 and Figure 4.47 present these simulations. The experimental result had the particle volume fraction increase along the composite length and reach to its maximum value at the end of the composite.

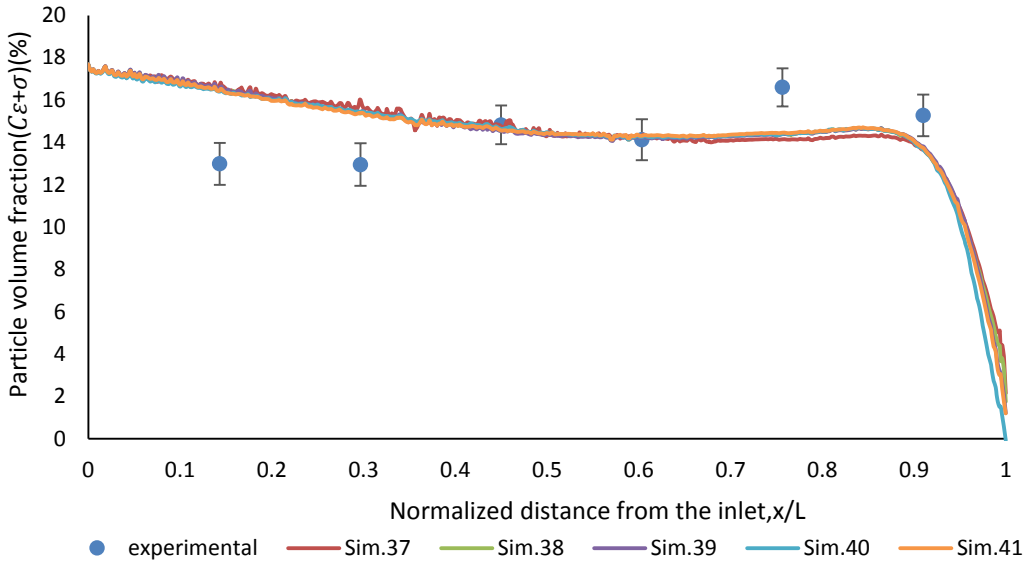

Figure 4.45 Simulation results for particle filler volume fraction distributions along the composite in CRTM(C_o=20(%) v_{fo} =27 (%)$v_{fo,initial}$ =16(%))

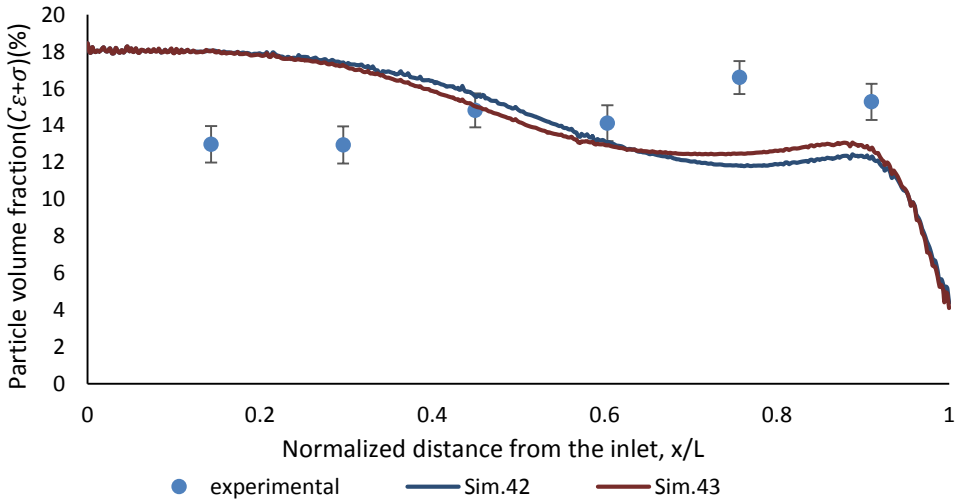

Figure 4.46 Simulation results for particle filler volume fraction distributions along the composite in CRTM (C_o=20(%) v_{fo} =27 (%)$v_{fo,initial}$ =16(%))

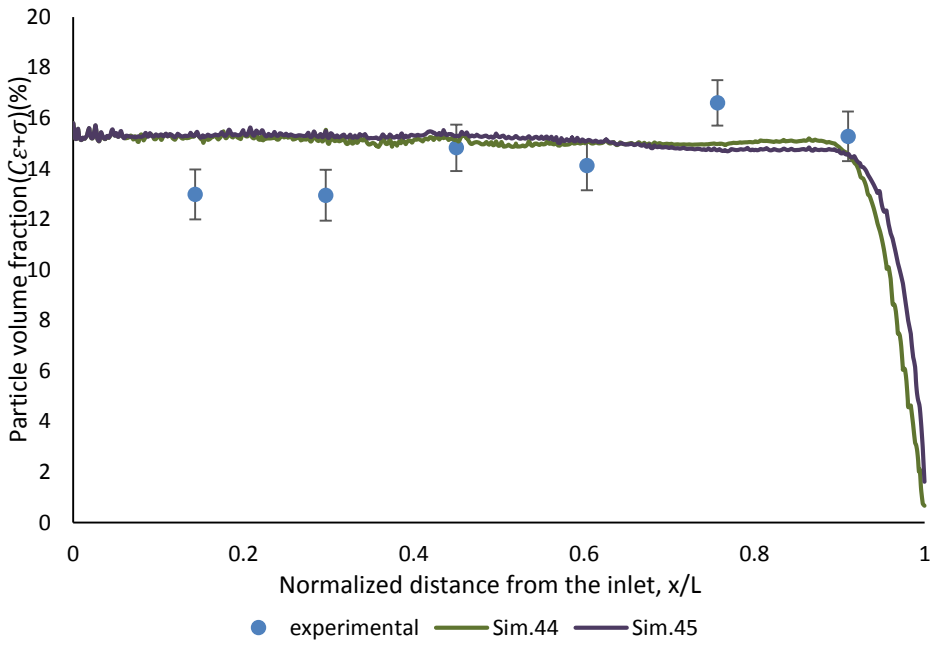

Figure 4.47 Simulation results for particle filler volume fraction distributions along the composite in CRTM (C_o=20(%) v_{fo} =27 (%)$v_{fo,initial}$ =16(%))

There is not a difference between the result of Sim. 37 and Sim. 38 that show the change of α_0 in compression phase does not affect the particle distribution in composite. The same result is presented between Sim.42 and Sim.43 also Sim.44 and Sim.45. In Sim.39 and Sim.40 there is not a difference on the particle distribution in composite with a significant change in $\boldsymbol{k_2}$ at compression phase(one of them is negative while the other is positive). The change of $\boldsymbol{k_1}$ in compression phase does not show a significiant effect on the particle distribution in composite (Sim.37 and Sim.41) Therefore, it is seen that the particle distribution trend of simulations is mainly affected by the model constants which are used in injection phase.

Table 4.22 presents the simulation parameters and the experiment which were simulated. Figure 4.48 and Figure 4.49 present these simulations. In Figure 4.48, the filtration coefficients in compression phase do not show a difference on the particle distribution in composite in Sim.29, Sim.30, Sim.31. This is also shown in Figure 4.49. The most effective constant on particle distribution is α_0 used in injection phase.

Table 4.22 Simulation parameters and experimental conditions that are simulated for filtration model constants determination in CRTM

Conditions of experiment that is simulated	Simulation Label	Injection phase			Compression phase		
		α_0	k_1	k_2	α_0	k_1	k_2
C_o=30(%) v_{fo} =23(%) $v_{fo,initial}$ =16 (%) CRTM-Exp.6*	Sim.29	0.5	500	-1*10^4	0.2	500	-2*10^4
	Sim.30	0.5	500	-1*10^4	0.5	500	-1*10^4
	Sim.31	0.5	500	-1*10^4	0.2	-500	2*10^4
	Sim.32	1	500	-2*10^4	1	500	-2*10^4
	Sim.33	0.2	500	-2*10^4	0.5	-500	-2*10^4
	Sim.34	0.2	500	-2*10^4	0.5	500	-2*10^4
	Sim.35	0.1	1000	-2*10^4	0.1	1000	-2*10^4
	Sim.36	0.1	1000	-2*10^4	0.1	2000	-2*10^4

*per Table 4.6

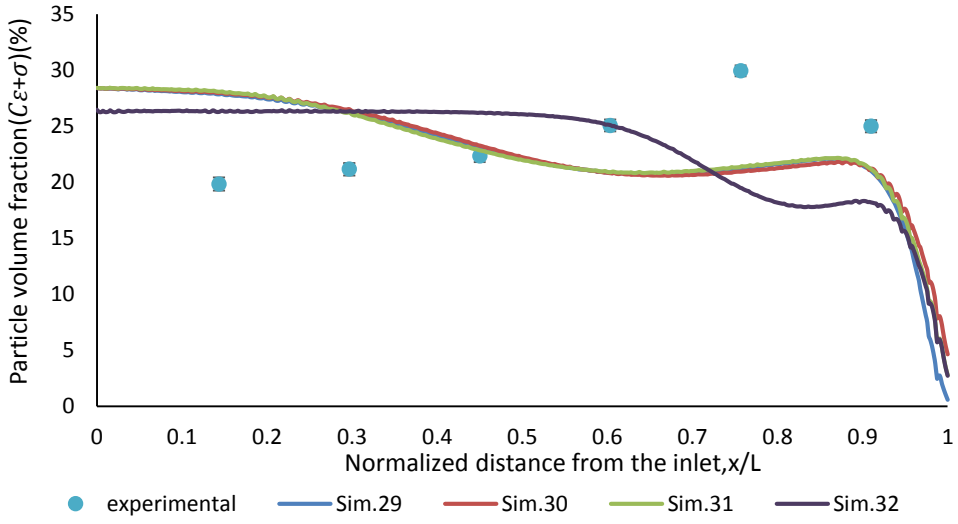

Figure 4.48 Simulation results for particle filler volume fraction distributions along the composite in CRTM (C_o=30(%) v_{fo} =23(%),$v_{fo,initial}$ =16(%))

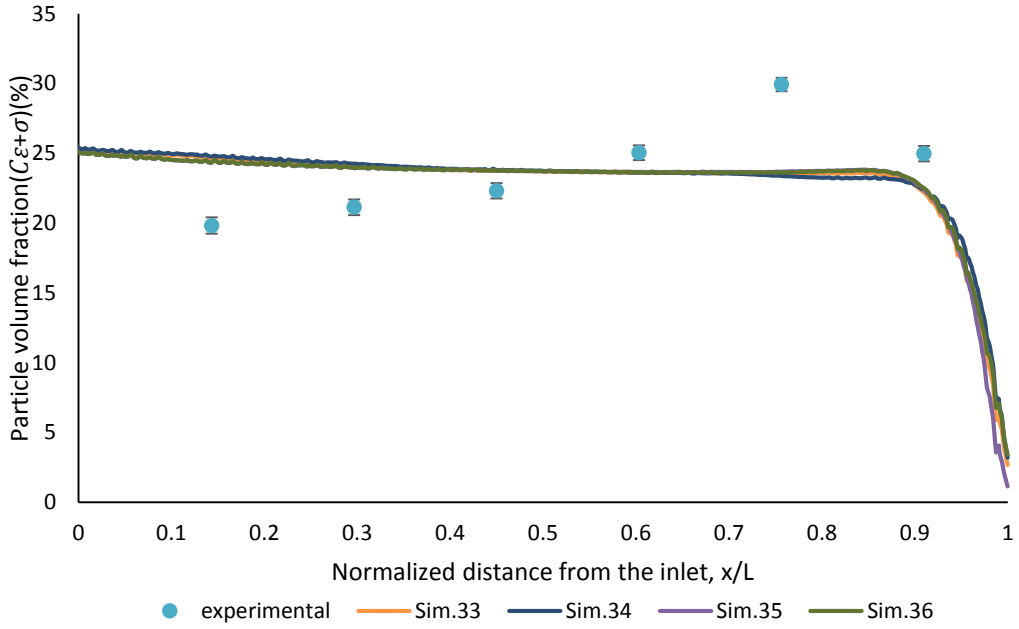

Figure 4.49 Simulation results for particle filler volume fraction distributions along the composite in CRTM (C_o=30(%) v_{fo} =23(%),$v_{fo,initial}$ =16(%))

Since the constants of filtration coefficients in the compression phase do not show a significiant effect on the particle distribution, in the last set of simulations involving the simulation of 40 % particle concentration injection filtration coefficient constants of injection phase are used for the compression phase as well as (Table 4.23).Figure 4.50 presents these simulations. The experimental particle filler content increases and decreases in alternating pattern.

Table 4.23 Simulation parameters and experimental conditions that are simulated for filtration model constants determination in CRTM

Conditions of experiment that is simulated	Simulation Label	Injection phase			Compression phase		
		α_0	k_1	k_2	α_0	k_1	k_2
C_o=40(%) v_f =22(%) $v_{fo,inj}$ =16(%) CRTM-Exp.7*	Sim.46	0.2	500	-2*10^4	0.2	500	-2*10^4
	Sim.47	0.3	500	-2*10^4	0.3	500	-2*10^4
	Sim.48	0.5	500	-2*10^4	0.5	500	-2*10^4

*per Table 4.6

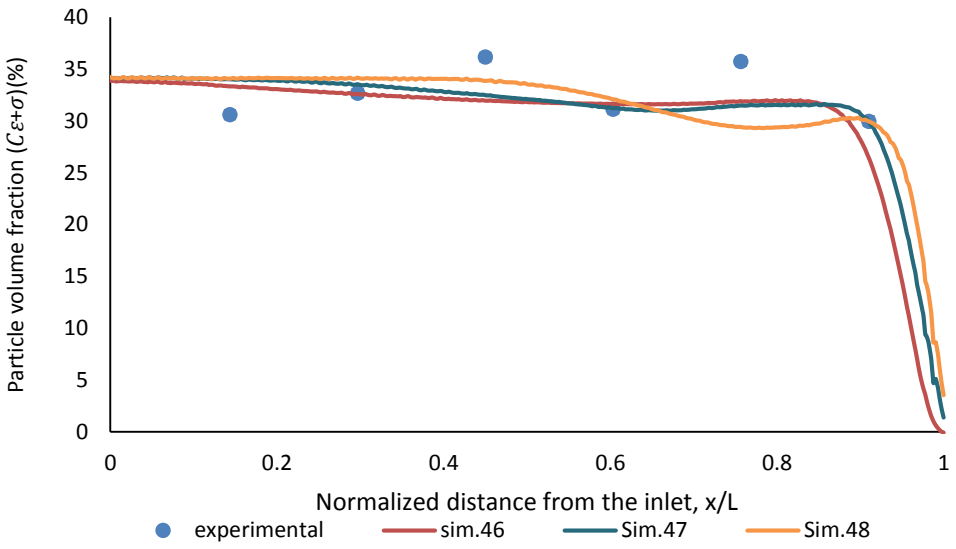

Figure 4.50 Simulation results for particle filler volume fraction distributions along the composite in CRTM (C_o=40(%) v_{fo} =22 (%) $v_{fo,initial}$ =16(%))

The comparison of experimental and numerical particle volume fraction distributions along the flow direction in the composite are presented for three CRTM experiments.

Unlike RTM process where the particle distribution trends are nearly uniform and in some cases, have a slight decrease in particle volume fraction values towards the end of composite, in CRTM, particle distribution trend increases towards the end of the composite followed by a clear decrease. The simulation results can not capture this trend. Therefore, the used filtration coefficient model is not appropriate for CRTM.

CHAPTER 5

CONCLUSIONS AND FUTURE WORK

In this study, an experimental work has been perfomed to investigate the particle distribution in particle-filled, continuous fiber-reinforced composites produced via two liquid molding methods: RTM and CRTM. Composite specimens which are produced with these processes are characterized for particle distribution to compare and understand the effect of various process parameters on the composite microstructure (particle distribution) in each experiment. The particle-filled resin impregnation through the fibrous preform in each process has been simulated using a previously developed Darcy-flow based impregnation model coupled with particle filtration. A particular aim of the current work was to adjust the filtration kinetics model based on experimental data by tuning the model parameters in filtration coefficient until simulated particle filler distributions matched with experimental ones. The numerical implementation and solution of the impregnation model was performed on Comsol Multiphysics ® version 4.3, a commercial software package.

The following have been found and concluded in this thesis

- A nearly constant particle distribution profile along the flow direction was found in all produced composites, indicating little filtration in RTM
- These results were obtained for composites made of epoxy resin, glass fiber and glass particles at fiber volume fraction near 20 % and for suspension 20 %, 30 %, 40 %. Here the 40 % particle content showed a slightly increasing particle content along flow direction in composite.

- In CRTM, particle content in composite increased towards the end of the flow length in composite.
- The experimental viscosity results for the suspension successfully fitted to an appropriate viscosity model from literature.
- The experimental permeability data (for 20 % and 30 % fiber volume fraction) was presented as a porosity function.
- High fiber volume fractions which are difficult to achieve in RTM due to the tremendous increase in inlet pressure, can be used in CRTM.
- The injection speed of the particle filler-resin suspension does not have a significant effect on the particle distribution, though it is very effective on flow pressure.
- The simulation results for particle distribution in composite are found to match nearly experimental results by an appropriate adjustment of the constants of filtration coefficient, in RTM. In RTM, for lower particle concentrations in the injected suspension (20 % and 30 % by volume), the model and experimental results for particle distributions in composite were found to be in reasonable agreement. At the high (40 %) particle concentration, some deviation from the experimental results was observed in simulations.
- In CRTM, the simulation results for particle distribution in composite can not capture the experimental trend.

The following are recommended for future work related to this thesis topic

- The experimental analysis can be extended to other composite constituents (different particles, fibers, resin) and fiber volume fraction values to assess the effect of these processing parameters on particle distribution within the composite for both RTM and CRTM processes. This analysis would give a more complete picture of particle deposition mechanisms in composites.
- The filtration phenomenon at higher fiber volume fraction can be studied using a resin with an especially low viscosity or a suspension with low particle filler concentration, as the pressure rises rapidly in high fiber volume fraction impregnations.

- In order to tune the constants of the filtration kinetics model more accurately, an optimization work can be undertaken with an appropriate software program that can be linked to Comsol Multiphysics®.
- The permeability model for particle-filled impregnation (equation 3.25) can be fine-tuned using the experimental results.
- The results of such work can be used towards designing on RTM or CRTM process for which a desired particle distribution within the produced composite can be obtained. An accurate flow model (one that predicts particle distributions accurately) would help design the mold as well as determine the optimum process parameters that would yield the desired particle distribution in composite.

REFERENCES

[1] Mazumdar SK, Composites Manufacturing, Crc Press, 2002.

[2] Lefevre D, Comas-Cardona S, Binétruy C, Krawczak P. Modelling the flow of particle-filled resin through a fibrous preform in liquid composite molding technologies. Composites Part A: Applied Science and Manufacturing 2007;38:2154–63.

[3] Shojaei A. Numerical simulation of three-dimensional flow and analysis of filling process in compression resin transfer moulding. Composites Part A: Applied Science and Manufacturing 2006;37:1434–50.

[4] Shojaei A. A numerical study of filling process through multilayer preforms in resin injection/compression molding. Composites Science and Technology 2006;66:1546–57.

[5] Young W-B. Three-dimensional nonisothermal mold filling simulations in resin transfer molding. Polymer Composites 1994;15:118–27.

[6] Phealan FR. Simulation of the Injection Process in Resin Transfer 1997;18: 460-476.

[7] Shojaei A. An Experimental Study of Saturated and Unsaturated Permeabilities in Resin Transfer Molding Based on Unidirectional Flow Measurements. Journal of Reinforced Plastics and Composites 2004;23:1515–36.

[8] Bhat P, Merotte J, Simacek P, Advani SG. Process analysis of compression resin transfer molding. Composites Part A: Applied Science and Manufacturing 2009;40:431–41.

[9] Buntain MJ, Bickerton S. Modeling forces generated within rigid liquid composite molding tools. Part A: Experimental study. Composites Part A: Applied Science and Manufacturing 2007;38:1729–41.

[10] Chang C-Y. Simulation of Mold Filling in Simultaneous Resin Injection/Compression Molding. Journal of Reinforced Plastics and Composites 2006;25:1255–68.

[11] Jiao W, Liu Y, Qi G. Studies on mechanical properties of epoxy composites filled with the grafted particles PGMA/Al_2O_3. Composites Science and Technology 2009;69:391–5.

[12] Huang G, Wang S, Song P, Wu C, Chen S, Wang X. Combination effect of carbon nanotubes with graphene on intumescent flame-retardant polypropylene nanocomposites. Composites Part A: Applied Science and Manufacturing 2014;59:18–25.

[13] Mohan N, Natarajan S, KumareshBabu SP. Abrasive wear behaviour of hard powders filled glass fabric–epoxy hybrid composites. Materials & Design 2011;32:1704–9.

[14] Visconti IC, Langella A, Durante M. The wear behaviour of composite materials with epoxy matrix filled with hard powder 2001:179–89.

[15] Yamamoto N, Guzman de Villoria R, Wardle BL. Electrical and thermal property enhancement of fiber-reinforced polymer laminate composites through controlled implementation of multi-walled carbon nanotubes. Composites Science and Technology 2012;72:2009–15.

[16] Tian Y, Gao B, Silvera-Batista C, Ziegler KJ. Transport of engineered nanoparticles in saturated porous media. Journal of Nanoparticle Research 2010;12:2371–80.

[17] Erdal M. Impregnation molding of continuous fiber-reinforced ceramic-ceramic composites using preceramic polymers. Mechanical Engineering, University of Illinois at Chicago, 1998.

[18] Erdal M, Guceri SI, Danforth SC. Impregnation molding of particle-filled preceramic polymers: Process Modeling. Journal of the American Ceramic Society 1999;82:2017–28.

[19] Sas H, Erdal M. Modeling of particle–resin suspension impregnation in compression resin transfer molding of particle-filled, continuous fiber reinforced composites. Heat and Mass Transfer 2014;50:397–414.

[20] Reia da Costa EF, Skordos A a., Partridge IK, Rezai A. RTM processing and electrical performance of carbon nanotube modified epoxy/fibre composites. Composites Part A: Applied Science and Manufacturing 2012;43:593–602.

[21] Fan Z, Hsiao K-T, Advani SG. Experimental investigation of dispersion during flow of multi-walled carbon nanotube/polymer suspension in fibrous porous media. Carbon 2004;42:871–6.

[22] Nordlund M, Fernberg SP, Lundström TS. Particle deposition mechanisms during processing of advanced composite materials. Composites Part A: Applied Science and Manufacturing 2007;38:2182–93.

[23] Shojaei A., Ghaffarian SR, Karimian SMH. Modeling and simulation approaches in the resin transfer molding process: A review. Polymer Composites 2003;24:525–44.

[24] Simacek P., Advani SG. Desirable features in mold filling simulations for Liquid composite molding processes. Polymer Composites n.d.;25:355–67.

[25] Bruschke M V., Advani SG. A finite element/control volume approach to mold filling in anisotropic porous media. Polymer Composites 1990;11:398–405.

[26] Matsuzaki R, Seto D, Todoroki A, Mizutani Y. Void formation in geometry–anisotropic woven fabrics in resin transfer molding. Advanced Composite Materials 2014;23:99–114.

[27] Devillard M, Hsiao K.T., Advani SG. Flow sensing and control strategies to address race-tracking disturbances in resin transfer molding—part II: automation and validation. Composites Part A: Applied Science and Manufacturing 2005;36:1581–9.

[28] Trochu F., Gauvin R., Gao D.M. Numerical Analysis of the resin transfer molding process by the finite element method. Advances in Polymer Technologies 1993;12:329–342.

[29] Laurenzi S, Grilli a., Pinna M, De Nicola F, Cattaneo G, Marchetti M. Process simulation for a large composite aeronautic beam by resin transfer molding. Composites Part B: Engineering 2014;57:47–55.

[30] Poodts E, Minak G, Mazzocchetti L, Giorgini L. Fabrication, process simulation and testing of a thick CFRP component using the RTM process. Composites Part B: Engineering 2014;56:673–80.

[31] Pham X.T, Trochu F. Simulation of Compression Resin Transfer Molding to Manufacture Thin Composite Shells 1999;20.

[32] Merotte J, Simacek P, Advani SG. Resin flow analysis with fiber preform deformation in through thickness direction during Compression Resin Transfer Molding. Composites Part A: Applied Science and Manufacturing 2010;41:881–7.

[33] Merotte J, Simacek P, Advani SG. Flow analysis during compression of partially impregnated fiber preform under controlled force. Composites Science and Technology 2010;70:725–33.

[34] Bickerton S, Buntain MJ. Modeling forces generated within rigid liquid composite molding tools. Part B: Numerical analysis. Composites Part A: Applied Science and Manufacturing 2007;38:1742–54.

[35] Chang C-Y. Effect of Process Variables on the Quality of Compression Resin Transfer Molding. Journal of Reinforced Plastics and Composites 2006;25:1027–37.

[36] Lefevre D, Comas-Cardona S, Binetruy C, Krawczak P. Coupling filtration and flow during liquid composite molding: Experimental investigation and simulation. Composites Science and Technology 2009;69:2127–34.

[37] Chohra M, Advani SG, Gokce A, Yarlagadda S. Modeling of Filtration Through Multiple Layers of Dual Scale Fibrous Porous Media. Polymer Composites 2006;27: 570-581.

[38] Hwang WR, Advani SG, Walsh S. Direct simulations of particle deposition and filtration in dual-scale porous media. Composites Part A: Applied Science and Manufacturing 2011;42:1344–52.

[39] Reia da Costa EF, Skordos A. Modelling flow and filtration in liquid composite moulding of nanoparticle loaded thermosets. Composites Science and Technology 2012;72:799–805.

[40] Mgs H. Laminating resin MGS ® L 160 Data Sheet 2006;49.

[41] Standard Terminology for Composite Materials. ASTM International, D3878-03.

[42] Naik NK, Sirisha M, Inani a. Permeability characterization of polymer matrix composites by RTM/VARTM. Progress in Aerospace Sciences 2014;65:22–40.

[43] Darcy H., Les fontaines publiques de la ville de Dijon. 1856.

[44] Coulter JP, Güçeri SI. Resin impregnation during composites manufacturing: Theory and experimentation. Composites Science and Technology 1989;35:317–30.

[45] Tan CP, Springer GS. Composite Manufacturing: Simulation of 3-D Resin Transfer Molding. Journal of Composite Materials 1999;33:1716–42.

[46] Herzig JP, Leclerc DM, Goff PL. Flow of Suspensions through Porous Media—Application to Deep Filtration. Industrial & Engineering Chemistry 1970;62:8–35.

[47] J IK. The Scientific basis of filtration. Proceedings of the NATO Advanced Study Institute on the Scientific Basis of Filtration, Noordhoof Int. Pub Co.; 1975, p. 183–224.

[48] Bai R, Tien C. Effect of Deposition in Deep-Bed Filtration: Determination and Search of Rate Parameters. Journal of Colloid and Interface Science 2000;231:299–311.

[49] T. Kataoka, T. Kitano, M. Sasahara KN. Viscosity of particle filled polymer melts. Rheologica Acta 1978;17:149–55.

[50] Bickerton S, Abdullah MZ. Modeling and evaluation of the filling stage of injection/compression moulding. Composites Science and Technology 2003;63:1359–75.

[51] http://www.comsol.com/products , last accessed on 10 September 2014.

APPENDIX A

A GUIDE FOR MONITORING DATA

The control unit that used in experimental setup consists of a graphical interface and data acquisition card. As data acquisition card, Arduino Uno is used. A NPN Power Darlington Transistor (TIP 120) is used with an Arduino to drive motors. The TIP120 acts as a power broker or gatekeeper between the Arduino realm and the high power realm composed of the linear actuator and power supply. Through the Base pin, the Arduino can tell the TIP120 how much power to supply to the motor from the external power but the Arduino does not share any of its power or share pins with actuator. Pin configurations are shown in Table A.1. Figure A.1 shows the circuit which was used to run the actuator in more details.

Table A.1 Pin Configuration

Arduino Pin	Connected to
A0	Pressure transducer data
A1	Linear actuator potentiometer data
5V	Linear actuator potentiometer power
GND	Linear actuator potentiometer and Pressure transducer GND
~11	TIP 120 Transistor Base

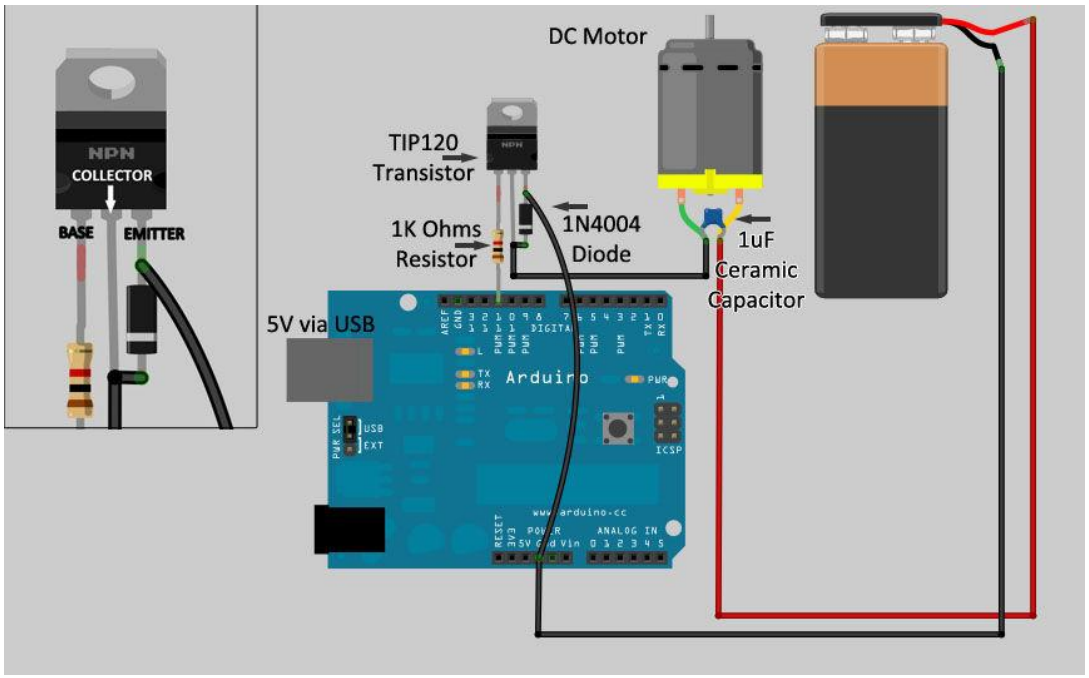

Figure A.1 The circuit for monitoring

The interface (Figure A.2) which is written in LabVIEW is used to run and monitor the injection setup. Mold inlet pressure, injection piston position and speed are plotted with respect to the time simultaneously. Furthermore, inlet pressure and piston position are shown using graphical indicators. Before running the interface, following items should be set:

1. Connect the Arduino to the computer via USB port.
2. Select the pressure transducer according to its maximum range. There are two options to select, 4 and 25 bar transducers.
3. Set the injection piston speed in mm/s. Note that the maximum applicable speed is 7 mm/s.
4. In order to know injected resin volume, click on “Set pos.” button.
5. In PID Controller window, set PID constants.
6. Set the Arduino Pulse Width Modulation (PWM) range. Set Output Low to 0 and Output High to 255.
7. Data sample rate can be set using Delay time box. For instance, if delay time set to 100 ms, 10 samples per second will be recorded.
8. Indicate the COM port which Arduino uses.

9. To reduce noise, statistical filters (mean value) are used. This operator computes the mean of the values in the set of the input data points specified using sample rate. Adjust the sample rate for piston position and velocity.
10. Active PID controller by clicking on PID button.
11. Click on RUN button.

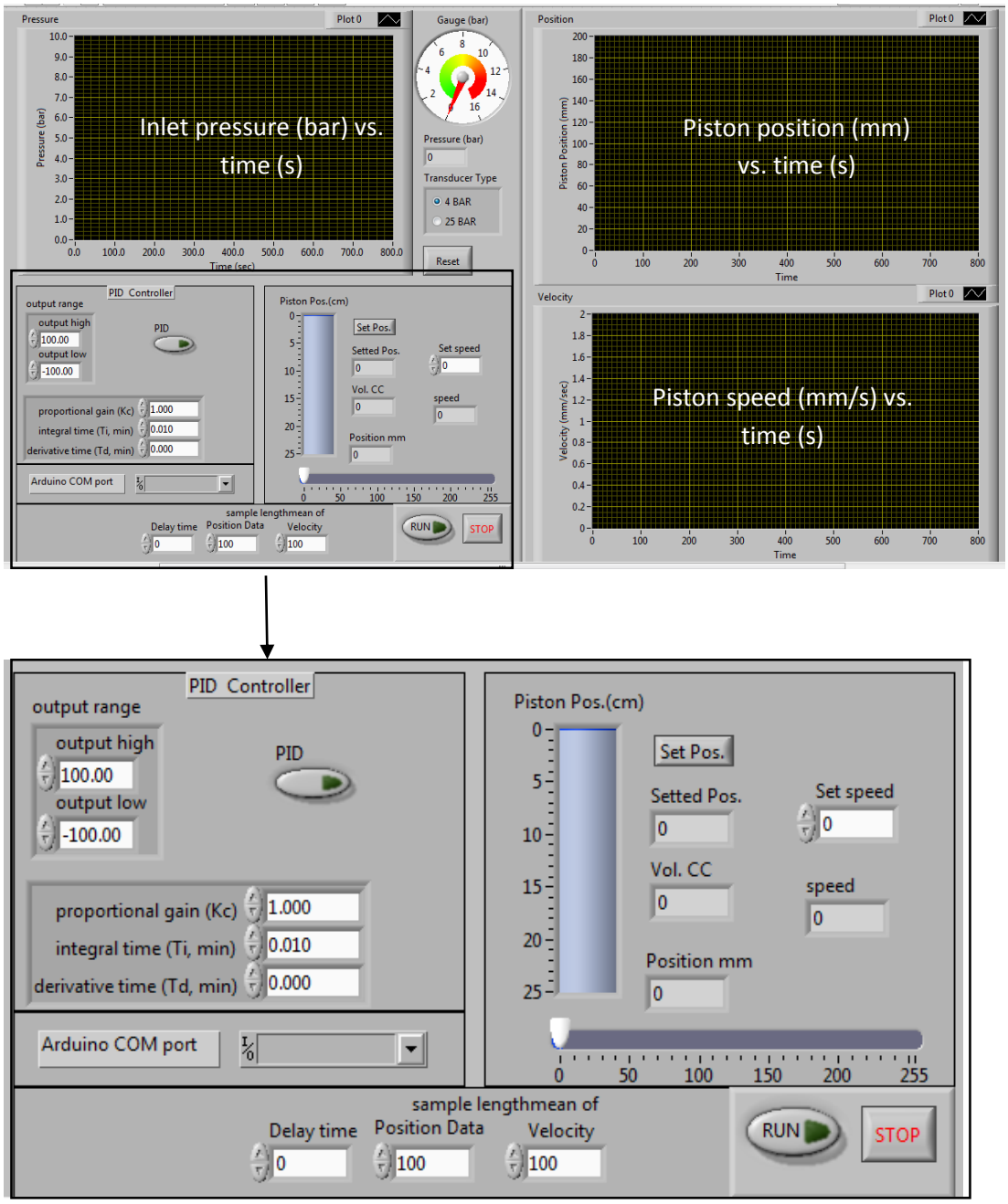

Figure A.2 The interface of the Labview®